

KINEMATIC SYNTHESIS AND ANALYSIS TECHNIQUES  
TO IMPROVE PLANAR RIGID-BODY GUIDANCE

Dissertation

Submitted to

The School of Engineering of the

UNIVERSITY OF DAYTON

In Partial Fulfillment of the Requirements for

The Degree

Doctor of Philosophy in Mechanical Engineering

by

David H. Myszka

UNIVERSITY OF DAYTON

Dayton, Ohio

August 2009

KINEMATIC SYNTHESIS AND ANALYSIS TECHNIQUES TO IMPROVE PLANAR  
RIGID-BODY GUIDANCE

APPROVED BY:

---

Andrew P. Murray, Ph.D.  
Advisor Committee Chairman  
Associate Professor, Dept. of  
Mechanical and Aerospace Engineering

---

James P. Schmiedeler, Ph.D.  
Committee Member  
Associate Professor, Dept. of  
Mechanical Engineering, University of  
Notre Dame

---

Ahmad Reza Kashani, Ph.D.  
Committee Member  
Professor, Dept. of Mechanical and  
Aerospace Engineering

---

Raúl Ordóñez, Ph.D.  
Committee Member  
Associate Professor, Dept. of Electrical  
and Computer Engineering

---

Malcolm W. Daniels, Ph.D.  
Associate Dean of Graduate Studies  
School of Engineering

---

Joseph E. Saliba, Ph.D.  
Dean  
School of Engineering

© Copyright by

David H. Myszka

All rights reserved

2009

## **ABSTRACT**

### **KINEMATIC SYNTHESIS AND ANALYSIS TECHNIQUES TO IMPROVE PLANAR RIGID-BODY GUIDANCE**

Name: Myszka, David H.  
University of Dayton

Advisor: Dr. Andrew P. Murray

Machine designers frequently need to conceive of a device that exhibits particular motion characteristics. Rigid-body guidance refers to the design task that seeks a machine with the capacity to place a link (or part) in a set of prescribed positions. An emerging research area in need of advancements in these guidance techniques is rigid-body, shape-change mechanisms.

This dissertation presents several synthesis and analysis methods that extend the established techniques for rigid-body guidance. Determining link lengths to achieve prescribed task positions is a classic problem. As the number of task positions increases, the solution space becomes very limited. Special arrangements of four and five task positions were discovered where the introduction of prismatic joints is achievable.

Once dimensions of link lengths are determined, solutions with defects must be eliminated. Defects include linkages that do not remain on the same assembly circuit, cross branch points where the mechanism cannot be driven, or achieve the task positions in the wrong order. To address the circuit defect, a general strategy was formulated that determines the number of assembly configurations that exist in a linkage and the sensitivity of the motion to a link length. To address the branch defect, extensible equations that generate a concise expression of the singularity conditions

of mechanisms containing a deformable closed loop was developed. To address the order defect, an intuitive method to ensure that rigid-bodies will reach design positions in the proper order has been developed. The result of the dissertation is a suite of methodologies useful in the synthesis and analysis of planar mechanisms to accomplish rigid-body guidance.

To Kim and our children: Jordan, Taylor, Payton and Riley

## ACKNOWLEDGMENTS

The writing of this dissertation was a tremendous undertaking and not possible without the personal and practical support of several people. To that point, my sincere gratitude goes to my family, my advisor and my committee members for their support and patience over the last few years.

First, I thank my advisor Dr. Andrew Murray, for his encouragement, guidance, and friendship. I am grateful that Drew took a very active approach throughout my research. He showed me how to strive for the underlying explanation for observations encountered in research work. He taught me different ways to approach a problem and the need to be persistent to accomplish an objective. I greatly admire his passion for kinematics, mathematical savvy and commitment to his students.

I also wish to express appreciation to Dr. James Schmeidler for his guidance and careful review of several concepts, theories and writings. His mastery of kinematic principles and foresight into possibilities is remarkable. I admire his knowledge, insightfulness and dedication to his profession.

Besides my advisors, I would like to thank the other members of my doctoral committee: Dr. Raúl Ordóñez and Dr. Reza Kashani who asked stimulating questions and offered useful input.

Finally, it would have been impossible to pursue my research goal without my family's love and support. This dissertation is dedicated to them.

## TABLE OF CONTENTS

	Page
ABSTRACT . . . . .	iii
DEDICATION . . . . .	v
ACKNOWLEDGMENTS . . . . .	vi
LIST OF FIGURES . . . . .	xi
LIST OF TABLES . . . . .	xvi
 CHAPTERS:	
I. INTRODUCTION . . . . .	1
1.1 Shape Changing, Rigid-Body Mechanisms . . . . .	2
1.2 General Synthesis Concepts . . . . .	4
1.2.1 Two-Position Guidance . . . . .	9
1.2.2 Three-Position Guidance . . . . .	10
1.2.3 Four-Position Guidance . . . . .	10
1.2.4 Five-Position Guidance . . . . .	11
1.2.5 Greater than Five-Position Guidance . . . . .	11
1.3 Solution Rectification . . . . .	11
1.3.1 Circuit Defects . . . . .	12
1.3.2 Branch Defects . . . . .	13
1.3.3 Order Defects . . . . .	14
1.4 Objectives . . . . .	15
1.5 Organization . . . . .	16
II. POSITION AND POLE ARRANGEMENTS THAT INTRODUCE PRISMATIC JOINTS INTO THE DESIGN SPACE OF FOUR AND FIVE POSITION RIGID-BODY SYN- THESIS . . . . .	19
2.1 Introduction . . . . .	19
2.2 Four Position Cases . . . . .	21



2.2.1	Poles, the Compatibility Linkage, and Center-point Curves . . . . .	21
2.2.2	Transition Linkage . . . . .	24
2.2.3	Opposite Pole Quadrilateral with $T_1 = T_2 = T_3 = 0$ : A Rhombus . . . .	25
2.2.4	Opposite Pole Quadrilateral with $T_1 = T_2 = 0$ : A Parallelogram . . . .	28
2.2.5	Opposite Pole Quadrilateral with $T_1 = T_3 = 0$ or $T_2 = T_3 = 0$ : A Kite .	31
2.2.6	Opposite Pole Quadrilateral with $T_1 = 0$ or $T_2 = 0$ or $T_3 = 0$ . . . . .	33
2.3	Synthesizing PR Dyads . . . . .	35
2.4	Synthesizing RP Dyads . . . . .	40
2.5	Three Position Case . . . . .	43
2.5.1	Collinear Poles . . . . .	44
2.5.2	Equilateral Triangle . . . . .	46
2.6	Five Position Cases . . . . .	46
2.6.1	Case 1: Movable Compatibility Platform . . . . .	47
2.6.2	Case 2: Alternate Configuration of the Movable Compatibility Platform .	48
2.7	Example 2.1 . . . . .	53
2.8	Summary . . . . .	53
III.	USING A SINGULARITY LOCUS TO EXHIBIT THE NUMBER OF GEOMETRIC INVERSIONS, TRANSITIONS, AND CIRCUITS OF A LINKAGE . . . . .	57
3.1	Introduction . . . . .	57
3.2	Loop Closure Equations . . . . .	60
3.2.1	Input/Output Function . . . . .	61
3.3	Singularity Function . . . . .	63
3.4	Projection of the Singularity Locus . . . . .	66
3.5	Circuits . . . . .	68
3.6	Transition Functions . . . . .	70
3.7	Motion Possibilities . . . . .	71
3.8	Examples . . . . .	75
3.8.1	Example 3.1: Slider-Crank Mechanism . . . . .	75
3.8.2	Example 3.2: Watt II Mechanism . . . . .	78
3.8.3	Example 3.3: Stephenson III Mechanism, Actuated through the Four-Bar Loop . . . . .	79
3.8.4	Example 3.4: Stephenson III Mechanism, Actuated through the Five-Bar Loop . . . . .	85
3.9	Summary . . . . .	87
IV.	SINGULARITY ANALYSIS OF AN EXTENSIBLE KINEMATIC ARCHITECTURE: ASSUR CLASS $N$ , ORDER $N - 1$ . . . . .	90
4.1	Introduction . . . . .	90

4.2	Assur Class Mechanisms . . . . .	91
4.3	Singularity Analysis of a Mechanism with Three Links in the Closed Contour . .	93
4.4	Singularity Analysis of a Mechanism with a Four-Link Deformable Closed Con- tour: Assur IV/3 . . . . .	96
4.5	Singularity Analysis of a Mechanism with a Five-Link Deformable Closed Con- tour: Assur V/4 . . . . .	100
4.6	Singularity Analysis of a Mechanism with an $N$ -Link Deformable Closed Con- tour: Assur $N/(N - 1)$ . . . . .	102
4.7	Singularity Equation of a Mechanism with a Six-Link Deformable Closed Con- tour: Assur VI/5 . . . . .	104
4.8	Singularity Equation of a Mechanism with a Seven-Link Deformable Closed Contour: Assur VII/6 . . . . .	105
4.9	Examples . . . . .	108
4.9.1	Example 4.1: Combination of physical and joint parameters resulting in a singularity . . . . .	108
4.9.2	Example 4.2: Singularity with adjacent parallel links . . . . .	109
4.9.3	Example 4.3: Singularity with isolated parallel links . . . . .	110
4.10	Summary . . . . .	112
V.	ASSESSING POSITION ORDER IN RIGID BODY GUIDANCE: AN INTUITIVE APPROACH TO FIXED PIVOT SELECTION . . . . .	114
5.1	Introduction . . . . .	114
5.2	Ordered Dyads . . . . .	115
5.3	Center-Point Theorem . . . . .	115
5.4	Necessary Pole Condition . . . . .	118
5.5	Sufficient Pole Condition . . . . .	120
5.6	Propeller Theorem . . . . .	121
5.7	Examples . . . . .	123
5.7.1	Example 5-1 . . . . .	124
5.7.2	Example 5-2 . . . . .	124
5.7.3	Example 5-3 . . . . .	128
5.7.4	Example 5-4 . . . . .	128
5.8	Summary . . . . .	130
VI.	CONCLUSIONS AND FUTURE WORK . . . . .	132
6.1	Contributions of the Dissertation . . . . .	132
6.2	Directions for Future Work . . . . .	134

## APPENDICES:

A.	SLIDER CRANKS AS COMPATIBILITY LINKAGES FOR PARAMETERIZING CENTER POINT CURVES . . . . .	136
A-1	Introduction . . . . .	136
A-2	Compatibility Linkage . . . . .	136
A-3	Algebraic form of Center-point Curves . . . . .	138
A-4	Alternative Compatibility Linkages . . . . .	141
A-5	Slider-Crank Compatibility Linkages . . . . .	143
A-6	Parameterizing the Center-point Curve with the Slider-Crank Linkage . . . . .	146
A-7	Curve Types and the Generating Slider-Crank . . . . .	148
A-7.1	Example A-1: Unicursal, Center-point Curve . . . . .	149
A-7.2	Example A-2: Bicursal, Center-point Curve . . . . .	149
A-7.3	Example A-3: Double-point, Center-point Curve . . . . .	150
A-7.4	Example A-4: Circle-degenerate, Center-point Curve . . . . .	152
A-7.5	Example A-5: Hyperbola-degenerate, Center-point Curve . . . . .	153
A-8	Summary . . . . .	155
	BIBLIOGRAPHY . . . . .	156

## LIST OF FIGURES

<u>Figure</u>	<u>Page</u>
1.1 Four segments are used to match the two design profiles. . . . .	3
1.2 Mechanism to guide shape change among a set of open curve, target profiles. . . .	5
1.3 Mechanism to guide shape change among an set of closed curve, target profiles. . .	6
1.4 Three target positions for a moving lamina. . . . .	6
1.5 Coordinate transformation. . . . .	7
1.6 RR dyad. . . . .	8
1.7 Singularity of a rigid-body, shape-changing mechanism that approximates open curves. . . . .	14
1.8 Additional singularity of a shape-changing mechanism approximating open curves, with actuation outside of the four-bar sub-linkage. . . . .	15
1.9 Singularity of a shape-changing mechanism that approximates closed curves. . . .	16
2.1 Five different center-point curve forms. . . . .	22
2.1 Five different center-point curve forms (con't). . . . .	23
2.2 Displacement pole. . . . .	23
2.3 The behavior of a 4R linkage is defined by $a$ , $b$ , $g$ , and $h$ . . . . .	25
2.4 Four positions that produce an opposite pole quadrilateral with sides of equal length.	28

2.4	Four positions that produce an opposite pole quadrilateral with sides of equal length (cont'). . . . .	29
2.5	Four positions that produce an opposite pole quadrilateral that with two pairs of equal side legs. . . . .	32
2.6	Four positions that produce an opposite pole quadrilateral with two pairs of equal side legs. . . . .	34
2.7	Four positions that produce an opposite pole quadrilateral with $T_1 = 0$ . . . . .	36
2.8	General PR dyad. . . . .	38
2.9	Opposite pole quadrilateral forming a rhombus. . . . .	40
2.10	A PR dyad can be oriented in any direction when the center-point curve is a hyperbola. . . . .	41
2.11	General RP dyad. . . . .	42
2.12	Opposite pole quadrilateral forming a parallelogram. . . . .	44
2.13	RP dyads are synthesized from arbitrary points on the center-point curve. . . . .	45
2.14	Compatibility structure for five position synthesis. . . . .	47
2.15	Five positions with a compatibility structure that has motion. . . . .	49
2.15	Five positions with a compatibility structure that has motion (con't). . . . .	50
2.16	Center-point curve for five task positions. . . . .	51
2.16	Center-point curve for five task positions (con't). . . . .	52
2.17	Pole locations that generate a center-point curve for five task positions. . . . .	52
2.18	Two fixed pivot locations exist for the five target positions of Table 2.2. . . . .	54
2.19	Shifted target positions to reorient the poles into a Case 2 compatibility platform. . . . .	55
2.20	An RRPR linkage to nearly achieve the five task positions. . . . .	56

3.1	Two degree-of-freedom, RRRPR linkage. . . . .	61
3.2	Input/output function (blue) of the RRRPR mechanism in Fig. 3.1 with $a_1 = 5$ , $a_2 = 3$ , and $a_3 = 4$ . The singularity function is also included (red). . . . .	63
3.3	Geometric inversions of the RRRPR mechanism in Fig. 3.1 with $a_1 = 5$ , $a_2 = 3$ , and $a_3 = 4$ plotted in reduced configuration space. . . . .	64
3.4	Input/output curve with a self-intersection. . . . .	66
3.5	Singularities of the RRRPR mechanism in Fig. 3.1 with $a_1 = 5$ , $a_2 = 3$ , and $a_3 = 4$ plotted in reduced configuration space. . . . .	67
3.6	Singularity locus for an RRRPR mechanism with $a_1 = 5$ , $a_2 = 3$ , and $a_3 = 4$ . . . .	68
3.7	Choice of output should represent all geometric inversions. . . . .	69
3.8	Singularity and circuit map for a five-bar mechanism with $a_1 = 5$ , $a_2 = 3$ , and $a_3 = 4$ . . . . .	70
3.9	2 circuits with 2 GIs and 4 singularities. . . . .	72
3.10	Slider-Crank Mechanism. . . . .	76
3.11	Design Map for a Slider-Crank Mechanism. . . . .	76
3.12	Watt II Mechanism. . . . .	79
3.13	Design Map for a Watt II Mechanism. . . . .	80
3.14	Stephenson III Mechanism. . . . .	81
3.15	Singularity locus for a Stephenson III mechanism with $\theta_4$ as input. . . . .	82
3.16	Transition configurations for Stephenson III of Fig. 3.14. . . . .	83
3.16	Transition configurations for Stephenson III of Fig. 3.14 (cont'd). . . . .	84
3.16	Transition configurations for Stephenson III of Fig. 3.14 (cont'd). . . . .	85

3.17	Singularity locus for a Stephenson III mechanism with $\theta_1$ as input. . . . .	86
3.18	Stephenson III greater than one revolution, non-crank. . . . .	88
3.19	Stephenson III greater than one revolution, non-crank. . . . .	89
4.1	AKC that becomes an Assur Mechanism by adopting the pivot shown in gray. . . .	92
4.2	Mechanism with three links in the closed-contour. . . . .	94
4.3	Assur IV/3 mechanism. . . . .	97
4.4	Assur V/4 mechanism. . . . .	101
4.5	Assur $N/(N - 1)$ mechanism. . . . .	103
4.6	Singularity discussed in Example 4.1. . . . .	109
4.7	Singularity discussed in Example 4.2. . . . .	111
4.8	Singularity discussed in Example 4.3. . . . .	112
5.1	The relationship between the fixed pivot of two positions, the pole and the crank angle. . . . .	116
5.2	An alternative relationship between the fixed pivot of two positions, the pole and the crank angle. . . . .	117
5.3	The relationship between the fixed pivot, the poles and three positions. . . . .	117
5.4	The angle between line $\overline{\mathbf{GP}_{ij}}$ and $\overline{\mathbf{GP}_{jk}}$ is $\beta_{ik}/2$ . . . . .	119
5.5	Equations 5.18 and 5.20 ensure the order of all $N$ positions. . . . .	122
5.6	The four-position application of the propeller method in Example 5-1, with the regions that satisfy the theorem crosshatched. . . . .	125
5.7	The special four-position application of the propeller method in Example 5-2. . . .	126
5.7	The special four-position application of the propeller method in Example 5-2 (con't). 127	

5.8	The five-position application of the propeller method from Example 5-3, with ordered regions crosshatched. . . . .	129
5.9	The five-position problem from Example 5-4, without any ordered regions. . . . .	130
A-1	Compatibility linkage used to generate a feasible center point. . . . .	137
A-2	Q Points are on the center-point curve. . . . .	138
A-3	Graphical construction of the principal focus. . . . .	139
A-4	Feasible center-point views opposite sides in equal, or supplementary, angles. . . . .	139
A-5	Compatibility linkage with alternate vertices. . . . .	143
A-6	Slider-crank compatibility linkage. . . . .	144
A-7	Slider-crank compatibility linkage from example A-1. . . . .	147
A-8	Center-point curve generated from a slider-crank compatibility linkage. . . . .	149
A-9	Slider-crank compatibility linkage from example A-2. . . . .	151
A-10	Slider-crank compatibility linkage from example A-3. . . . .	152
A-11	Slider-crank compatibility linkage from example A-4. . . . .	153
A-12	Alternate compatibility linkage from example A-5. . . . .	154
A-13	RPRP compatibility linkage from example 5. . . . .	155



## LIST OF TABLES

<u>Table</u>	<u>Page</u>
2.1 Summary of the four position distinctive cases. . . . .	37
2.2 Target Positions for Example. . . . .	53
3.1 One circuit motion possibilities. . . . .	72
3.2 Two circuit motion possibilities. . . . .	73
3.3 Three circuit motion possibilities. . . . .	74
3.3 Three circuit motion possibilities (con't). . . . .	75
3.4 Four circuit motion possibilities. . . . .	77
3.4 Four circuit motion possibilities (con't). . . . .	78
4.1 Mechanism parameters for Example 4.1, $\beta = 223^\circ$ and $f = 2.3865$ . . . . .	108
4.2 Mechanism parameters for Example 4.2, $\beta = 221^\circ$ . . . . .	110
4.3 Mechanism parameters for Example 4.3, $\beta = 194^\circ$ . . . . .	112

## **CHAPTER I**

### **INTRODUCTION**

Design engineers regularly desire a planar mechanism that places a body in several distinct and arbitrarily prescribed positions. Kinematic synthesis of such a linkage involves specifying an arrangement of links and determining their dimensions to achieve the desired motion. The category of linkage synthesis that places a link in prescribed positions is termed rigid-body guidance or motion generation.

Applications of linkages designed for rigid-body guidance are numerous. Pick-and-place mechanisms common to manufacturing and assembly processes involve two-position rigid-body guidance [1]. Such a mechanism is required to pick an object that is presented at some initial position and move the object to a final position. The initial and final positions become the targets for guidance. Intermediate positions can be inserted between the pick and place destinations to avoid obstacles [2].

Athletic training and rehabilitation equipment is designed to conform to trajectories of sports movements. Three precision points have been used to successfully synthesize a linkage to accurately follow selected body points during cyclic two-dimensional running motion [3]. The linkage was used in a mechanical device that correctly guides an athlete through proper running motions to improve performance. Three precision points have also been used to successfully synthesize a

vehicle suspension [4], to guide the bin for a tipper/dump truck [5], and to direct the forming tool in a mechanical forming press [6].

Four precision points were used to guide the bucket of a front loader [7]. The target positions were specified so that the bucket achieves a high reach and does not arc back toward the operator. Four positions were also used to synthesize an autoclave door linkage [7]. The positions ensure that the door is stored inside the unit when open, swings closed within the space limitations, and forms a tight seal against the frame.

Five precision points were used to synthesize a distinctive steering linkage [8]. The target positions were specified to ensure that the axis of each steerable wheel intersects on the axis of the non-steerable wheels. Five points were also used in the design of a chair foot-rest [9] and an assembly machine to insert electrical connectors into a telephone [7].

## **1.1 Shape Changing, Rigid-Body Mechanisms**

A novel application of rigid-body guidance synthesis is shape-changing mechanisms [10, 11]. Planar linkages, comprising a chain of rigid links connected with revolute joints, are designed to approximate a shape change defined by a set of “morphing” curves. A variety of applications exist for mechanical systems that change geometric shape in a controlled manner. Systems with such requirements include morphing airfoils [12], active aperture antennas [13] and deformable mirrors for optic systems [14]. Significant research has been undertaken in actuating shape-changing systems with smart materials technology [15, 16]. Rigid-body mechanisms have advantages such as higher load-carrying capabilities, the ability to attain higher displacements, and fewer required actuators. Along with the applications mentioned, military aircraft turrets, automotive spoilers, extrusion dies and kinetic artwork are also being explored.

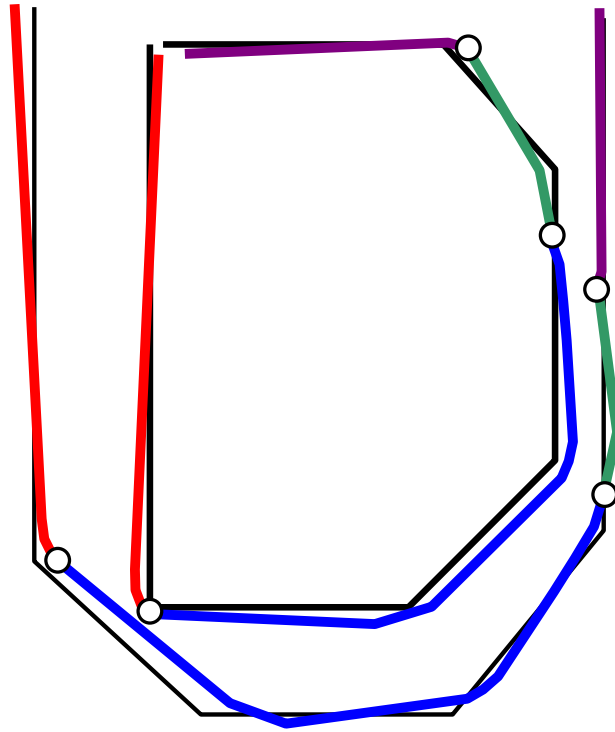


Figure 1.1: Four segments are used to match the two design profiles.

The synthesis process of rigid-body, shape-changing mechanisms begins by dividing the  $p$  target profiles into  $N$  rigid-body segments. The segments are optimized such that one edge satisfactorily matches the shape of the corresponding segments for all  $p$  profiles. An example of four rigid-link segments ( $N = 4$ ) matching two target profiles ( $p = 2$ ) is given in Fig. 1.1. A greater number of segments will improve the approximation to the design profiles. Yet, a balance is needed since more rigid-body segments produces a more complex mechanical system.

After segmentation, the mechanization stage defines the full shape of the rigid bodies and adds links to reduce the system's degrees of freedom (DOF). Multi-DOF mechanisms may provide a

better match to the target profiles. However, the reduced actuation requirements of a single-DOF linkage are usually preferred, but may come at a cost to accurately matching the profiles.

A shape-changing mechanism that guides rigid links between an open set of target profiles is shown in Fig. 1.2. The open chain of  $N$  rigid links is connected with  $N - 1$  revolute joints. These rigid links can be constrained with  $N + 1$  additional links to yield a single-DOF shape-changing mechanism. In the most common constraining case, of the  $N$  links forming the open contour, one is a quaternary link, while  $N - 1$  are ternary links. The other revolute joints on the quaternary and ternary links connect constraining dyads. The mechanism shown in Fig. 1.2 has four links ( $N = 4$ ) in the deformable open contour. The quaternary link and two constraining dyads forms a four-bar sub-linkage, which usually provides actuation. Single dyads constrain the other three ( $N - 1 = 3$ ) open-chain links. Placing the four-bar centrally and actuating the linkage through it will decrease the likelihood of reaching a singularity, which will be discussed later.

A shape-changing mechanism that guides rigid-links between a closed set of target profiles is shown in Fig. 1.3. The closed chain of  $N$  rigid links is connected with  $N$  revolute joints. These rigid links can be constrained with  $N - 1$  additional links to yield a single-DOF shape-changing mechanism. In this case, of the  $N$  links forming the closed contour, one remains a binary link, while  $N - 1$  are ternary links. The mechanism shown in Fig. 1.3 has five links ( $N = 5$ ) in the deformable closed contour. The other revolute joints on the ternary links connect four ( $N - 1 = 4$ ) constraining dyads.

## 1.2 General Synthesis Concepts

Prior to presenting the planar kinematic synthesis and analysis theories developed in this dissertation, general synthesis concepts are reviewed first. Figure 1.4 illustrates the path of a moving

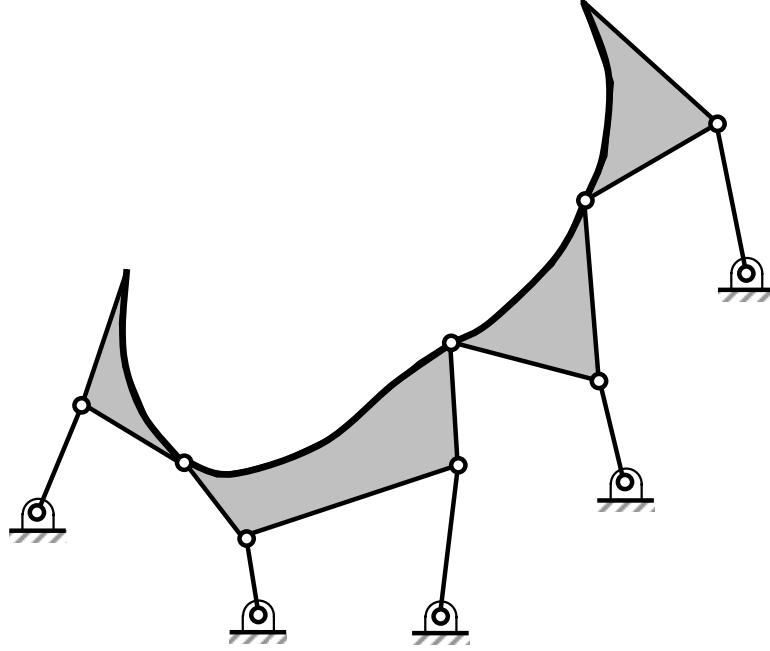


Figure 1.2: Mechanism to guide shape change among a set of open curve, target profiles.

lamina, highlighted in three task positions. The linkage resulting from the rigid-body guidance synthesis will guide a coupler as a whole through the task positions.

Since any object in a plane has three DOF, the location of one point and the orientation of one line segment fully describe the pose of the lamina. Each task position is described by a coordinate system  $M$  defined by a location vector  $\mathbf{d} = \{d_x \ d_y\}^T$  and an orientation angle  $\theta$ , both relative to a fixed frame  $F$ . Figure 1.5 shows an arbitrary moving coordinate frame  $M_i$ . The coordinates of a general point in  $F$  are  $\mathbf{X}_i = \{X_i \ Y_i\}^T$  and in  $M_i$  are  $\mathbf{x} = \{x \ y\}^T$  and are related through

$$\mathbf{X}_i = A_i \mathbf{x} + \mathbf{d}_i, \quad (1.1)$$

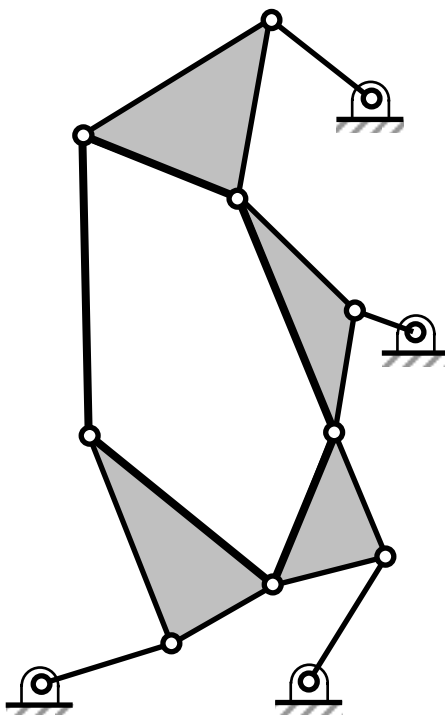


Figure 1.3: Mechanism to guide shape change among an set of closed curve, target profiles.

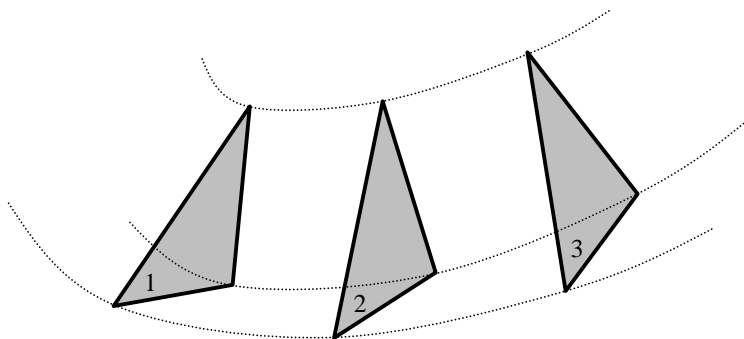


Figure 1.4: Three target positions for a moving lamina.

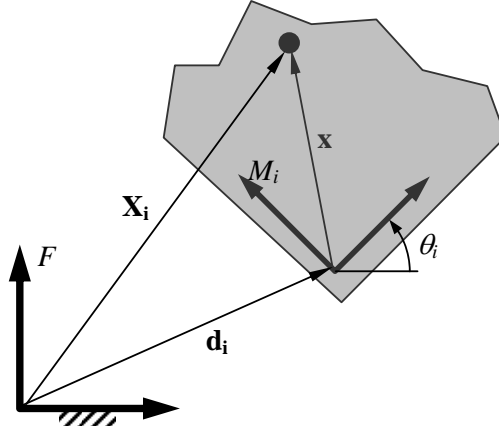


Figure 1.5: Coordinate transformation.

where

$$A_i = \begin{bmatrix} \cos \theta_i & -\sin \theta_i \\ \sin \theta_i & \cos \theta_i \end{bmatrix}. \quad (1.2)$$

Dimensional synthesis for rigid body guidance is a classical problem in linkage design. Well established methods have been developed to generate a revolute-revolute (RR) dyad to exactly reach as many as five arbitrary target positions [2, 7, 17, 18, 19, 20, 21, 22, 23]. Figure 1.6 illustrates an RR dyad in two positions.

The fixed pivot, also known as the center-point, is located in the fixed frame with  $\mathbf{G}$ . The link attached to the fixed pivot, also known as the crank, has a length  $l$  and is oriented with a crank angle  $\phi$ . A crank vector associated with target position  $i$  is

$$\mathbf{l}_i = l \{\cos \phi_i \quad \sin \phi_i\}^T. \quad (1.3)$$



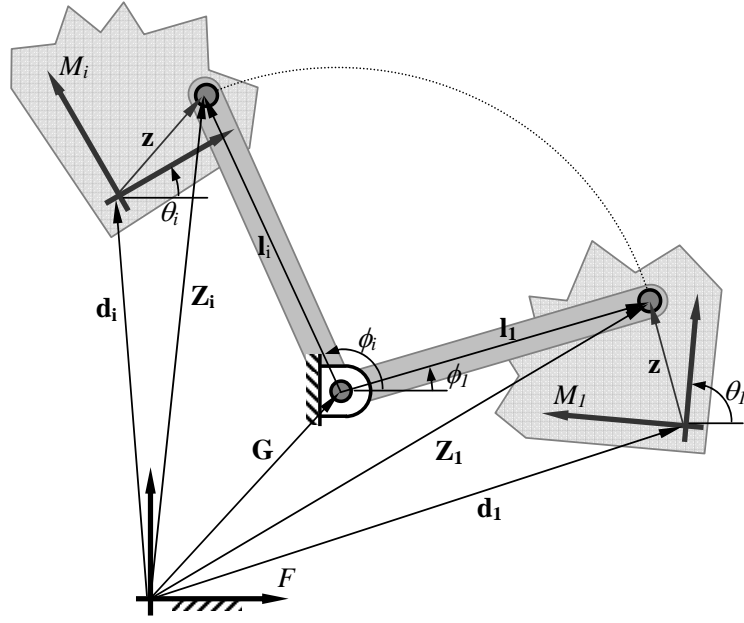


Figure 1.6: RR dyad.

The location of the moving pivot, also known as the circle-point, relative to the moving frame is  $\mathbf{z}$ . Using Eq. 1.1, the location of the moving pivot relative to the fixed frame is

$$\mathbf{Z}_i = A_i \mathbf{z} + \mathbf{d}_i. \quad (1.4)$$

Alternatively, the location of the moving pivot relative to the fixed frame as constrained by the crank is

$$\mathbf{Z}_i = \mathbf{G} + \mathbf{l}_i. \quad (1.5)$$

Dimensional synthesis of an RR dyad amounts to determining appropriate values of  $\mathbf{G}$  and  $\mathbf{z}$ . The fundamental synthesis equation ensures a constant crank length and is given by combining

Eqs. 1.4 and 1.5 and squaring, giving

$$\begin{aligned} l^2 &= (A_1 \mathbf{z} + \mathbf{d}_1 - \mathbf{G})^T (A_1 \mathbf{z} + \mathbf{d}_1 - \mathbf{G}) \\ &= (A_i \mathbf{z} + \mathbf{d}_i - \mathbf{G})^T (A_i \mathbf{z} + \mathbf{d}_i - \mathbf{G}). \end{aligned} \quad (1.6)$$

Equation 1.6 relates the required values of the target positions ( $\mathbf{d}_i$  and  $\theta_i$ ) to the synthesis values ( $\mathbf{G}$  and  $\mathbf{z}$ ).

A four-bar linkage is often the simplest mechanism capable of single-DOF rigid-body guidance and consequently, is widely used. Two RR dyads can be coupled to form a four-bar linkage that can be directly incorporated into a design. Additional RR dyads can be used to form multi-loop linkages that can open the design space for rigid-body guidance [24]. Planar four-bar synthesis methods are readily extended to include prismatic joints [25, 26].

### 1.2.1 Two-Position Guidance

With two target positions, Eq. 1.6 becomes

$$2\mathbf{G} \cdot (\mathbf{Z}_1 - \mathbf{Z}_2) + \mathbf{Z}_2^T \mathbf{Z}_2 - \mathbf{Z}_1^T \mathbf{Z}_1 = 0, \quad (1.7)$$

giving a single equation with four synthesis values. Thus, three synthesis values can be arbitrarily selected. Any point on the moving lamina can be chosen as the moving pivot, defining  $\mathbf{z}$ . Additionally, one component of the ground pivot vector  $\mathbf{G}$  can be arbitrarily selected. Equation 1.7 is used to determine the second vector component of  $\mathbf{G}$ . Alternatively, both components of  $\mathbf{G}$  and one of  $\mathbf{z}$  can be arbitrarily selected, solving for the second vector component of  $\mathbf{z}$ .

### 1.2.2 Three-Position Guidance

With three target positions, Eq. 1.6 becomes

$$\begin{bmatrix} 2(\mathbf{Z}_1 - \mathbf{Z}_2)^T \\ 2(\mathbf{Z}_1 - \mathbf{Z}_3)^T \end{bmatrix} \mathbf{G} + \begin{Bmatrix} \mathbf{Z}_2^T \mathbf{Z}_2 - \mathbf{Z}_1^T \mathbf{Z}_1 \\ \mathbf{Z}_3^T \mathbf{Z}_3 - \mathbf{Z}_1^T \mathbf{Z}_1 \end{Bmatrix} = 0, \quad (1.8)$$

giving two equations with four synthesis values. Thus, two synthesis values can be arbitrarily selected. Any point on the moving lamina can be chosen as the moving pivot, again defining  $\mathbf{z}$ . Equation 1.8 is used to determine the location of the corresponding center-point  $\mathbf{G}$ . Conversely, any center-point can be selected, and the corresponding moving pivot will be established.

### 1.2.3 Four-Position Guidance

With four target positions, Eq. 1.6 becomes

$$\begin{bmatrix} 2(\mathbf{Z}_1 - \mathbf{Z}_2)^T \\ 2(\mathbf{Z}_1 - \mathbf{Z}_3)^T \\ 2(\mathbf{Z}_1 - \mathbf{Z}_4)^T \end{bmatrix} \mathbf{G} + \begin{Bmatrix} \mathbf{Z}_2^T \mathbf{Z}_2 - \mathbf{Z}_1^T \mathbf{Z}_1 \\ \mathbf{Z}_3^T \mathbf{Z}_3 - \mathbf{Z}_1^T \mathbf{Z}_1 \\ \mathbf{Z}_4^T \mathbf{Z}_4 - \mathbf{Z}_1^T \mathbf{Z}_1 \end{Bmatrix} = 0, \quad (1.9)$$

giving three equations with four synthesis values. Thus, a single synthesis value can be arbitrarily selected. Suppressing  $\mathbf{G}$  in Eq. 1.9,

$$\det \begin{bmatrix} 2(\mathbf{Z}_1 - \mathbf{Z}_2)^T & \mathbf{Z}_2^T \mathbf{Z}_2 - \mathbf{Z}_1^T \mathbf{Z}_1 \\ 2(\mathbf{Z}_1 - \mathbf{Z}_3)^T & \mathbf{Z}_3^T \mathbf{Z}_3 - \mathbf{Z}_1^T \mathbf{Z}_1 \\ 2(\mathbf{Z}_1 - \mathbf{Z}_4)^T & \mathbf{Z}_4^T \mathbf{Z}_4 - \mathbf{Z}_1^T \mathbf{Z}_1 \end{bmatrix} = 0, \quad (1.10)$$

which generates a relationship in terms of  $z_x$  and  $z_y$ , called a circle-point curve. Thus, a moving pivot  $\mathbf{z}$  must be selected as a point on the circle-point curve. After selecting the moving pivot from the circle-point curve, any two equations from Eq. 1.9 can be used to determine the corresponding fixed pivot.

Alternatively, the four-position equation development can be written in terms of the moving reference frame to produce a relationship in terms of  $G_x$  and  $G_y$ , called a center-point curve. Thus, the fixed pivot  $\mathbf{G}$  must be selected as a point on a center-point curve. The center-point curve is the

locus of feasible fixed pivot locations for a planar 4R linkage that will guide the coupler through four finitely separated positions. The theory, originally formulated by Burmester [27], is described in numerous classic sources [17, 18, 20] and continues to be an essential element of more recent machine theory textbooks [2, 21, 22]. After selecting the fixed pivot on the center-point curve, the location of the corresponding moving pivot will be established.

#### **1.2.4 Five-Position Guidance**

With five target positions, Eq. 1.6 generates four equations in terms of the four synthesis values. The four equations are solved to produce sets of specific solution points. That is, up to four sets of circle-points and center-points may be used to create a dyad. The fixed pivot solution points are the intersection of all five center-point curves that are generated by taking each combination of four target positions. There are either 0, 2 or 4 intersection points [23].

#### **1.2.5 Greater than Five-Position Guidance**

Beyond five positions, numerical optimization techniques must be used to determine the linkage parameters that best fit the attainment of the task positions [28]. Least-squares [29] and kinematic mapping [30, 31, 32] have emerged as common techniques for performing dimensional synthesis of exact and approximate rigid-body guidance.

### **1.3 Solution Rectification**

Equation 1.6 can produce unacceptable solutions that suffer from any of three defects, as detailed by Chase and Mirth [33, 34]. With a circuit defect, the linkage must be disconnected and reassembled to achieve all positions. This defective solution is associated with linkage configurations that lie on two distinct coupler curves. With a branch defect, a single crank cannot be actuated

to move the linkage through all positions. This defective solution occurs when the crank orients the linkage into a stationary, or toggle, orientation between the given positions. An order defect occurs when the coupler moves through the target positions in the wrong order as the crank is driven in a uniform direction. While the branch and circuit defects are associated with an entire mechanism, the order defect is related solely on the selection of a driving dyad.

Solution rectification refers to the elimination of defects from a mechanism synthesis result. Balli and Chand [35] provide a comprehensive overview of linkage defects and solution rectification beginning with Filemon's [36] pioneering graphical process for the four-position synthesis of a crank-rocker. That process involves constructing a dyad for numerous points along the center-point curve and plotting the resulting dyad angles and crank lengths as a function of the arc length along the center-point curve. From this plot, one can identify fixed pivots for the crank and rocker that are more likely to provide a defect-free linkage. This procedure, however, does not guarantee success.

### **1.3.1 Circuit Defects**

Chase and Mirth [33] defined a circuit of a mechanism as the set of all possible orientations of links that can be realized without disconnecting any of the joints. Foster and Cipra [37, 38] use the term assembly configuration to refer to a circuit. If a mechanism must be disassembled to move from one position to another, the two positions reside on separate circuits. The circuits of a mechanism are independent of the choice of driving link(s) [33]. Established methods to identify different circuits rely on geometric insights of a particular mechanism [37, 38, 34, 24, 39].

### 1.3.2 Branch Defects

During the operation of a mechanism, a configuration can arise in which the input link is no longer able to move the mechanism. The mechanism becomes stationary, and the mechanical advantage reduces to zero [40]. This stationary position of a mechanism is termed a singular configuration or toggle position and must be avoided when attempting to operate the mechanism with a single input crank. Mathematically, a singular configuration occurs when the matrix that relates the input speeds to the output speeds becomes rank deficient, as discussed by Gosselin and Angeles [41]. Singularity analysis of a particular mechanism is the study of the conditions that lead to the stationary configuration.

#### Singularities in Shape-Change Mechanisms

Singularities in shape-changing mechanisms that approximate open curves are associated with geometric relationships. When the linkage is actuated with a dyad in the four-bar sub-linkage, a singularity will exist if the coupler and a dyad become collinear as shown in Fig. 1.7. When the linkage is actuated with a dyad that is not in the four-bar sub-linkage, a singularity will exist [42] if

1. The coupler and a pivoted link become collinear.
2. The lines through the coupler attached to the actuated link and two other pivoted links meet at a common point as shown in Fig. 1.8.

As stated earlier, actuating through the four-bar sub-linkage is given preference. This is because of the fewer geometric considerations to avoid encountering a singularity.

Singularities in shape-changing mechanisms that approximate closed curves are more difficult to avoid. The linkage shown in Fig. 1.9 is in a singularity position. It is noted that no two links are

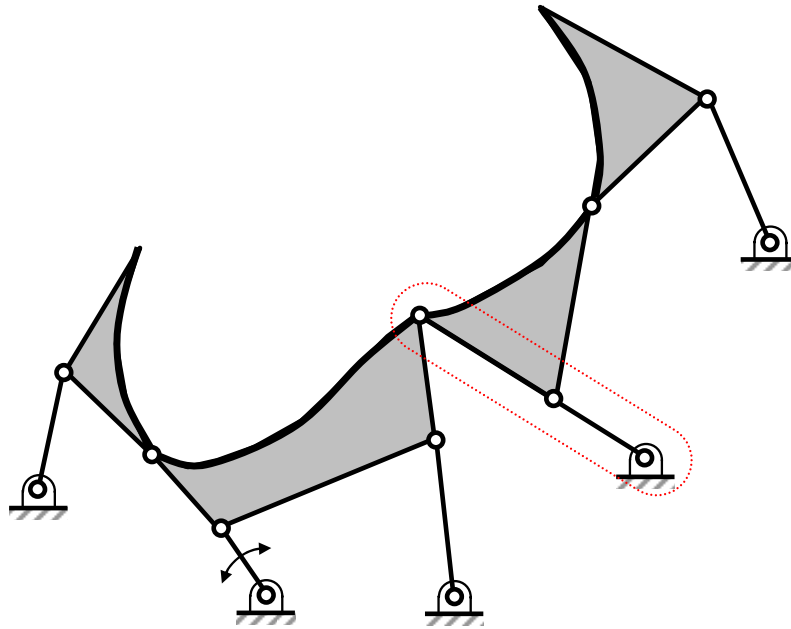


Figure 1.7: Singularity of a rigid-body, shape-changing mechanism that approximates open curves.

parallel. Further, lines are extended through each link to illustrate that three lines do not intersect at a point.

### 1.3.3 Order Defects

The order defect occurs when the coupler moves through the task positions in the wrong order as the input link is driven in a uniform direction. While an individual dyad cannot suffer from branch and circuit defects, it can have an order defect, which is relevant only if it is the driving dyad since the driven dyad that completes the four-bar linkage need not exhibit order. Of the three defects, only order can be assessed by examining the potential driving dyad, and thus, only order can be addressed during, and even prior to, synthesizing a single dyad. Waldron [43, 44, 45] addressed the order problem by mapping permissible segments of the circle-point curve that, when synthesized,

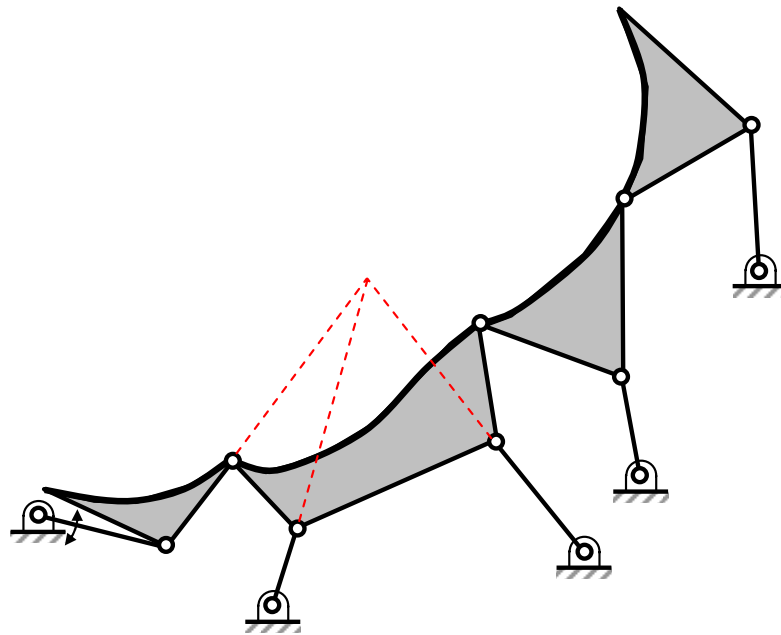


Figure 1.8: Additional singularity of a shape-changing mechanism approximating open curves, with actuation outside of the four-bar sub-linkage.

obtain dyads that achieve the design positions in order. Prentis [46] presented a process to delineate areas in a four-position problem within which the center-point curve must lie based on how the potential crank center views the displacement poles. Further, he identified regions where a crank center would generate ordered solutions.

## 1.4 Objectives

The objectives of this dissertation study are: 1) exploring the design space of rigid-body guidance and identifying conditions that introduce prismatic joints, 2) provide a general methodology



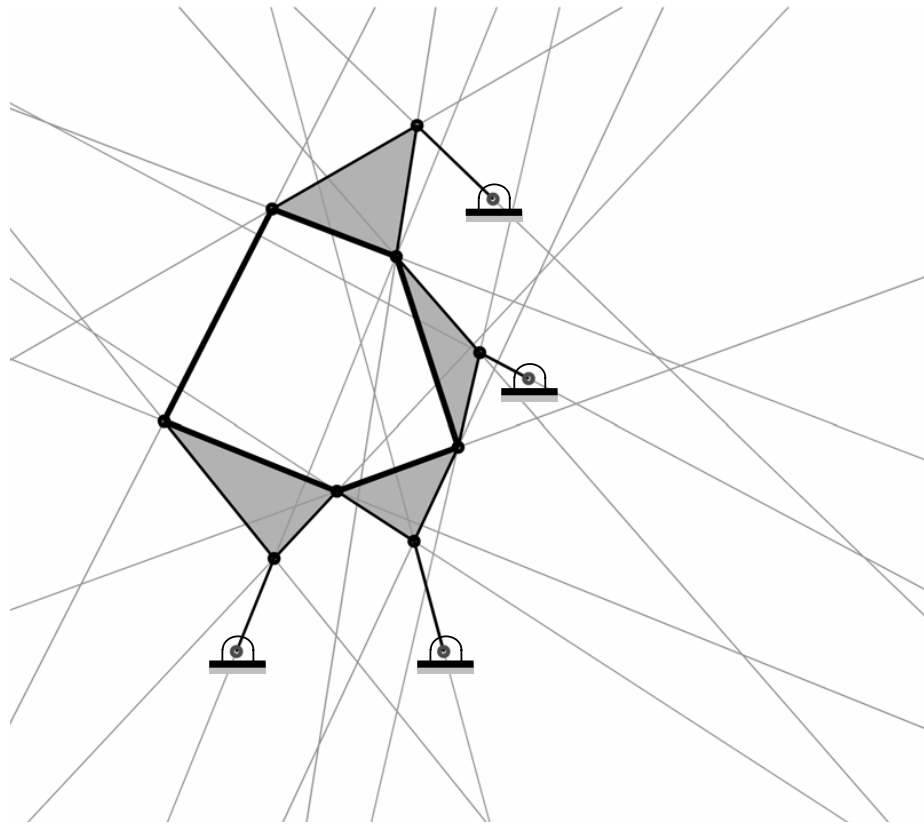


Figure 1.9: Singularity of a shape-changing mechanism that approximates closed curves.

to understand and analyze the assembly circuits of a given linkage, 3) detect singularities of linkages that approximate closed curves, and 4) produce a method to ensure that the task positions are achieved in proper order.

## 1.5 Organization

Chapter 2 focuses on synthesis options for rigid-body guidance. The chapter provides a thorough discussion of center-point curves. The curve is a circular cubic that can take one of five different forms. The center-point curve can be generated with a compatibility linkage obtained

from an opposite pole quadrilateral of the four design positions. This chapter identifies four- and five-position pole configurations for which the associated center-point curve(s) includes the line at infinity. With a center-point line at infinity, a PR dyad with line of sliding in any direction can be synthesized to achieve the design positions. Further, four- and five-position pole configurations are identified for which the associated circle-point curve(s) includes the line at infinity. With a circle-point that includes a line at infinity, an RP dyad originating anywhere on a center-point curve can be synthesized to achieve the design positions. If the rigid-body guidance problem is approximate, small changes to the positions may result in the introduction of a one-parameter family of dyads including a prismatic joint.

Chapter 3 focuses on gaining insight to assembly circuits. This chapter extends the established methods for analyzing multi-DOF platforms to gain insight into single-actuated linkages. A singularity locus is projected onto the input joint space. From this plot, the number of singularities, geometric inversions, and circuit regimes are revealed. The input/output motion of the linkage can be inferred from the locus. The methodology to produce the singularity locus is general and does not rely on geometric insights of a particular mechanism. By using the locus, desired operational features can be readily identified, such as a fully rotatable crank. Unique motion characteristics, such as a greater than  $360^\circ$  non-rotatable crank, can be also be detected. Further, it is observed that transition linkages serve as bounds between the regions of circuit change. The method is illustrated with several linkages, including the Stephenson III which serves as a foundation of shape-changing mechanisms that approximate open curves.

Chapter 4 focuses on detecting branch points. The chapter presents an analysis to create a general singularity condition for an Assur mechanism that contains a deformable closed contour. This kinematic architecture is used in rigid-link, shape-changing mechanisms that approximate closed

curves. The analysis is repeated for alternative input links. The general singularity equations are reduced to a condensed form, which allows geometric relationships to be readily detected. A method for formulating the singularity condition for an Assur Class  $N$  mechanism, knowing the condition for a Class  $N - 1$ , is given. This approach is illustrated with several examples.

Chapter 5 focuses on eliminating an order defect. The chapter extends the work of Prentis and presents an organized and concise method to detect whether a single dyad will achieve the task positions in order. The method can be used to assess the suitability of a candidate fixed pivot location by determining whether an ordered dyad will be generated. This evaluation can be performed prior to the actual process of dimensional synthesis. The benefit of this assessment process is that linkage designers can limit the work of dimensional synthesis to evaluating only viable fixed pivot locations. The method is illustrated with several examples

Chapter 6 summarizes the contributions of this dissertation. Suggestions for future work are also included.

The Appendix includes a study of compatibility linkages and parameterization of the center-point curve. While not directly related to synthesis to rigid-body guidance mechanisms, this study is an extension of Chapter 2 and resulted in a new finding. It is widely known that the center-point curve can be parameterized by a 4R compatibility linkage. In this study, a slider crank is presented as a suitable compatibility linkage to generate the center-point curve. Further, the center-point curve can be parametrized by the crank angle of a slider crank linkage. It is observed that the center-point curve is dependent on the classification of the slider crank. Lastly, a direct method to calculate the principal focus of the center-point curve is revealed.

## CHAPTER II

### POSITION AND POLE ARRANGEMENTS THAT INTRODUCE PRISMATIC JOINTS INTO THE DESIGN SPACE OF FOUR AND FIVE POSITION RIGID-BODY SYNTHESIS

#### 2.1 Introduction

A center-point curve is the locus of feasible fixed pivot locations for a planar linkage that will guide the coupler through four finitely separated positions. To guide a coupler through five positions, the fixed pivot is limited to the intersections of the five center-point curves generated by taking all five combinations of four positions [23].

The equation of the center-point curve is

$$(C_1x + C_2y)(x^2 + y^2) + C_3x^2 + C_4y^2 + C_5xy + C_6x + C_7y + C_8 = 0, \quad (2.1)$$

which is classified as a circular cubic. Keller [47] shows that the constants  $C_i$  are not independent but functions of the coordinates of an opposite pole quadrilateral, which is formally defined in the next section. Thus, the opposite pole quadrilateral dictates the shape of the center-point curve.

Sandor and Erdman [7] present an algebraic formulation for the center-point curve that is similar in form to a closure equation for a four-bar linkage. Further, they introduce the concept of a “compatibility linkage” as a conceptual linkage whose solution for various crank orientations will generate points on the center-point curve. They show that the curve can be parameterized based on

the conceptual crank angle of the compatibility linkage. McCarthy [48] shows that the opposite pole quadrilateral serves as a compatibility linkage and uses its crank angle to parameterize the center-point curve. Murray and McCarthy [49] state that there is a two dimensional set of quadrilaterals that can generate a given center-point curve. Within this dissertation, a slider-crank linkage was found to be a suitable compatibility linkage. The development and justification is included in the Appendix.

Barker [50] classified four-bar mechanisms based on the permissible motions. Schaaf and Lammers [51] applied Barker's classifications to compatibility linkages to distinguish the geometric forms of the associated center-point curves. Beyer [18] illustrates five possible geometric forms of the center-point curve. Chase et al. [52] observe that the form of the center-point curve is dependent on the motion type of the compatibility linkage. They show that a Grashof compatibility linkage (one in which at least one link can make a full revolution) generates a disjointed (bicursal) center-point curve, as shown in Fig. 2.1a. A non-Grashof compatibility linkage (one in which no link is able to make a full revolution) generates a continuous (unicursal) center-point curve, as shown in Fig. 2.1b. Schaaf and Lammers [51] expand the work of Chase et al. and note that a change-point linkage (transition between Grashof and non-Grashof) will generate three less common forms. A double-point form is the transition between a unicursal and bicursal curve where the branches are joined at a self-intersection, as shown in Fig. 2.1c. When the compatibility linkage is a change-point linkage and all sides are unequal, a double-point center-point curve will be generated. The circle-degenerate form consists of a circle intersected by a straight line. The hyperbolic-degenerate form is an equilateral hyperbola and a line at infinity. A change-point linkage that has two equal pairs or all equal lengths will generate either a circular-degenerate or a hyperbolic-degenerate center-point curve. This chapter shows that if the configuration of the compatibility linkage is open (does not

overlap itself), a hyperbolic-degenerate curve will result, as shown in Fig. 2.1e. If the compatibility linkage is crossed, a circular-degenerate curve will result, as shown in Fig. 2.1d.

The study presented in this chapter identifies position and pole arrangements that introduce a one parameter family of solutions to rigid-body guidance. Specifically, pole arrangements for four and five position cases are identified that have a center point at infinity, allowing a PR dyad that achieves the task positions to be synthesized in any sliding direction. Additionally, pole arrangements for four- and five-position cases that have a circle point at infinity allow an RP dyad to be selected from anywhere along a center-point curve to achieve the task positions. With the aforementioned restrictions on four- and five-position guidance, adjusting the positions such that the poles are configured into the special orientations will include additional possibilities for prismatic joints.

## 2.2 Four Position Cases

### 2.2.1 Poles, the Compatibility Linkage, and Center-point Curves

Any displacement of a rigid body from position  $j$  to position  $k$ , and vice versa, can be accomplished by a pure rotation about the displacement pole  $\mathbf{P}_{jk} = \mathbf{P}_{kj}$ , as shown in Fig. 2.2. The displacement pole is calculated as

$$\begin{aligned}\mathbf{P}_{jk} &= A_j[A_j - A_k](\mathbf{d}_k - \mathbf{d}_j) + \mathbf{d}_j \\ &= A_k[A_j - A_k](\mathbf{d}_k - \mathbf{d}_j) + \mathbf{d}_k,\end{aligned}\tag{2.2}$$

where  $\mathbf{d}_j$  is the vector locating task position  $j$  and  $A_j$  is the rotation matrix associated with its orientation  $\theta_j$ .

Given four specified positions, six displacement poles exist ( $\mathbf{P}_{12}, \mathbf{P}_{13}, \mathbf{P}_{14}, \mathbf{P}_{23}, \mathbf{P}_{24}$  and  $\mathbf{P}_{34}$ ).

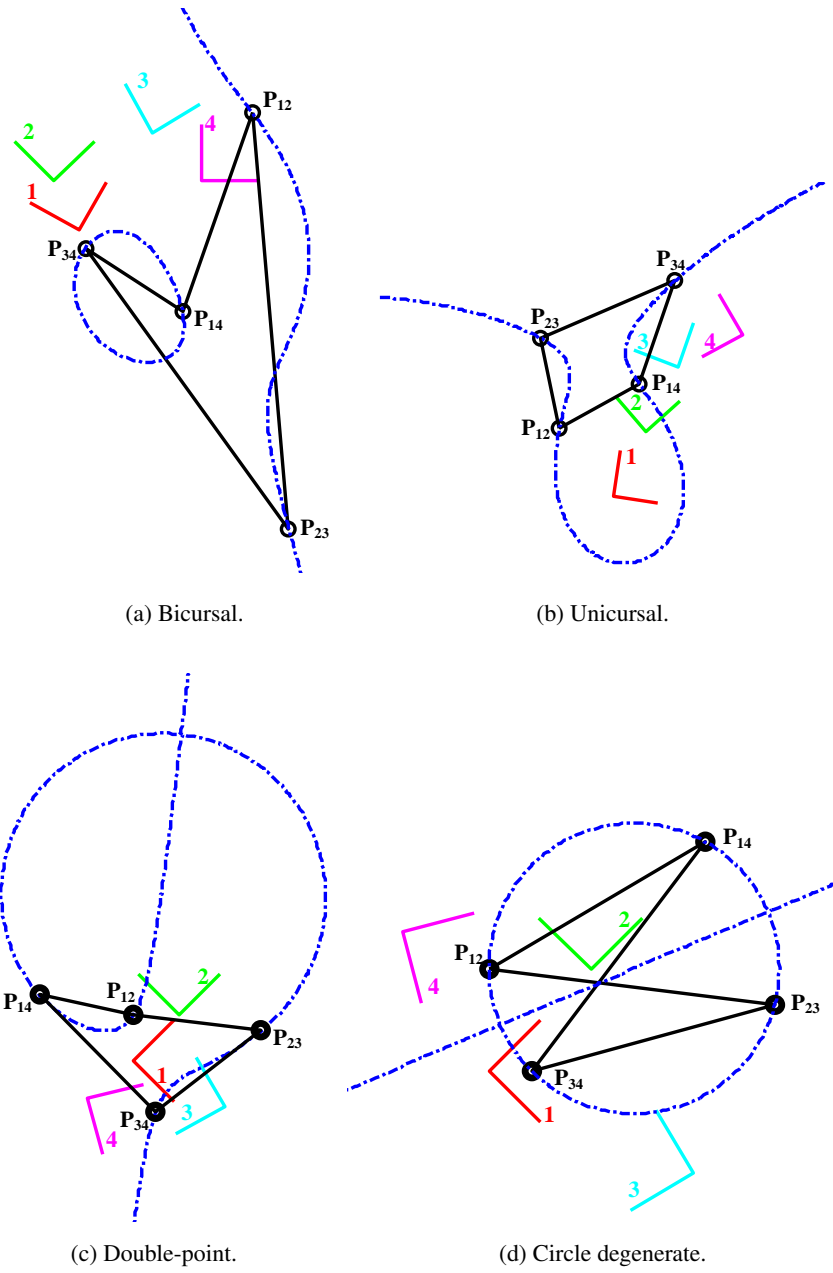
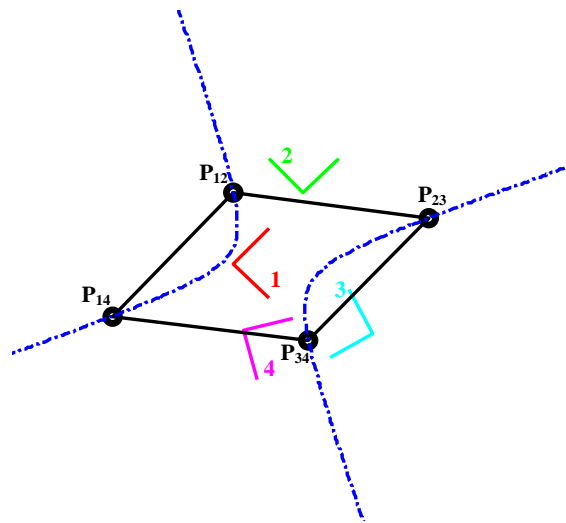


Figure 2.1: Five different center-point curve forms.



(e) Hyperbola degenerate.

Figure 2.1: Five different center-point curve forms (con't).

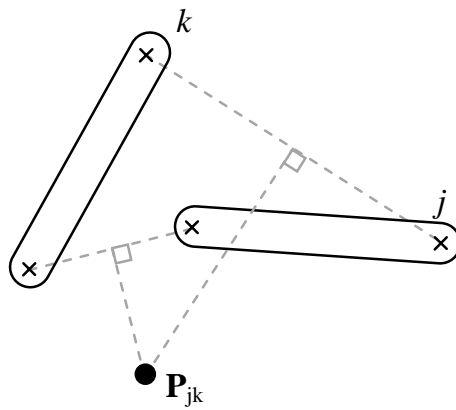


Figure 2.2: Displacement pole.



An opposite pole quadrilateral is defined by four poles such that the poles along the diagonal do not share an index. For the four-position case, three different opposite pole quadrilaterals can be formed with vertices:  $\mathbf{P}_{12}\mathbf{P}_{23}\mathbf{P}_{34}\mathbf{P}_{14}$ ,  $\mathbf{P}_{12}\mathbf{P}_{24}\mathbf{P}_{34}\mathbf{P}_{13}$ , and  $\mathbf{P}_{13}\mathbf{P}_{23}\mathbf{P}_{34}\mathbf{P}_{14}$ . It has been observed that as a distinctive shape is formed with one opposite pole quadrilateral, the others form that same shape. The development presented in the remaining sections of the chapter focuses on the quadrilateral formed from the poles  $\mathbf{P}_{12}\mathbf{P}_{23}\mathbf{P}_{34}\mathbf{P}_{14}$ .

A technique will be presented that uses three task positions to determine a fourth task position that forms various shapes of the opposite pole quadrilateral. A characteristic length is defined by the poles that are fully specified by the three positions as

$$L = |\mathbf{P}_{12} - \mathbf{P}_{23}|. \quad (2.3)$$

### 2.2.2 Transition Linkage

A transition linkage, as described by Murray et al. [53], has a configuration where the non-square matrix defined by the derivative of the loop closure equations with respect to the joint variables loses rank. A transition linkage is independent of the choice of input and output joints and can be identified based on the physical parameters of the linkage. Transition functions outline relationships among the physical parameters such that there exists a configuration where the non-square matrix loses rank. Thus, any linkage where one of the transition functions evaluates to zero is a transition linkage.

Applied to a planar 4R linkage, as shown in Fig. 2.3, the transition linkage identifies bounds between motion types. As stated, Chase et al. [52] observe that the shape of the center-point curve is dependent on the motion type of the compatibility linkage.

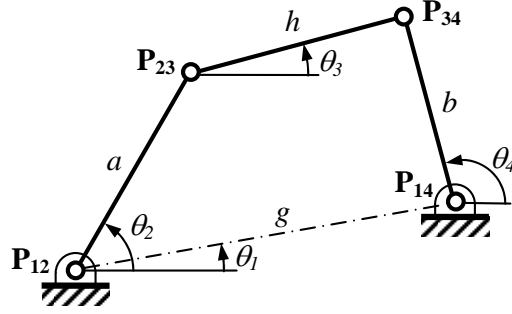


Figure 2.3: The behavior of a 4R linkage is defined by  $a$ ,  $b$ ,  $g$ , and  $h$ .

Barker [50] refers to the transition between Grashof and non-Grashof 4R linkages as change-point and categorizes them based the shortest link. The transition function approach more distinctly classifies the different types of change-point linkages. McCarthy [23] refers to the transition as folding linkages and presents the three transition functions to categorize them:

$$T_1 = a + h - g - b, \quad (2.4)$$

$$T_2 = a - h + g - b, \quad (2.5)$$

$$T_3 = a - h - g + b. \quad (2.6)$$

### 2.2.3 Opposite Pole Quadrilateral with $T_1 = T_2 = T_3 = 0$ : A Rhombus

A compatibility linkage having all sides of equal length is described by

$$L^2 = |\mathbf{P}_{23} - \mathbf{P}_{34}|^2 = |\mathbf{P}_{14} - \mathbf{P}_{12}|^2 = |\mathbf{P}_{14} - \mathbf{P}_{34}|^2. \quad (2.7)$$

Barker [50] identified a linkage having all sides of equal length as a class 6, change-point linkage.

A shape having all sides with equal lengths and parallel opposite sides is a rhombus. Equation 2.7

can also represent a folded rhombus, where two poles are coincident. A set of poles that conform to Eq. 2.7 is the most constrained case of the change point compatibility linkages. Identifying positions that create this distinctive shape of the opposite pole quadrilateral is completed by fully specifying three positions and solving for the location and orientation of the fourth position. The three relations of Eq. 2.7 expand into three constraining functions

$$f_1 = [(\mathbf{P}_{23x} - \mathbf{P}_{34x})^2 + (\mathbf{P}_{23y} - \mathbf{P}_{34y})^2] - L^2 = 0, \quad (2.8)$$

$$f_2 = [(\mathbf{P}_{12x} - \mathbf{P}_{14x})^2 + (\mathbf{P}_{12y} - \mathbf{P}_{14y})^2] - L^2 = 0, \quad (2.9)$$

$$f_3 = [(\mathbf{P}_{14x} - \mathbf{P}_{34x})^2 + (\mathbf{P}_{14y} - \mathbf{P}_{34y})^2] - L^2 = 0. \quad (2.10)$$

As each pole is a function of the positions, Eq. 2.2 substituted into Eqs. 2.8, 2.9 and 2.10 gives

$$f_i = B_i(d_{4x}^2 + d_{4y}^2) + C_i d_{4x} + D_i d_{4y} + E_i = 0, \quad (2.11)$$

where  $B_i, C_i, D_i$  and  $E_i$  are functions of  $\theta_4$  for  $i = 1, 2, 3$ . For a solution to Eqs. 2.11 to exist,

$$\det \begin{bmatrix} B_1 & C_1 & E_1 \\ B_2 & C_2 & E_2 \\ B_3 & C_3 & E_3 \end{bmatrix} = \det \begin{bmatrix} C_1 & D_1 & E_1 \\ C_2 & D_2 & E_2 \\ C_3 & D_3 & E_3 \end{bmatrix} = \det \begin{bmatrix} B_1 & D_1 & E_1 \\ B_2 & D_2 & E_2 \\ B_3 & D_3 & E_3 \end{bmatrix} \equiv 0. \quad (2.12)$$

Evaluating any of the determinants will obtain a single function of  $\theta_4$  of the form

$$K [a \sin(\theta_4) + b \cos(\theta_4) + c \sin(2\theta_4) + d \cos(2\theta_4) + e \sin(3\theta_4) + f \cos(3\theta_4)] = 0, \quad (2.13)$$

where  $K$  is a constant. Equation 2.13 generates three solutions for  $\theta_4$ .

To solve for the corresponding location of the fourth task position, Eqs. 2.11 with  $i = 1, 2$  are combined to eliminate the squared terms, giving

$$\begin{aligned} f_4 &= f_1 - (B_1/B_2)f_2 \\ &= (C_1 - C_2 B_1/B_2)d_{4x} + (D_1 - D_2 B_1/B_2)d_{4y} + (E_1 - E_2 B_1/B_2) \\ &= C_4 d_{4x} + D_4 d_{4y} + E_4 = 0. \end{aligned} \quad (2.14)$$

Rewriting Eq. 2.14 gives

$$d_y = (-C_4 d_{4x} - E_4)/D_4. \quad (2.15)$$

Substituting Eq. 2.15 into Eq. 2.11 with  $i = 3$  gives

$$\begin{aligned} f_3 = B_3 d_{4x}^2 + B_3 [(-D_4 d_{4x} - E_4)/E_4]^2 + C_3 d_{4x} \\ + D_3 [(-D_4 d_{4x} - E_4)/E_4] + F_3 = 0. \end{aligned} \quad (2.16)$$

Equation 2.16 produces two solutions of  $d_{4x}$  for each of the three values of  $\theta_4$ . Each value of  $d_{4x}$  can be substituted into Eq. 2.15 to obtain the corresponding  $d_{4y}$ . In all, six solutions for position 4 will generate an opposite pole quadrilateral with equal length sides. This will represent both an open and folded rhombus. Schaaf and Lammers [51] identify that the center-point curves for a class 6, change-point compatibility linkage will appear as hyperbolic-degenerate or circle-degenerate.

As an example, three positions are given as  $\mathbf{d}_1 = (0, 0)^T$ ,  $\theta_1 = -45^\circ$ ,  $\mathbf{d}_2 = (1, 1)^T$ ,  $\theta_2 = 45^\circ$ ,  $\mathbf{d}_3 = (2, -1)^T$ ,  $\theta_3 = 120^\circ$ . Solutions according to the procedure outlined above, along with the opposite pole quadrilateral and center-point curve, are shown in Fig. 2.4. Values for the fourth position include  $\mathbf{d}_4 = (2.7071, -2.2247)^T$  and  $\theta_4 = 30.0^\circ$  (shown in Fig. 2.4a),  $\mathbf{d}_4 = (-2.000, -1.000)^T$  and  $\theta_4 = 30.0^\circ$  (shown in Fig. 2.4b),  $\mathbf{d}_4 = (0.7753, -2.2247)^T$  and  $\theta_4 = -120.0^\circ$  (shown in Fig. 2.4c),  $\mathbf{d}_4 = (0.7321, 3.7321)^T$  and  $\theta_4 = -120.0^\circ$  (shown in Fig. 2.4d),  $\mathbf{d}_4 = (2.8993, 3.5280)^T$  and  $\theta_4 = -150.0^\circ$  (shown in Fig. 2.4e),  $\mathbf{d}_4 = (1.3032, -2.6065)^T$  and  $\theta_4 = -150.0^\circ$  (shown in Fig. 2.4f). Notice that the folded rhombi are associated with a circle-degenerate form of the center-point curve. The center-point curves for all open rhombuses appear as intersecting lines, which is a limiting case of the hyperbolic-degenerate form. This observation has been observed for all situations explored.

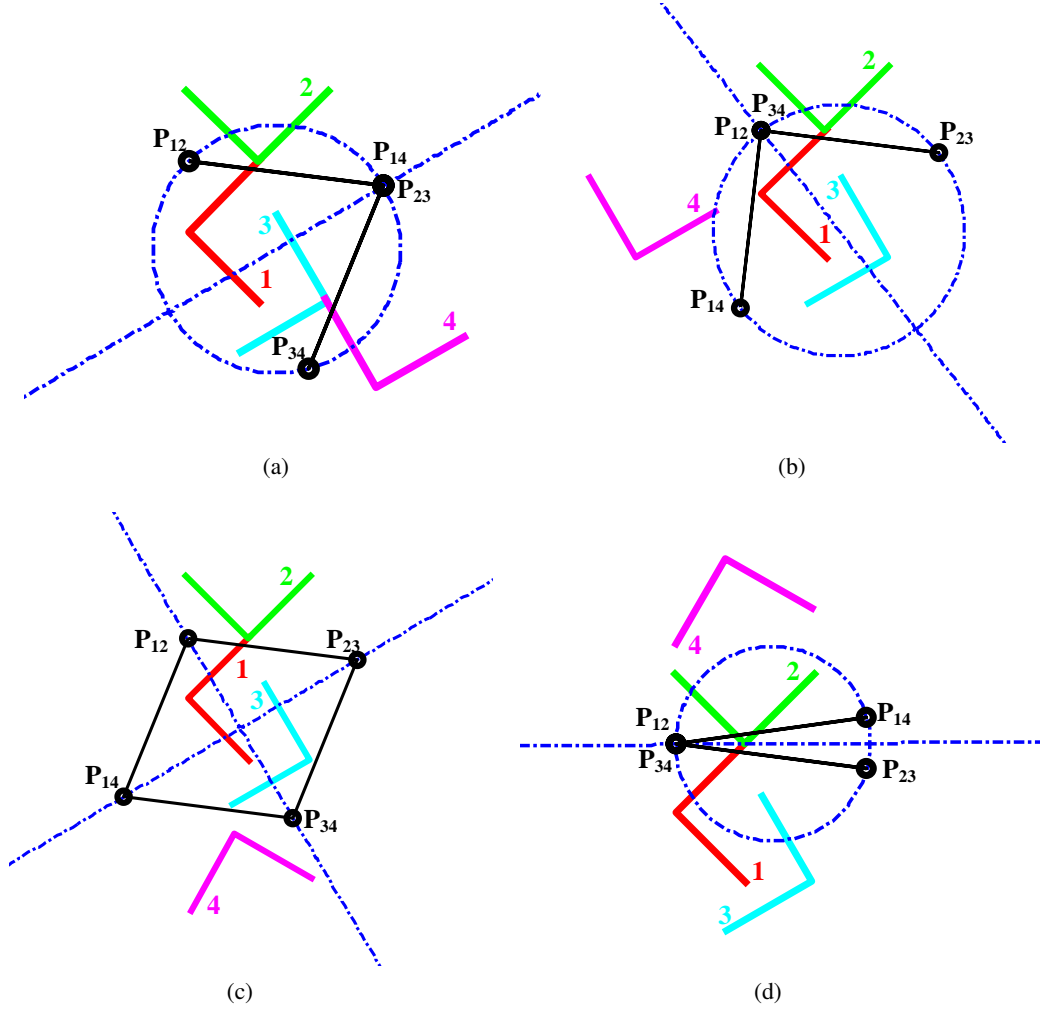


Figure 2.4: Four positions that produce an opposite pole quadrilateral with sides of equal length.

#### 2.2.4 Opposite Pole Quadrilateral with $T_1 = T_2 = 0$ : A Parallelogram

A parallelogram, where the two sets of opposite sides have the same length, is described as

$$|\mathbf{P}_{14} - \mathbf{P}_{34}|^2 = L^2, \quad (2.17)$$

$$|\mathbf{P}_{12} - \mathbf{P}_{14}|^2 = |\mathbf{P}_{23} - \mathbf{P}_{34}|^2.$$

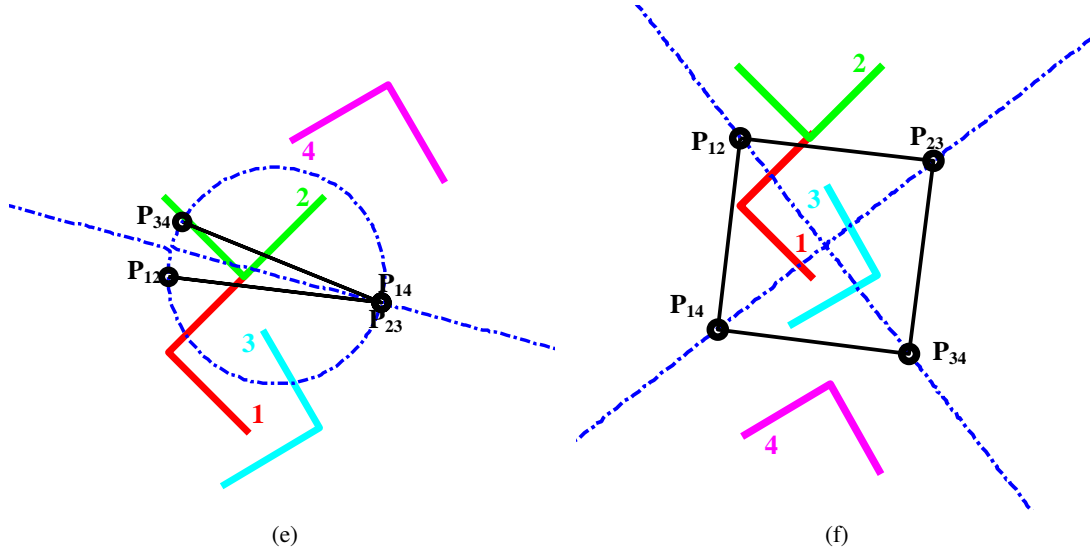


Figure 2.4: Four positions that produce an opposite pole quadrilateral with sides of equal length (cont').

Barker [50] identified a linkage having two sets of opposite sides with the same length as a class 5 change-point linkage. A shape having two pairs of opposite sides that are parallel and the same length is a parallelogram. Equation 2.17 can also represent a crossed parallelogram, where two sets of equal length sides are not parallel. Identifying positions that create these distinctive shapes of the opposite pole quadrilateral is completed by fully specifying three positions and the orientation of the fourth position, then solving for the location of the fourth position. The two relations of Eq. 2.17 expand into two constraining functions

$$f_1 = [(\mathbf{P}_{14x} - \mathbf{P}_{34x})^2 + (\mathbf{P}_{14y} - \mathbf{P}_{34y})^2] - L^2 = 0, \quad (2.18)$$

$$f_2 = [(\mathbf{P}_{12x} - \mathbf{P}_{14x})^2 + (\mathbf{P}_{12y} - \mathbf{P}_{14y})^2] - [(\mathbf{P}_{23x} - \mathbf{P}_{34x})^2 + (\mathbf{P}_{23y} - \mathbf{P}_{34y})^2] = 0. \quad (2.19)$$

Of course, each pole is a function of the relative positions as given in Eq. 2.2, which can be substituted into Eqs. 2.18 and 2.19, resulting in

$$f_i = B_i(d_{4x}^2 + d_{4y}^2) + C_i d_{4x} + D_i d_{4y} + E_i = 0, \quad (2.20)$$

where  $B_i, C_i, D_i$ , and  $E_i$  are constant for  $i = 1, 2$ .

Like the rhombus, solving for the corresponding location of the fourth task position, Eqs. 2.20 with  $i = 1, 2$  are combined to eliminate the squared terms, giving

$$\begin{aligned} f_3 &= f_1 - (B_1/B_2)f_2 \\ &= (C_1 - C_2 B_1/B_2)d_{4x} + (D_1 - D_2 B_1/B_2)d_{4y} + (E_1 - E_2 B_1/B_2) \\ &= C_4 d_{4x} + D_4 d_{4y} + E_4 = 0. \end{aligned} \quad (2.21)$$

Rewriting Eq. 2.21 gives

$$d_{4y} = (-D_4 d_{4x} - E_4)/E_4. \quad (2.22)$$

Substituting Eq. 2.22 into Eq. 2.18 gives

$$\begin{aligned} f_1 &= B_3 d_{4x}^2 + B_3 [(-D_4 d_{4x} - E_4)/E_4]^2 + C_3 d_{4x} \\ &\quad + D_3 [(-D_4 d_{4x} - E_4)/E_4] + F_3 = 0. \end{aligned} \quad (2.23)$$

Equation 2.23 produces two solutions of  $d_{4x}$ . Each value of  $d_{4x}$  can be substituted into Eq. 2.22 to obtain the corresponding  $d_{4y}$ . The solutions will represent both an open and crossed form of a parallelogram. Burmester [27] originally recognized that as the opposite pole quadrilateral is arranged as a parallelogram, the center-point curve will degenerate into the line at infinity and an equilateral hyperbola. Schaaf and Lammers [51] further identified that the center-point curves for a class 5 change-point compatibility linkage will appear as circle-degenerate or hyperbolic-degenerate forms.

As an example of the parallelogram, three positions are given as  $\mathbf{d}_1 = (0, 0)^T$ ,  $\theta_1 = -45^\circ$ ,  $\mathbf{d}_2 = (1, 1)^T$ ,  $\theta_2 = 45^\circ$ ,  $\mathbf{d}_3 = (2, -1)^T$ ,  $\theta_3 = 120^\circ$ , and the orientation of the fourth position is given as  $\theta_4 = -75^\circ$ . Solutions according to the procedure outlined above, along with the opposite pole quadrilateral and center-point curve, are shown in Fig. 2.5. Locations for the fourth position include  $\mathbf{d}_4 = (0.1466, -0.9675)^T$  (shown in Fig. 2.5a) and  $\mathbf{d}_4 = (-0.8395, 1.3653)^T$  (shown in Fig. 2.5b). Notice that the open parallelogram is associated with a hyperbolic-degenerate form of the center-point curve. The center-point curve for the crossed parallelogram is circle-degenerate. This observation has been observed for all situations explored.

### 2.2.5 Opposite Pole Quadrilateral with $T_1 = T_3 = 0$ or $T_2 = T_3 = 0$ : A Kite

The constraining equations for a kite, where the two sets of adjacent sides have the same length, is given as

$$f_1 = |\mathbf{P}_{14} - \mathbf{P}_{14}|^2 - L^2, \quad (2.24)$$

$$f_2 = |\mathbf{P}_{23} - \mathbf{P}_{34}|^2 - |\mathbf{P}_{14} - \mathbf{P}_{34}|^2, \quad (2.25)$$

or

$$f_1 = |\mathbf{P}_{23} - \mathbf{P}_{34}|^2 - L^2, \quad (2.26)$$

$$f_2 = |\mathbf{P}_{12} - \mathbf{P}_{14}|^2 - |\mathbf{P}_{14} - \mathbf{P}_{34}|^2. \quad (2.27)$$

Like the parallelogram, Barker [50] identified this as a class 5 change-point linkage. Identifying positions that create these distinctive shapes of the opposite pole quadrilateral is completed by fully specifying three positions and the orientation of the fourth position, then solving for the location of the fourth position.



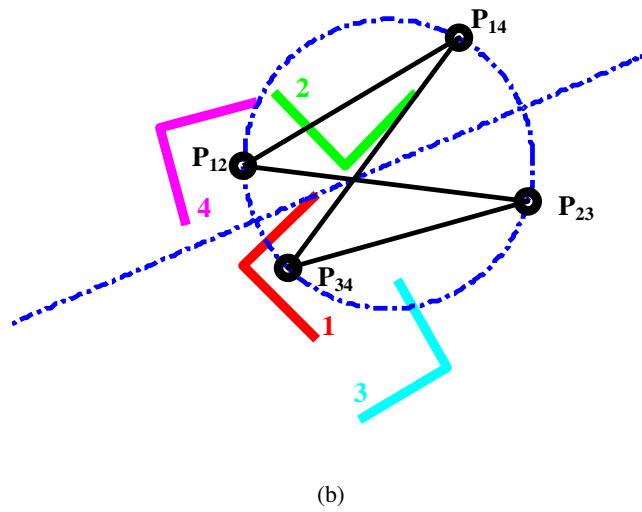
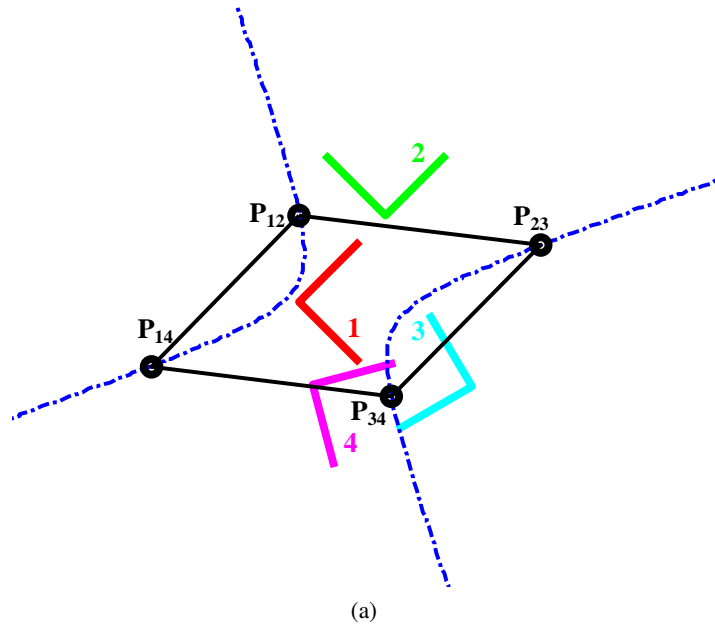


Figure 2.5: Four positions that produce an opposite pole quadrilateral that with two pairs of equal side legs.

Substituting Eq. 2.2 into expanded versions of Eqs. 2.24 and 2.25, or Eqs. 2.26 and 2.27, results in an equation in the form given in 2.20. Obtaining the location of the fourth position proceeds identically to the procedure outlined in the parallelogram case. The solutions will represent both an open and folded form of a kite. Schaaf and Lammers [51] identify that the center-point curves for a class 5 change-point compatibility linkage will appear as either a double-point or circle-degenerate form.

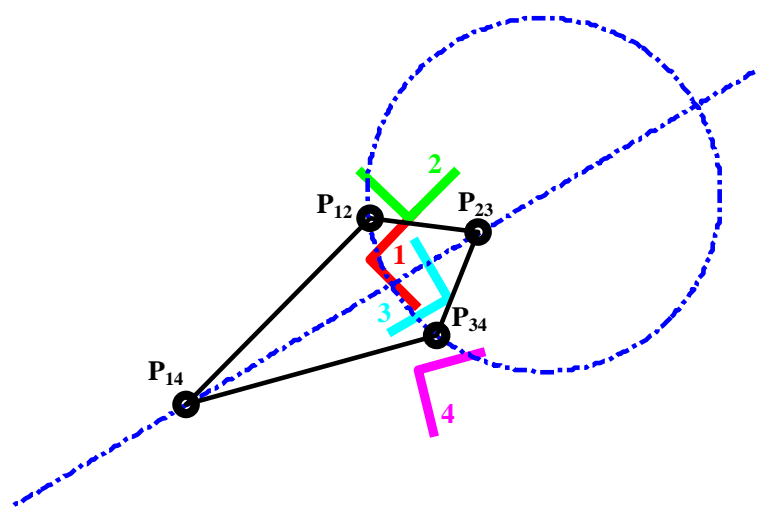
As an example of the kite, the same three positions are given as  $\mathbf{d}_1 = (0, 0)^T$ ,  $\theta_1 = -45^\circ$ ,  $\mathbf{d}_2 = (1, 1)^T$ ,  $\theta_2 = 45^\circ$ ,  $\mathbf{d}_3 = (2, -1)^T$ ,  $\theta_3 = 120^\circ$ , and the orientation of the fourth position is given as  $\theta_4 = -75^\circ$ . Solutions according to the procedure outlined above, along with the opposite pole quadrilateral and center-point curve, are shown in Fig. 2.6. Locations for the fourth position include  $\mathbf{d}_4 = (1.2412, -2.8320)^T$ , resulting in the open kite shown in Fig. 2.6a, and  $\mathbf{d}_4 = (-1.4142, 3.4459)^T$ , resulting in a closed kite shown in Fig. 2.6b. Notice that the open kite is associated with a circle-degenerate form of the center-point curve. The center-point curve for the closed kite is a double-point form. This observation has been observed for all situations explored.

### 2.2.6 Opposite Pole Quadrilateral with $T_1 = 0$ or $T_2 = 0$ or $T_3 = 0$

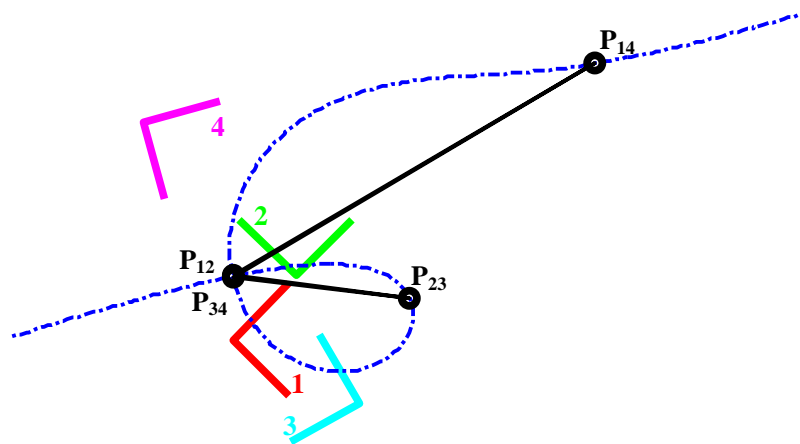
This category of compatibility linkage is a general transition linkage and characterized when the sum of two sides equals the sum of the other two. Barker [50] identified these as class 1 through 3 change-point linkages, depending on which sides are combined. A transition linkage with  $T_1 = 0$  is described by

$$f_1 = |\mathbf{P}_{12} - \mathbf{P}_{14}| + |\mathbf{P}_{14} - \mathbf{P}_{34}| - |\mathbf{P}_{23} - \mathbf{P}_{34}| - L.$$

Identifying positions that create this distinctive shape of the opposite pole quadrilateral is completed by fully specifying three positions, the orientation and one location coordinate of the fourth position,



(a)



(b)

Figure 2.6: Four positions that produce an opposite pole quadrilateral with two pairs of equal side legs.

then solving for the other location coordinate. In a similar fashion to the method presented in the preceding two sections, Eq. 2.2 is substituted into Eq. 2.28, resulting in the rather complex equation

$$f_1 = Ad_{4y}^2 + Bd_{4y} + C + \sqrt{Dd_{4y}^2 + Ed_{4y} + F} = 0. \quad (2.28)$$

Eq. 2.28 produces two solutions of  $d_{4y}$  which represent both an open and crossed form of the transition linkage. Schaaf and Lammers [51] identify that the center-point curves for a class 1,2 or 3 change-point compatibility linkage will appear as a double-point form.

As an example of the general transition compatibility linkage, the same three positions are given as  $\mathbf{d}_1 = (0, 0)^T$ ,  $\theta_1 = -45^\circ$ ,  $\mathbf{d}_2 = (1, 1)^T$ ,  $\theta_2 = 45^\circ$ ,  $\mathbf{d}_3 = (2, -1)^T$ ,  $\theta_3 = 120^\circ$ . The orientation of the fourth position is  $\theta_4 = -75^\circ$ , and  $d_{4x} = -1$ . Solutions according to the procedure outlined above, along with the opposite pole quadrilateral and center-point curve, are shown in Fig. 2.7. The remaining location coordinates for the fourth position include  $d_{4y} = -0.8406$  (shown in Fig. 2.7a) and  $d_{4y} = 1.2706$  (shown in Fig. 2.7b). Notice that both cases in Fig. 2.7 are associated with a double-point form of the center-point curve. This observation has been seen for all general transition situations explored.

All transition cases of the opposite pole quadrilateral (OPQ) and the associated form of the center-point curve (CPC) are summarized in Table 2.1.

### 2.3 Synthesizing PR Dyads

For a general case of four finitely separated positions, one unique prismatic-revolute chain (PR dyad) can be synthesized [23]. A general PR dyad is shown in Fig. 2.8. The location of the moving pivot relative to the fixed frame is

$$\mathbf{Z}_i = A_i \mathbf{z} + \mathbf{d}_i. \quad (2.29)$$

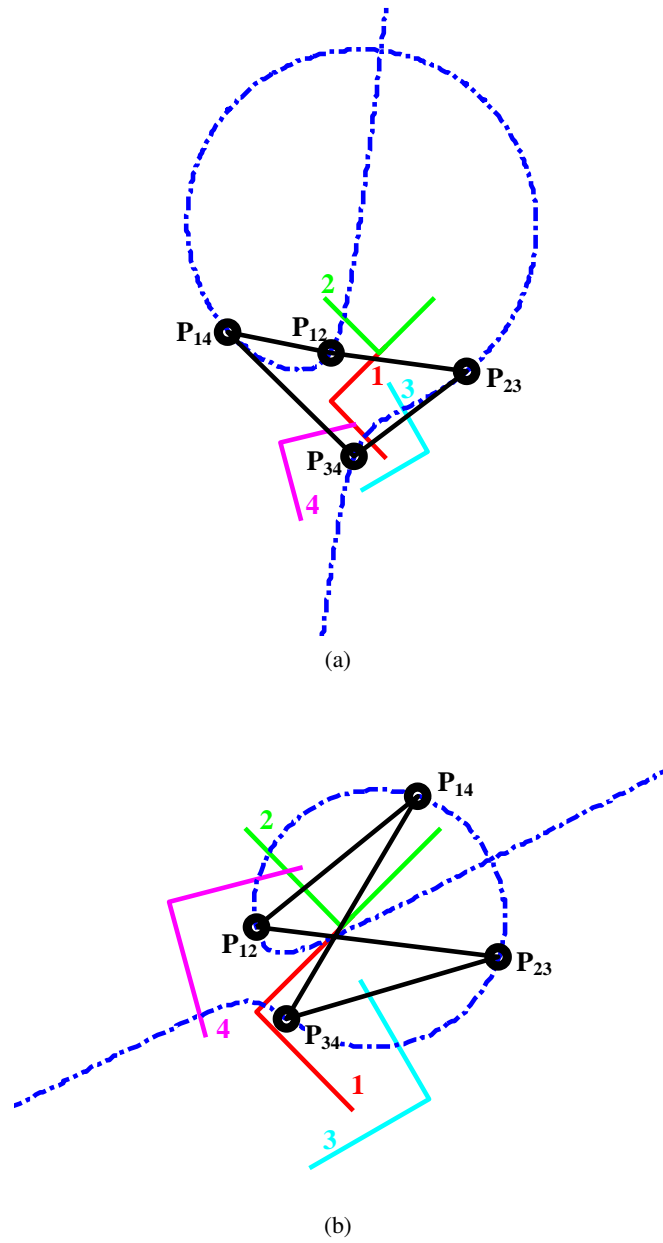


Figure 2.7: Four positions that produce an opposite pole quadrilateral with  $T_1 = 0$ .

Table 2.1: Summary of the four position distinctive cases.

Case	$T_1$	$T_2$	$T_3$	Shape of OPQ	Pose	CPC Form	Parameters Specified	No of Solns.
1	0	0	0	Rhombus	Open	Intersecting	$\mathbf{d}_1, \theta_1, \mathbf{d}_2, \theta_2, \mathbf{d}_3, \theta_3$	2
2	0	0	0	Rhombus	Closed	Circle-degenerate	$\mathbf{d}_1, \theta_1, \mathbf{d}_2, \theta_2, \mathbf{d}_3, \theta_3$	4
3	0	0		Parallelogram	Open	Hyperbola	$\mathbf{d}_1, \theta_1, \mathbf{d}_2, \theta_2, \mathbf{d}_3, \theta_3, \theta_4$	1
4	0	0		Parallelogram	Crossed	Circle-degenerate	$\mathbf{d}_1, \theta_1, \mathbf{d}_2, \theta_2, \mathbf{d}_3, \theta_3, \theta_4$	1
5	0		0	Kite	Open	Circle-degenerate	$\mathbf{d}_1, \theta_1, \mathbf{d}_2, \theta_2, \mathbf{d}_3, \theta_3, \theta_4$	1
6	0		0	Kite	Closed	Double-point	$\mathbf{d}_1, \theta_1, \mathbf{d}_2, \theta_2, \mathbf{d}_3, \theta_3, \theta_4$	1
7		0	0	Kite	Open	Circle-degenerate	$\mathbf{d}_1, \theta_1, \mathbf{d}_2, \theta_2, \mathbf{d}_3, \theta_3, \theta_4$	1
8		0	0	Kite	Closed	Double-point	$\mathbf{d}_1, \theta_1, \mathbf{d}_2, \theta_2, \mathbf{d}_3, \theta_3, \theta_4$	1
9	0			Folding	Open	Double-point	$\mathbf{d}_1, \theta_1, \mathbf{d}_2, \theta_2, \mathbf{d}_3, \theta_3, \theta_4, d_{4x}$	1
10	0			Folding	Crossed	Double-point	$\mathbf{d}_1, \theta_1, \mathbf{d}_2, \theta_2, \mathbf{d}_3, \theta_3, \theta_4, d_{4x}$	1
11		0		Folding	Open	Double-point	$\mathbf{d}_1, \theta_1, \mathbf{d}_2, \theta_2, \mathbf{d}_3, \theta_3, \theta_4, d_{4x}$	1
12		0		Folding	Crossed	Double-point	$\mathbf{d}_1, \theta_1, \mathbf{d}_2, \theta_2, \mathbf{d}_3, \theta_3, \theta_4, d_{4x}$	1
13			0	Folding	Open	Double-point	$\mathbf{d}_1, \theta_1, \mathbf{d}_2, \theta_2, \mathbf{d}_3, \theta_3, \theta_4, d_{4x}$	1
14			0	Folding	Crossed	Double-point	$\mathbf{d}_1, \theta_1, \mathbf{d}_2, \theta_2, \mathbf{d}_3, \theta_3, \theta_4, d_{4x}$	1

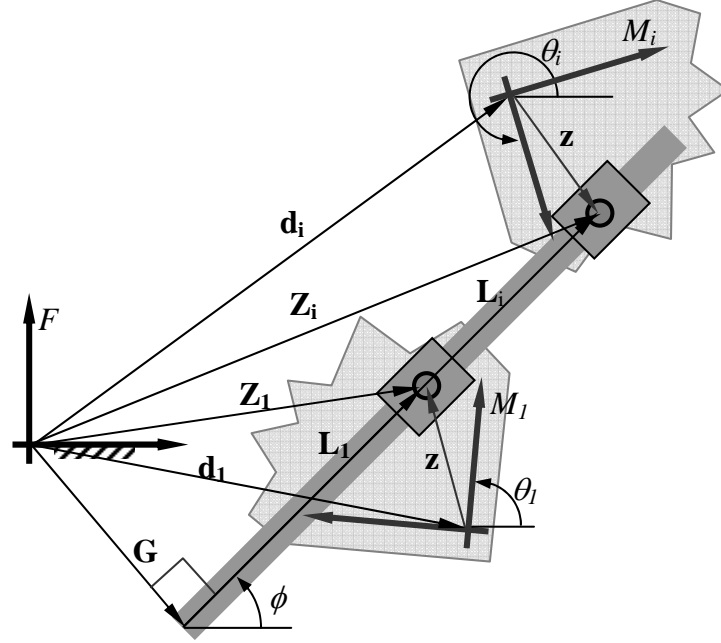


Figure 2.8: General PR dyad.

Alternatively, the location of the moving pivot relative to the fixed frame as constrained by the slide is

$$\mathbf{Z}_i = \mathbf{G} + L_i \begin{Bmatrix} \cos \phi \\ \sin \phi \end{Bmatrix}, \quad (2.30)$$

where  $L_i = \|\mathbf{L}_i\|$ . Combining Eqs. 2.29 and 2.30 for two positions  $i$  and  $j$  gives

$$(A_j - A_i)\mathbf{z} + (\mathbf{d}_j - \mathbf{d}_i) = L_{ij} \begin{Bmatrix} \cos \phi \\ \sin \phi \end{Bmatrix}, \quad (2.31)$$

where  $L_{ij} = L_i - L_j$ .

For four finitely separated positions, three independent versions of Eq. 2.31 can be expressed as

$$\begin{bmatrix} [A_4 - A_3] & -\cos \phi & 0 & 0 & \mathbf{d}_4 - \mathbf{d}_3 \\ & -\sin \phi & 0 & 0 & \\ [A_4 - A_2] & 0 & -\cos \phi & 0 & \mathbf{d}_4 - \mathbf{d}_2 \\ & 0 & -\sin \phi & 0 & \\ [A_4 - A_1] & 0 & 0 & -\cos \phi & \mathbf{d}_4 - \mathbf{d}_1 \\ & 0 & 0 & -\sin \phi & \end{bmatrix} \begin{Bmatrix} z_x \\ z_y \\ L_{34} \\ L_{24} \\ L_{14} \\ 1 \end{Bmatrix} = 0. \quad (2.32)$$

A PR solution exists only if the determinant of the matrix in Eq.2.32 is zero. For a general set of positions, a single value of  $\phi$  ( $0 \leq \phi < \pi$ ) is possible. The line of slide defined by  $\phi$  will be perpendicular to the asymptote of the center-point curve [7]. As the center-point curve approaches infinity, the highest order terms in Eq. 2.1 dominate. The equation of the asymptote is

$$C_1x + C_2y = 0, \quad (2.33)$$

which has a slope

$$m = y/x = -C_1/C_2. \quad (2.34)$$

Figure 2.4c is reproduced as Fig. 2.9. Also included as the dotted red curve is the circle-point curve associated with the first position, which has a circle-degenerate form. Since the center-point curve appears as a hyperbola, as in the open parallelogram and rhombus cases, the center-point curve exhibits two asymptotes and the line at infinity. For this special case where the center-point curve includes the line at infinity, the determinant of the matrix in Eq. 2.32 is zero for any  $\phi$ . This confirms that any five of the six equations can be solved for  $\mathbf{z}$ ,  $L_{14}$ ,  $L_{24}$ , and  $L_{34}$  with an arbitrary  $\phi$ . The solution will be consistent with the unused equation. Therefore, for these situations, a PR dyad to achieve the four positions can be synthesized with the line of slide in any direction. As an example, PR dyads are synthesized at arbitrary  $47^\circ$  and  $152^\circ$  to achieve the positions illustrated in Fig. 2.9 and are shown in Figs. 2.10a and 2.10b, respectively. The two PR dyads are joined to form an elliptical trammel linkage to achieve the four target positions as shown in Figs. 2.10c.



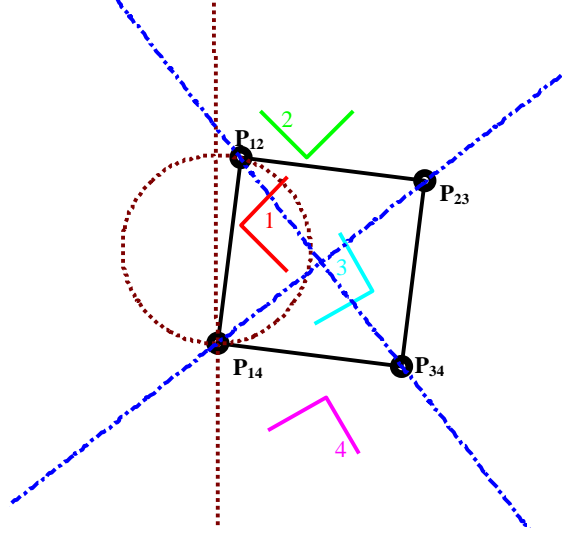


Figure 2.9: Opposite pole quadrilateral forming a rhombus.

Although the center-point curve degeneracies are thoroughly discussed in the literature, previous examples detailing the arbitrary line of slide for the P in a PR chain have not been encountered in the literature.

## 2.4 Synthesizing RP Dyads

For a general case of four finitely separated positions, one unique revolute-prismatic chain (RP dyad) can be synthesized. A general RP dyad is shown in Fig. 2.11. Similar to the PR dyad, the location of the prismatic joint can be represented through alternative vector paths, written relative to the moving reference frame  $M_i$  as

$$A_i^T (\mathbf{G} - \mathbf{d}_i) = \mathbf{z} + l_i \begin{Bmatrix} -\sin \psi \\ \cos \psi \end{Bmatrix}. \quad (2.35)$$

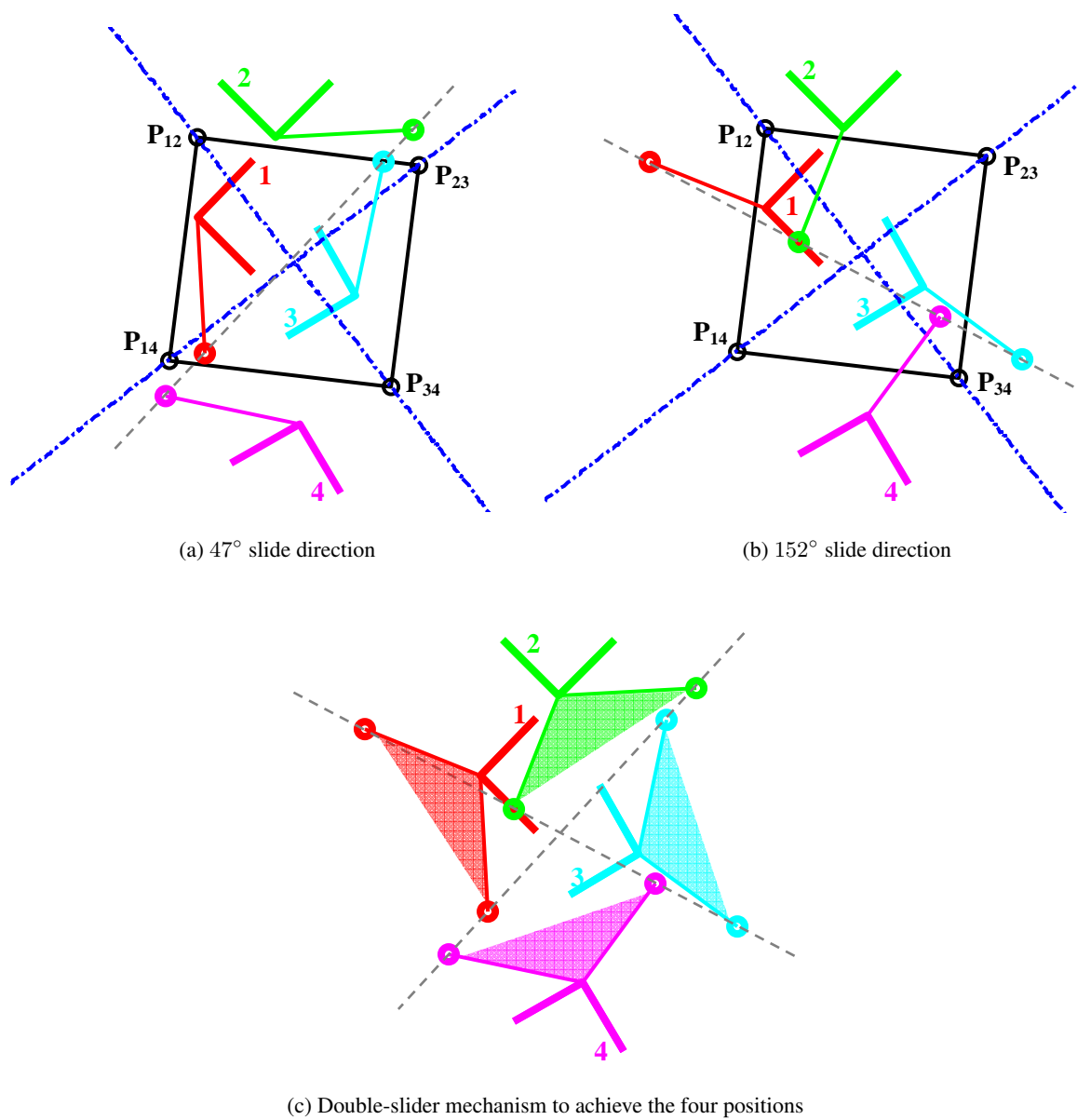


Figure 2.10: A PR dyad can be oriented in any direction when the center-point curve is a hyperbola.

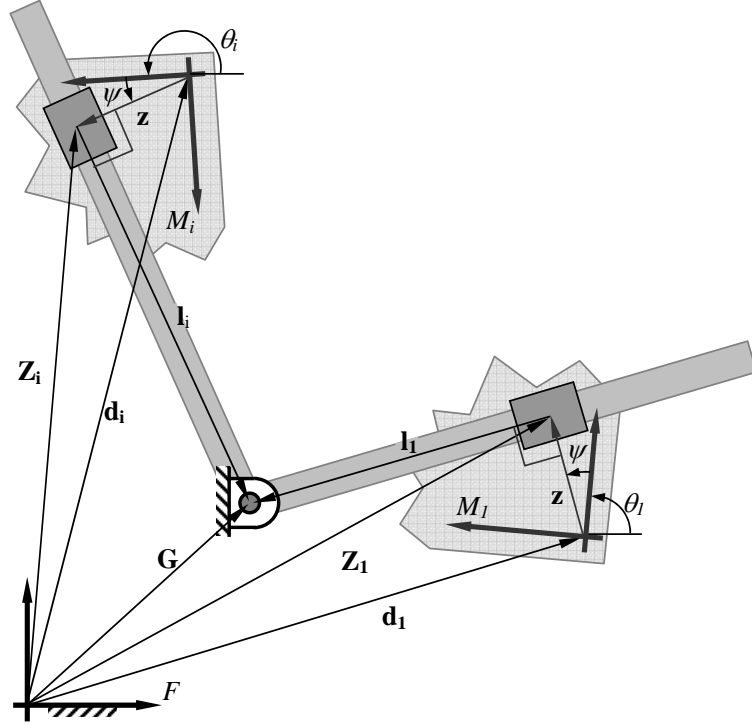


Figure 2.11: General RP dyad.

Writing Eq. 2.35 for two positions  $i$  and  $j$  and subtracting gives

$$\left( A_i^T - A_j^T \right) \mathbf{G} + l_{ij} \begin{Bmatrix} \sin \psi \\ -\cos \psi \end{Bmatrix} = \left( A_i^T \mathbf{d}_i - A_j^T \mathbf{d}_j \right), \quad (2.36)$$

where  $l_{ij} = |l_i - l_j|$ .

For the general case of four finitely separated positions, three independent versions of Eq. 2.36 can be expressed as

$$\begin{bmatrix} [A_4 - A_3]^T & \sin \psi & 0 & 0 & (A_3^T \mathbf{d}_3 - A_4^T \mathbf{d}_4) \\ [A_4 - A_2]^T & -\cos \psi & 0 & 0 & (A_2^T \mathbf{d}_2 - A_4^T \mathbf{d}_4) \\ [A_4 - A_1]^T & 0 & \sin \psi & 0 & (A_1^T \mathbf{d}_1 - A_4^T \mathbf{d}_4) \\ & 0 & -\cos \psi & 0 & \\ & 0 & 0 & \sin \psi & \\ & 0 & 0 & -\cos \psi & \end{bmatrix} \begin{Bmatrix} G_x \\ G_y \\ l_{34} \\ l_{24} \\ l_{14} \\ 1 \end{Bmatrix} = 0. \quad (2.37)$$

An RP solution exists only if the determinant of the matrix in Eq. 2.37 is zero. For a general set of positions, as in the case of the PR dyad, a single value of  $\psi$  ( $0 \leq \psi < \pi$ ) is possible.

Figure 2.5b is reproduced as Fig. 2.12. The circle-point curve associated with the first position has a circle-degenerate form and is included as the dotted red curve. When the circle-point curve appears as a hyperbola, as in the crossed parallelogram or folded rhombus, the circle-point curve exhibits two asymptotes and the line at infinity. For this special case where the circle-point curve includes the line at infinity, the determinant of the matrix in Eq. 2.37 is zero for any  $\phi$ . This confirms that any five of the six equations can be solved for  $\mathbf{G}$ ,  $L_{14}$ ,  $L_{24}$ , and  $L_{34}$  with an arbitrary  $\psi$ . The solution will be consistent with the unused equation. The corresponding fixed pivot  $\mathbf{G}$  will always lie along the circular portion of the center-point curve. Therefore, an RP dyad to achieve the special case of four positions can be synthesized for any point along the circular portion of the center-point curve. As an example, two RP dyads are synthesized from arbitrary points on the center-point curve illustrated in Fig. 2.12, is shown in Fig. 2.13. Two RP dyads are joined to form an RPPR linkage to achieve the four target positions as shown in Fig. 2.13c.

## 2.5 Three Position Case

In light of the discussion of the special cases for four task positions, special cases of three positions were explored. The purpose is that additional PR or RP dyads may be introduced with distinctive arrangements of the poles. With three task positions, only three poles exist:  $\mathbf{P}_{12}$ ,  $\mathbf{P}_{23}$  and  $\mathbf{P}_{13}$ . Special relationships between three poles include collinearity and an equilateral triangle. Both relationships are described by two constraint equations. Identifying positions that create these distinctive shapes of the pole triangle is completed by fully specifying two positions and the angle of the third position, then solving for the location of the third position.

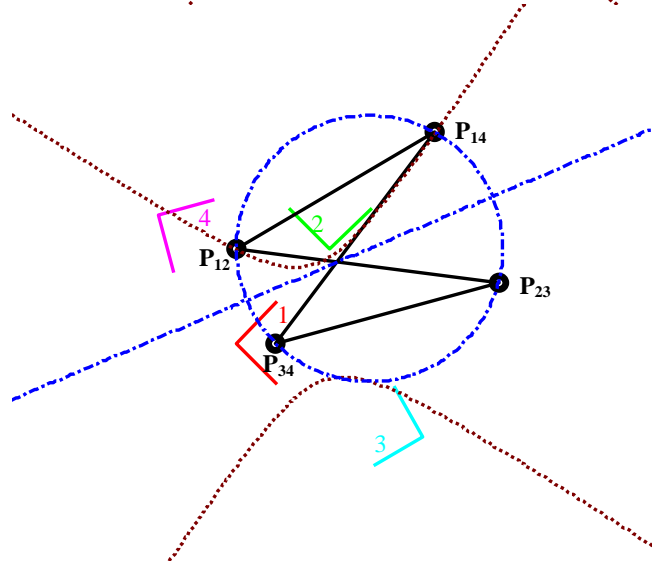


Figure 2.12: Opposite pole quadrilateral forming a parallelogram.

### 2.5.1 Collinear Poles

Three poles cannot be collinear. The constraining equations for the poles to lie along a line is generated by equating the slope of the line connecting the three poles

$$f_1 = \frac{P_{12y} - P_{13y}}{P_{12x} - P_{13x}} - \frac{P_{12y} - P_{23y}}{P_{12x} - P_{23x}} = 0, \quad (2.38)$$

$$f_2 = \frac{P_{12y} - P_{13y}}{P_{12x} - P_{13x}} - \frac{P_{13y} - P_{23y}}{P_{13x} - P_{23x}} = 0. \quad (2.39)$$

The two constraints in Eqs. 2.38 and 2.39 will not produce real solutions for  $\{d_{3x} \ d_{3y}\}$  with arbitrarily selected task orientations ( $\theta_1$ ,  $\theta_2$ , and  $\theta_3$ ). For collinear poles, the interior angles of the pole triangle must be  $0^\circ$  or  $180^\circ$ . As discussed in McCarthy [23], the interior angles of a pole triangle are one-half of the angle between the orientations. This implies that for collinear poles, the angle between the orientations is  $0^\circ$  or  $360^\circ$ . Since the pole of parallel task positions is at infinity, three

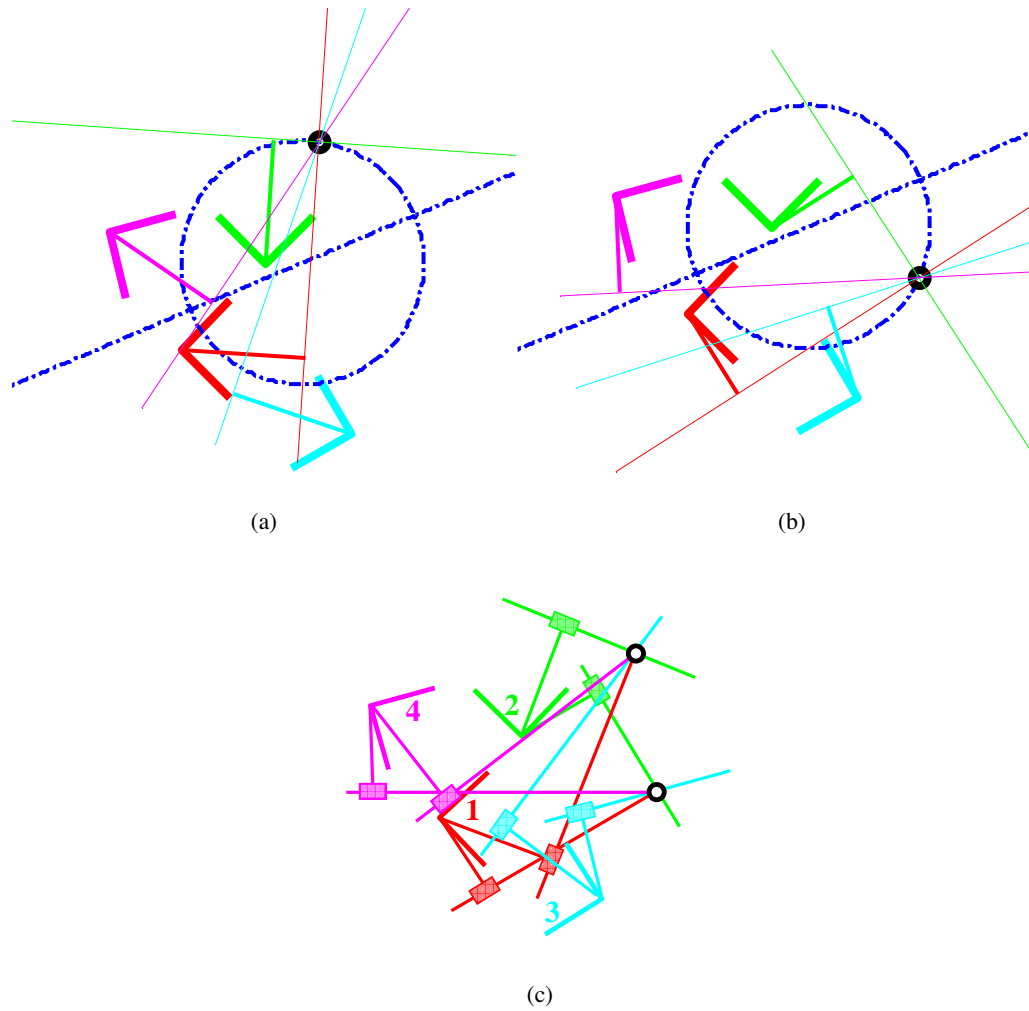


Figure 2.13: RP dyads are synthesized from arbitrary points on the center-point curve.

poles can not be collinear. Incidentally, the constraints are satisfied with arbitrary task orientations if the three poles collapse to a single point.

### 2.5.2 Equilateral Triangle

The constraining equations for the poles to form an equilateral triangle are generated by equating the length of the three sides

$$f_1 = |\mathbf{P}_{12} - \mathbf{P}_{13}| - |\mathbf{P}_{12} - \mathbf{P}_{23}| = 0, \quad (2.40)$$

$$f_2 = |\mathbf{P}_{12} - \mathbf{P}_{13}| - |\mathbf{P}_{13} - \mathbf{P}_{23}| = 0. \quad (2.41)$$

Like the previous case, the two constraints in Eqns. 2.40 and 2.41 will not produce real solutions for  $\{d_{3x} \ d_{3y}\}$  with arbitrarily selected task orientations ( $\theta_1$ ,  $\theta_2$ , and  $\theta_3$ ). For the equilateral triangle, the interior angles of the pole triangle are  $60^\circ$ . This implies that the angle between the orientations is  $120^\circ$  or  $240^\circ$ . Thus, any values of  $d_{3x}$  and  $d_{3y}$  will satisfy the constraints specified in Eqns. 2.40 and 2.41 if the task orientations are separated by  $120^\circ$  or  $240^\circ$ . That is, the poles of any 3 positions separated by  $120^\circ$  or  $240^\circ$  will form an equilateral triangle.

## 2.6 Five Position Cases

For five general task positions, a discrete number of locations (0, 2 or 4) are possible for a fixed pivot of an RR dyad. The fixed pivot locations are the intersections of all five center-point curves generated by taking every four-position combination. With five positions, 10 poles exist ( $\mathbf{P}_{12}$ ,  $\mathbf{P}_{13}$ ,  $\mathbf{P}_{14}$ ,  $\mathbf{P}_{15}$ ,  $\mathbf{P}_{23}$ ,  $\mathbf{P}_{24}$ ,  $\mathbf{P}_{25}$ ,  $\mathbf{P}_{34}$ ,  $\mathbf{P}_{35}$  and  $\mathbf{P}_{45}$ ). Three center-point curves will intersect at a pole as the two positions that define the pole are used in the generation of the center-point curves.

The triangle formed by  $\mathbf{P}_{23}$ ,  $\mathbf{P}_{34}$  and  $\mathbf{P}_{35}$  is considered to be a platform connected to ground by the RR dyads  $\mathbf{P}_{12}\mathbf{P}_{13}$ ,  $\mathbf{P}_{14}\mathbf{P}_{34}$  and  $\mathbf{P}_{15}\mathbf{P}_{35}$ . Murray and McCarthy [54] call this a compatibility platform. In general, a compatibility platform is a structure with zero DOF, yet it exhibits alternate assembly configurations. A compatibility platform is shown with the black lines in Fig. 2.14. An

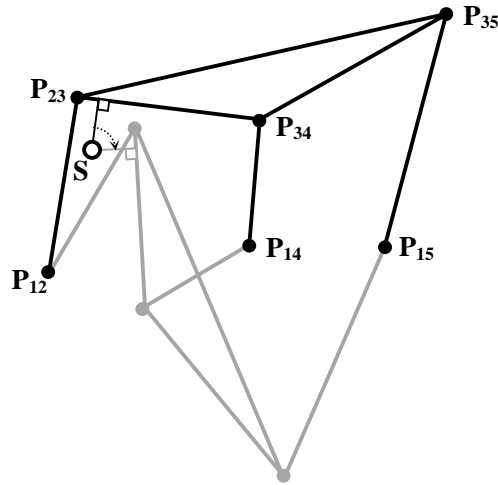


Figure 2.14: Compatibility structure for five position synthesis.

alternative assembly configuration of this structure is shown as gray lines. As Murray and McCarthy describe, the fixed pivot of an RR dyad compatible with five task positions is a pole of an assembly of the compatibility platform relative to its initial configuration. One such fixed pivot for an RR dyad to achieve all five positions is shown as  $S$  in Fig. 2.14. Note that  $S$  is coincident with the displacement pole of the gray configuration relative to the black configuration.

### 2.6.1 Case 1: Movable Compatibility Platform

A noteworthy case for the five-position guidance problem aligns the poles such that the compatibility platform contains three equal length and parallel cranks. As in the general case, this compatibility platform can have different assembly configurations revealing fixed pivots for an RR dyad. It is noteworthy in that because of the symmetry, the structure is able to move as a triple crank. The motion of the platform is an orbital translation in which each point on the platform



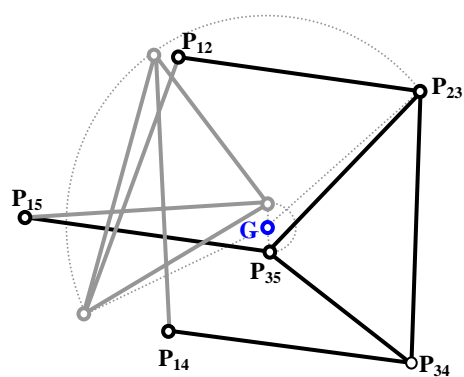
traces a circle, and the displacement poles form a line at infinity. Like the four-position cases in which the center-point curve includes a line at infinity, a PR dyad can be synthesized to achieve the five positions with the line of slide in any arbitrary direction.

As an example of a compatibility platform with motion, five positions are given as  $\mathbf{d}_1 = (0, 0)^T$ ,  $\theta_1 = -45^\circ$ ,  $\mathbf{d}_2 = (1, 1)^T$ ,  $\theta_2 = 45^\circ$ ,  $\mathbf{d}_3 = (2, -1)^T$ ,  $\theta_3 = 120^\circ$ ,  $\mathbf{d}_4 = (1.4691, -2.6237)^T$ ,  $\theta_4 = 200^\circ$ ,  $\mathbf{d}_5 = (0.1040, -0.8033)^T$ , and  $\theta_5 = 290^\circ$ . This movable compatibility platform and an alternate assembly configuration are shown in Fig. 2.15a. An RR dyad, synthesized from the displacement pole of the compatibility platform is shown in Fig. 2.15b. Two PR dyads are synthesized at arbitrary directions of  $57^\circ$  and  $162^\circ$  and shown in Fig. 2.15c.

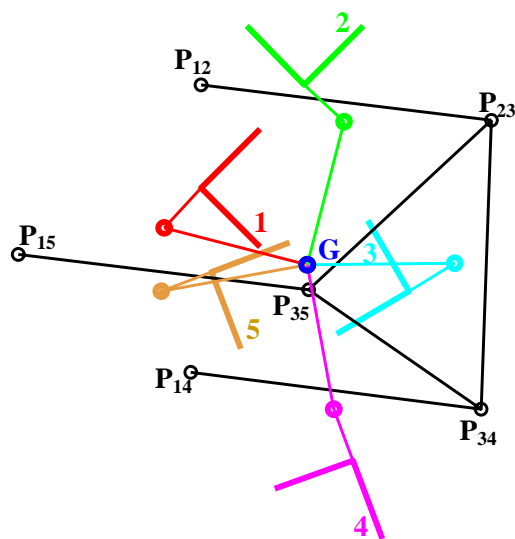
### 2.6.2 Case 2: Alternate Configuration of the Movable Compatibility Platform

A second interesting case is revealed if a movable compatibility platform, as in Fig. 2.15b, is placed in an alternate configuration. An alternate configuration is shown in gray in Fig. 2.15a. As described earlier, fixed pivot locations for the five positions correspond to the pole of the compatibility platform relative to the initial configuration. In this case, the other configuration is able to move, and the displacement pole becomes a curve. Thus, a center-point curve for five positions is obtained. However, the corresponding circle point for each center point on the curve is at infinity. As with the four-position case with a circle-point at infinity, an RP dyad can be constructed from any point on the center-point curve that achieves the five task positions.

Pole locations that place the compatibility platform of Fig. 2.15b into an alternate configuration are shown in Fig. 2.16a. Positions consistent with this set of poles are  $\mathbf{d}_1 = (0, 0)^T$ ,  $\theta_1 = 0^\circ$ ,  $\mathbf{d}_2 = (0.9914, 0.8692)^T$ ,  $\theta_2 = 82.5^\circ$ ,  $\mathbf{d}_3 = (-3.2602, 0.7422)^T$ ,  $\theta_3 = -195.0^\circ$ ,  $\mathbf{d}_4 = (1.6268, -1.3416)^T$ ,  $\theta_4 = -72.5^\circ$ ,  $\mathbf{d}_5 = (-3.2472, -1.7717)^T$ , and  $\theta_5 = -162.5^\circ$ . The



(a)



(b)

Figure 2.15: Five positions with a compatibility structure that has motion.

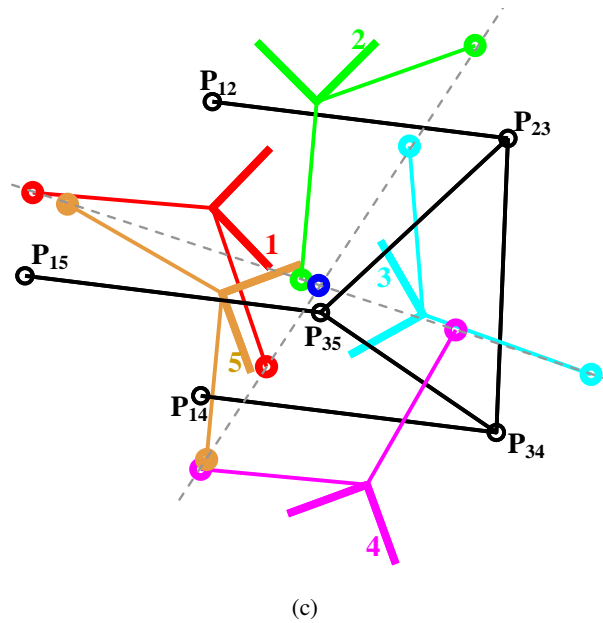
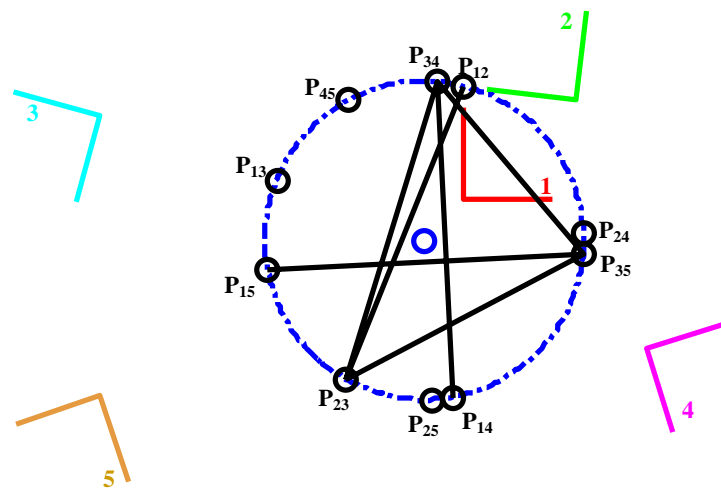


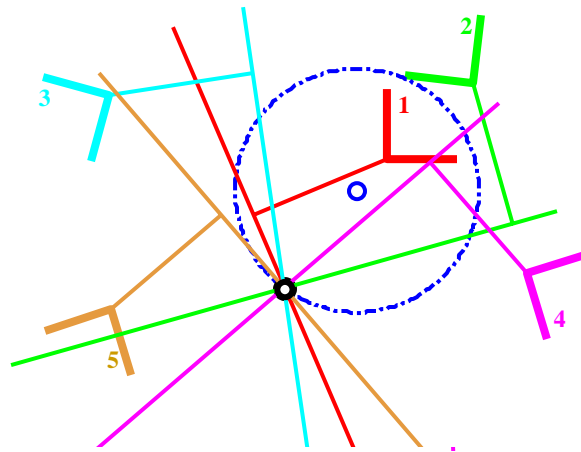
Figure 2.15: Five positions with a compatibility structure that has motion (con't).

center-point curve for these five positions is shown as blue in Fig. 2.16a. Two RP dyads are synthesized from arbitrary points on the center-point curve and shown in Figs. 2.16b and c.

The prescription for pole locations that generate the alternative compatibility platform is shown in Fig 2.17. The three poles  $P_{23}$ ,  $P_{34}$ , and  $P_{35}$  define a circle. An arbitrary distance  $l$  can be used from  $P_{23}$  to place  $P_{12}$  on the circle. Then, using the same length  $l$ ,  $P_{14}$  and  $P_{15}$  are placed on the circle in the same rotational direction as  $P_{12}$ . With this arrangement of poles, the design space for five positions includes an infinite number of RP dyads to solve the five-position rigid-body guidance problem.



(a)



(b)

Figure 2.16: Center-point curve for five task positions.

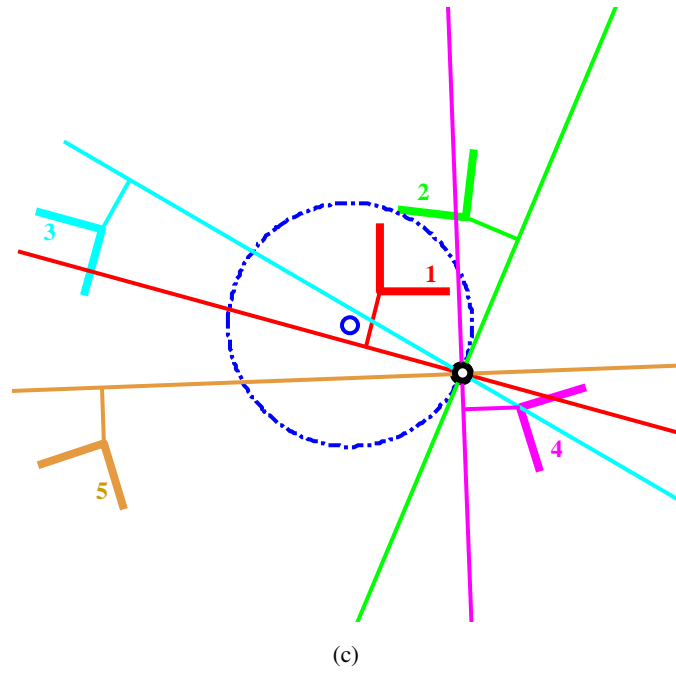


Figure 2.16: Center-point curve for five task positions (con't).

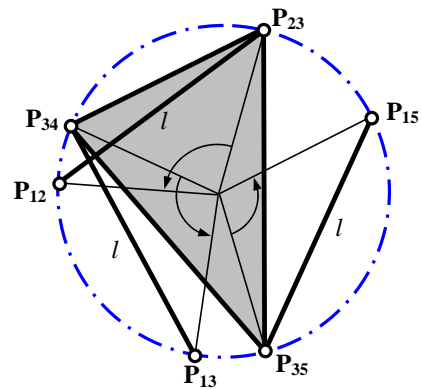


Figure 2.17: Pole locations that generate a center-point curve for five task positions.

Table 2.2: Target Positions for Example.

$i$	Target Positions			Shifted Positions		
	$\theta_i$	$d_{ix}$	$d_{iy}$	$\theta_i$	$d_{ix}$	$d_{iy}$
1	$40^\circ$	-0.5	2.5	$41.8^\circ$	-0.348	2.461
2	$30^\circ$	0.5	2.5	$29.9^\circ$	0.479	2.301
3	$-10^\circ$	1.5	1.5	$-8.9^\circ$	1.706	1.766
4	$-40^\circ$	2.8	2.5	$-41.8^\circ$	2.768	2.386
5	$-75^\circ$	5.5	2.5	$-76.5^\circ$	5.719	2.389

## 2.7 Example 2.1

A rigid-body guidance design task has the requirements shown in the left portion of Table 2.2. The task positions, poles, and five center-point curves are shown in Fig. 2.18. The five center-point curves all intersect at two points, shown as solid markers labeled  $\mathbf{G}_1$  and  $\mathbf{G}_2$  in Fig. 2.18. These are the only two locations that can serve as fixed pivots of an RR chain to achieve the five positions. The positions are shifted so the poles become arranged into a Case 2 compatibility platform, which exhibits a center-point curve. The shifted positions are indicated in the right portion of Table 2.2 and the arrangement of the poles and compatibility platform is shown in Fig. 2.19.

The center of the center-point circle is a feasible fixed pivot for an RR dyad. Any arbitrary point along the center-point circle can be selected as the fixed pivot of a RP dyad. Joining the two dyads, an RRPR linkage can be synthesized to achieve the five shifted positions as shown in Fig. 2.20.

## 2.8 Summary

The study presented in this chapter outlines a procedure to identify four finitely separated positions that create distinctive shapes of the center-point curve. This study is unique in determining a set of task positions that arrange the poles in specific shapes resulting in these center-point curves.

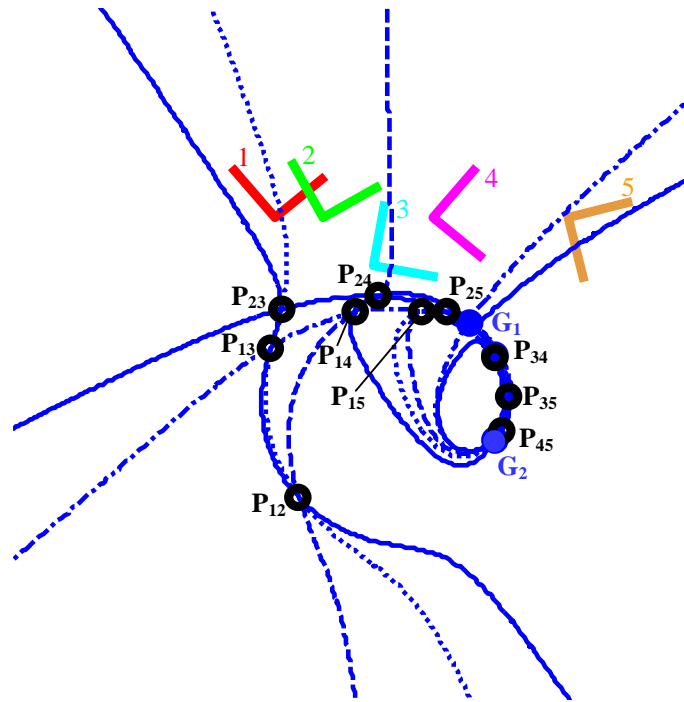


Figure 2.18: Two fixed pivot locations exist for the five target positions of Table 2.2.

Shapes explored include open and closed forms of a rhombus, kite, parallelogram, and quadrilaterals with the sum of the length of two sides equal to that of the other two. Further, the association between these distinctive compatibility linkages and the unusual center-point curves is noted. The process is expanded to generate distinctive pole arrangements in three- and five-position cases.

Four- and five-position pole configurations are identified in which the associated center-point curve(s) includes the line at infinity. With a center-point line at infinity, a PR dyad with a line of slide in any direction can be synthesized to achieve the task positions. Further, four- and five-position pole configurations are identified in which the associated circle-point curve(s) includes the line at infinity. With a circle-point that includes a line at infinity, an RP dyad originating anywhere on a center-point curve can be synthesized to achieve the task positions. If the rigid-body guidance

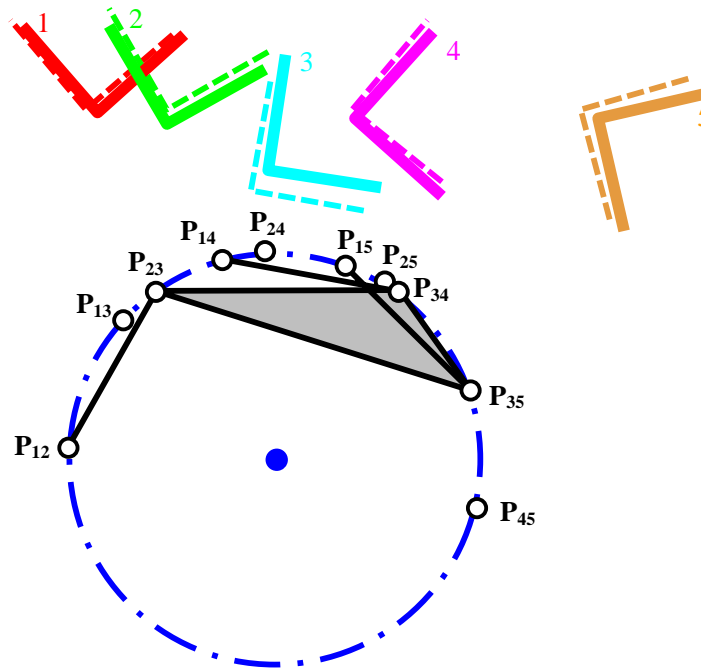


Figure 2.19: Shifted target positions to reorient the poles into a Case 2 compatibility platform.

problem is approximate, small changes to the positions may result in the introduction of a one-parameter family of dyads including a prismatic joint.



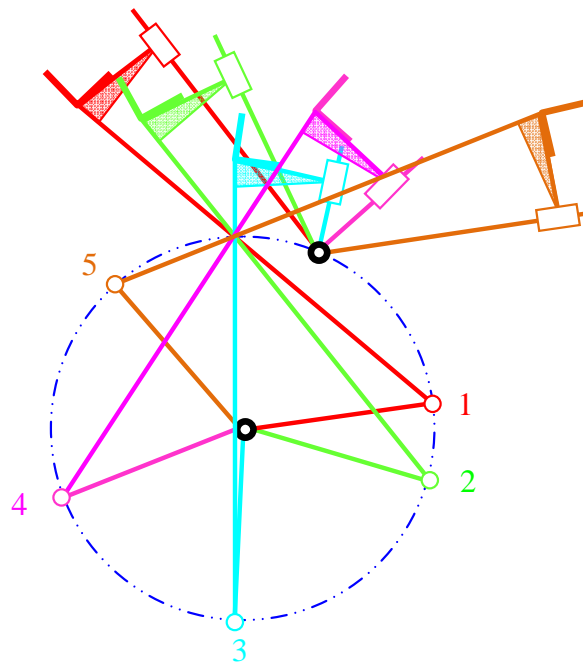


Figure 2.20: An RRPR linkage to nearly achieve the five task positions.

## **CHAPTER III**

### **USING A SINGULARITY LOCUS TO EXHIBIT THE NUMBER OF GEOMETRIC INVERSIONS, TRANSITIONS, AND CIRCUITS OF A LINKAGE**

#### **3.1 Introduction**

The circuit defect was introduced in Section 1.3.1. This chapter presents a process to infer the motion characteristics and number of circuits of a linkage, along with the sensitivity to an “adjustment” parameter. Among other examples, the method is applied to the Stephenson III linkage, actuated from within and outside the four-bar sub-chain. This linkage is important as it serves as the foundation for shape-changing mechanisms that approximate open curves.

Forward kinematic position analysis of a mechanism involves determining the orientation of links as an input link(s) is positioned. Since the governing position equations for the links in a mechanism are non-linear, multiple solutions are obtained. These different solutions are called geometric inversions [2]. Geometric inversions (GIs) are defined as the various configurations of a mechanism that can be realized for a given position of the input link(s). For a specific mechanism, the number of geometric inversions is dependent on the position of the input link(s).

Chase and Mirth [33] defined a circuit of a mechanism as the set of all possible orientations of links that can be realized without disconnecting any of the joints. Foster and Cipra [37, 38] use the term assembly configuration to refer to a circuit. If a mechanism must be disassembled to move from one position to another, the two positions reside on separate circuits. Each geometric

inversion may lie on a different circuit, but several geometric inversions can lie on the same circuit. The circuits of a mechanism are independent of the choice of driving link(s), and there is no direct relationship between the geometric inversions and circuits [33]. Established methods to identify different circuits rely on geometric insights of a particular mechanism [55, 37, 38, 56, 24, 39].

Stationary points, or singularities, can exist on a circuit when the driving link is no longer able to move the mechanism. The mechanism becomes stationary, and the mechanical advantage reduces to zero [40, 41]. Singular positions of a mechanism are dependent on the choice of driving link(s) and must be avoided when attempting to smoothly operate the mechanism. Chase and Mirth [33] defined the regions on a circuit between these singularities as branches. For single-actuated mechanisms, singularities are the input limits for that branch. Examples exist where a single branch can contain more than a full revolution of the input link [33, 39]. If a geometric inversion sits on a circuit that has no singularities, it can be driven with a fully rotatable crank.

For a mechanism to move between two or more task positions, the configurations must be on the same circuit. Once a mechanism has been synthesized, it is important to identify the assembly circuits in order to ensure that the design positions lie on the same circuit. Ensuring that two or more design configurations lie on the same circuit and branch is a primary part of the solution rectification process. Balli and Chand [35] provide a comprehensive overview of research on solution rectification.

Innocenti [57] identified a case of a two-degree-of-freedom mechanism, couched as a three-degree-of-freedom platform, that can be placed onto a different circuit without encountering a singularity. McAree and Daniel [58] displayed the geometric inversions of a 3-RPR platform on a plot of one output variable and two inputs, which they termed the reduced configuration space. Singularities were located and projected onto the input joint space in a plot termed a singularity locus

[59, 60]. The locus identifies input combinations that produce a singularity and regions with the same number of geometric inversions. The locus can be used to identify cusps that when encircled produce a “net-zero” activation sequence that places a platform in an alternative circuit. Zein et al. [61, 62] enhanced the analysis of the singularity locus by fixing one of the actuator joints and viewing two-dimensional slices of the joint space. Macho et al. [63] use the singularity locus and show a general condition for singularity-free, “net-zero” activation sequences that place a platform on a different circuit.

Murray et al. [53] use the transition linkage concept to classify single-degree-of-freedom mechanisms. Transition linkages contain link lengths that lie on the boundary of physically realizable linkages or between linkages with distinct motion characteristics. In the case of a four-bar linkage, for example, a transition linkage sits at the junction between a crank-rocker and a triple-rocker (non-Grashof linkage).

The work presented in this chapter extends the concepts of McAree and Zein to gain insight into single-actuated linkages. By generating a singularity locus, the number of singularities, geometric inversions, and circuit regimes are revealed. The input/output motion of the linkage can be inferred from the locus. The methodology to produce the singularity locus is general and does not rely on geometric insights of a particular mechanism. By using the locus, desired operational features, such as a fully rotatable crank, and unique motion characteristics, such as a greater than  $360^\circ$  non-rotatable crank can be identified. Further, it is observed that transition linkages serve as bounds between regions of different circuits.

### 3.2 Loop Closure Equations

Position analysis of planar linkages comprised of  $N$  links and  $j_p$  single-DOF joints is performed by representing each link with a position vector. For each loop  $i$ , a pair of closure equations are written of the form

$$\begin{aligned} f_{2i-1} &= \sum a_k \sin \theta_k = 0, \\ f_{2i} &= \sum a_k \cos \theta_k = 0, \end{aligned} \quad (3.1)$$

where  $k$  refers to link numbers that comprise the loop,  $a_k$ , is the length of link  $k$  and  $\theta_k$  is the corresponding revolute joint variable. For fixed links,  $\theta_k$  is constant. For links that contain prismatic joints,  $a_k$  is variable.

The number of driving links is dictated by the mobility  $m$  of the linkage, where excluding redundancies,  $m = 3(N - 1) - 2j_p$ . An  $m$ -dimensional input vector denoted  $\Theta_i$  corresponds to the number of independent inputs. The  $n$ -dimensional output vector denoted  $\Theta_o$  can represent output coordinates, joint angles or displacements. In general, the number of inputs ( $m$ ) does not need to be the same as the number of outputs ( $n$ ). However, the number of inputs will always be the same as the number of independent outputs.

An RRRPR planar linkage is shown in Fig. 3.1. For this mechanism, the loop closure equations are written as

$$\begin{aligned} f_1 &= a_2 \cos \theta_2 + a_3 \cos \theta_3 - a_1 - a_4 \cos \theta_4 = 0, \\ f_2 &= a_2 \sin \theta_2 + a_3 \sin \theta_3 - a_4 \sin \theta_4 = 0, \end{aligned} \quad (3.2)$$

where  $a_1$ ,  $a_2$ , and  $a_3$  are physical parameters and  $\theta_2$ ,  $\theta_3$ ,  $\theta_4$  and  $a_4$  are joint variables. This mechanism has two degrees of freedom, where  $\Theta_i = [\theta_2, a_4]^T$ . In this situation,  $\theta_2$  is declared the actuated

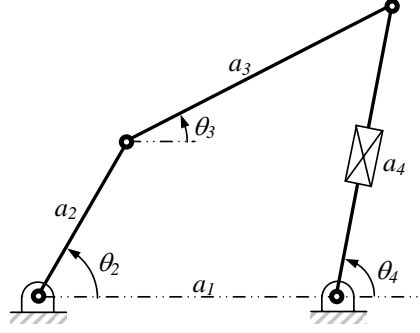


Figure 3.1: Two degree-of-freedom, RRRPR linkage.

input variable, and  $a_4$  is a secondary input which can be adjusted to achieve specific motion characteristics.

Forward kinematic position analysis determines the orientation of the mechanism links ( $\Theta_o$ ) as  $m$  input links are positioned ( $\Theta_i$ ) for a given set of physical parameters  $a_k$ . In the case of Fig. 3.1,  $\Theta_o = [\theta_3, \theta_4]^T$ . Since loop equations are written in pairs with trigonometric functions, an even set of  $\Theta_o$  solutions exist for a given  $\Theta_i$ .

### 3.2.1 Input/Output Function

In synthesizing a mechanism to accomplish a desired task, one of the output parameters is usually of higher importance and designated as  $\theta_o$ . This is specifically true for rigid-body guidance, function generation and robotic applications. Through algebraic manipulation and utilizing trigonometric identities, the loop closure of Eq. 3.1 can be reduced to a single input/output function

$$F = f(\Theta_i, \theta_o) = 0. \quad (3.3)$$

For the mechanism of Fig. 3.1,  $\theta_2$  and  $a_4$  are considered as input variables and  $\theta_4$  is designated as the output. Eliminating  $\theta_3$  from Eqs. 3.2 forms an input/output function for the mechanism in Fig. 3.1

$$F = a_1^2 + a_2^2 + a_3^2 - a_4^2 + 2a_2a_3 \sin \theta_2 \sin \theta_4 + 2a_2a_3 \cos \theta_2 \cos \theta_4 - 2a_1a_2 \cos \theta_2 - 2a_1a_3 \cos \theta_4 = 0, \quad (3.4)$$

which is  $2^{nd}$  order in  $\theta_4$ . This implies that a maximum of 2 geometric inversions are possible for a given  $\theta_2$  and  $a_4$ .

Supplying values for the physical parameters and holding  $a_4$  constant, Eq. 3.4 can be graphed, producing an input/output plot of a common four-bar mechanism. An example is shown as the blue curve in Fig. 3.2. The input/output curve of Fig. 3.2a shows that with  $a_4 = 5$ , two geometric inversions exist for all  $\theta_2$ . The input/output curve of Fig. 3.2b reveals that as  $a_4$  is changed to 7, two geometric inversions exist only over the range of  $-0.5855 \leq \theta_2 \leq 0.5855$ .

A series of the input/output plots at increasing values of  $a_4$  generates a 2-dof input/output manifold in reduced configuration space as shown in Fig. 3.3. This is equivalent to McAree and Daniel's [58] approach for the 3-RPR platform. The cyan, blue, maroon and magenta curves are slices taken at  $a_4 = 3, 5, 7$ , and  $10$ , respectively. Notice that the blue and maroon curves in Figs. 3.3 represent the input/output curves from Fig. 3.2.

In general, forward position analysis is completed by substituting values for the input variables into Eq. 3.3 and using tangent-half-angle substitutions for the output variable [64]. The substitution converts sine and cosine equations of  $\theta_o$  into a polynomial equation of a new variable,  $t = \tan(\theta_o/2)$ . Alternatively, Wampler [65] presents a method that uses complex formulation of the loop equations and solves bilinear equations of exponential variables. Since the loop equations

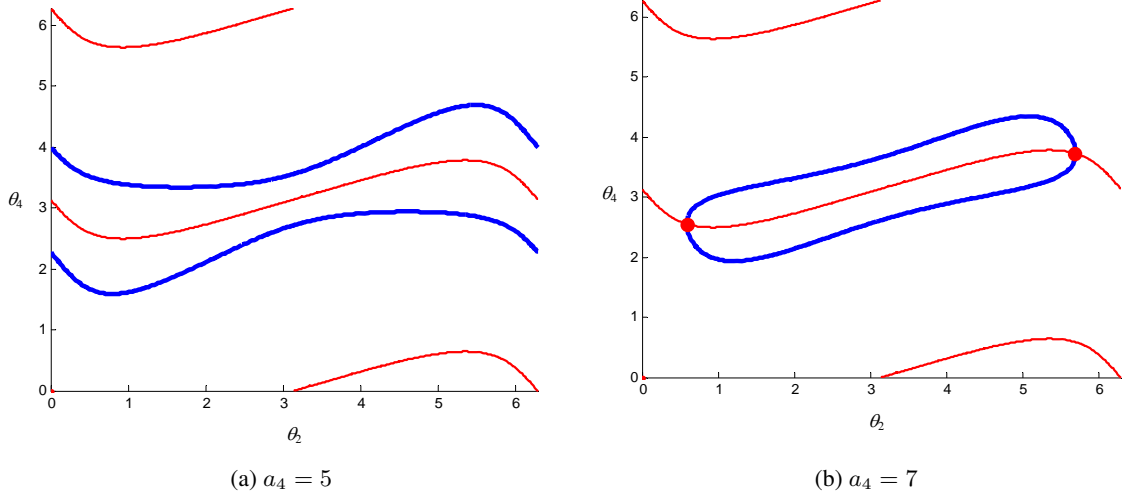


Figure 3.2: Input/output function (blue) of the RRRPR mechanism in Fig. 3.1 with  $a_1 = 5$ ,  $a_2 = 3$ , and  $a_3 = 4$ . The singularity function is also included (red).

are always generated in pairs with trigonometric functions, the order of the input/output equation will be an even value, yielding an even number of geometric inversions.

### 3.3 Singularity Function

Singular positions are associated with a mechanism configuration in which the matrix that relates the input speeds to the output speeds becomes rank deficient. The rank-deficient matrix is encountered as

$$F'_{\theta_o} = \frac{\partial F(\Theta_i, \theta_o)}{\partial \theta_o} = 0, \quad (3.5)$$

which is called a singularity function.

A singular position exists when both Eqs. 3.3 and 3.5 are satisfied. Gosselin and Angeles [41] refer to this as a Type 2 singularity, which corresponds to a configuration in which the output joint is



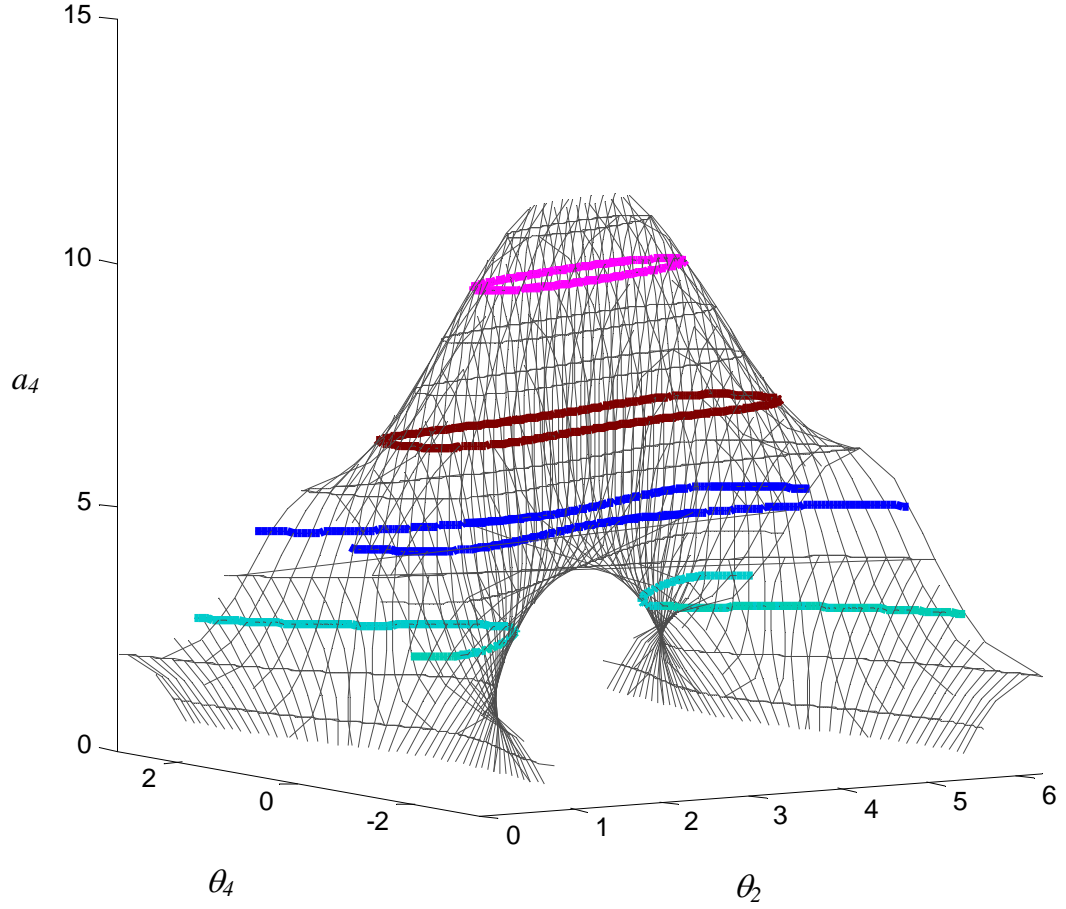


Figure 3.3: Geometric inversions of the RRRPR mechanism in Fig. 3.1 with  $a_1 = 5$ ,  $a_2 = 3$ , and  $a_3 = 4$  plotted in reduced configuration space.

locally movable even when the actuated joint is locked. It represents a set of points where different branches meet.

For the RRRPR mechanism in Fig 3.1 with the input/output function given in Eq. 3.4, the Type 2 singularity function is

$$F'_{\theta_4} = 2a_2a_3 \sin(\theta_2) \cos(\theta_4) - 2a_2a_3 \cos(\theta_2) \sin(\theta_4) + 2a_1a_3 \sin(\theta_4) = 0. \quad (3.6)$$

For the plots shown in Fig. 3.2, the red curve represents Eq. 3.6. Both Eqs. 3.4 and 3.6 are satisfied at the intersection of the input/output and singularity functions. In Fig. 3.2a, no intersections are present, revealing that both geometric inversions associated with  $\theta_2$  can rotate continuously without encountering a singularity. In Fig. 3.2b, the intersections are highlighted, showing that both geometric inversions associated with  $\theta_2$  meet at a singularity. Graphically, singularities exist as the slope of the input/output function becomes parallel with the axis of the output variable. In Fig. 3.2b, the red curve intersects the blue curve whenever the tangent of the blue curve becomes vertical. It is noted that the existence of singularities is dependent on the choice of input and unrelated to the choice of  $\theta_o$ .

For input/output functions that exhibit self-intersections, the  $F'$  curve will also intersect  $F$  at these points. Self-intersections are not singularities as the Jacobian of the loop equations relative to the output velocities does not lose rank. Thus, care must be taken as Eqs. 3.3 and 3.5 can result in extraneous solutions. As an example, an input/output plot for a Stephenson III mechanism that will be discussed in Section 3.8.3 is shown in Fig 3.4. Notice that the red curve crosses the blue at the self-intersection located at  $\theta_1 = -0.75$  and  $\theta_6 = 2.41$ . While these values satisfy  $F'$  and  $F$ , the linkage is not at a singularity.

A series of the singularity points at increasing values of  $a_4$  is superimposed on the 2-DOF input/output manifold of Fig. 3.3 and shown as Fig. 3.5. Again, this is equivalent to McAree and Daniel's [58] approach for the 3-RPR platform.

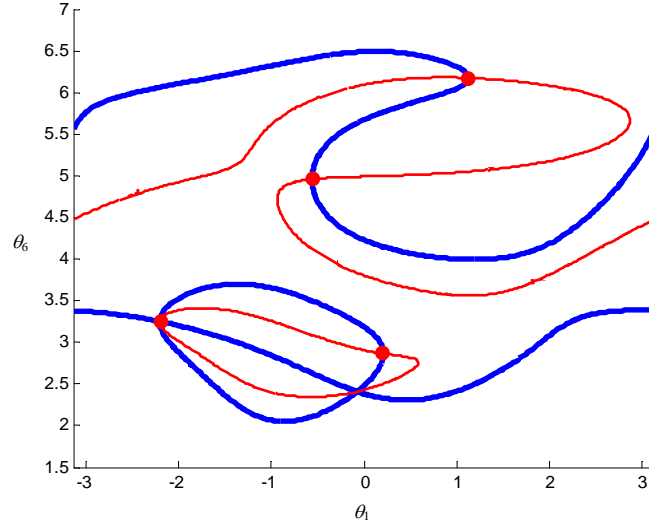


Figure 3.4: Input/output curve with a self-intersection.

### 3.4 Projection of the Singularity Locus

Equations 3.3 and 3.5 can be combined to eliminate  $\theta_o$  and form a function of the actuated joint variables and physical parameters. This function,

$$G(\Theta_i) = 0, \quad (3.7)$$

gives values of  $\Theta_i$  for which the mechanism will be in a singularity configuration. For the RRRPR linkage in Eq. 3.2,

$$\begin{aligned} G(\theta_2, a_4) = & 4a_3^2 \left( a_2^2 \sin^2(\theta_2) + a_2^2 \cos^2(\theta_2) + a_1^2 - 2a_1a_2 \cos(\theta_2) \right) \left( a_2^4 - 4a_1a_2^3 \cos(\theta_2) \right. \\ & + 4a_1^2a_2^2 \cos^2(\theta_2) - 4a_2^2a_3^2 \cos^2(\theta_2) + 2a_1^2a_2^2 + 2a_2^2a_3^2 - 4a_2^2a_3^2 \sin^2(\theta_2) \\ & - 2a_2^2a_4^2 - 4a_1a_2^3 \cos(\theta_2) + 4a_1a_2a_3^2 \cos(\theta_2) + 4a_1a_2a_4^2 \cos(\theta_2) + a_1^4 - 2a_1^2a_3^2 \\ & \left. + a_3^4 - 2a_1^2a_4^2 - 2a_3^2a_4^2 + a_4^4 \right) = 0. \end{aligned} \quad (3.8)$$

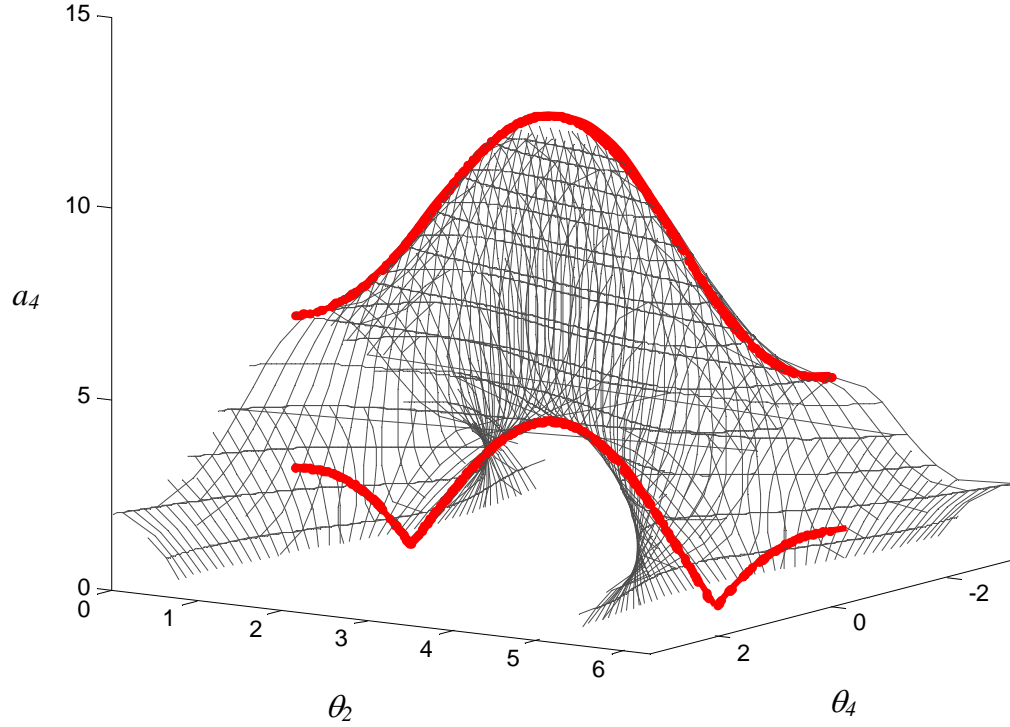


Figure 3.5: Singularities of the RRRPR mechanism in Fig. 3.1 with  $a_1 = 5$ ,  $a_2 = 3$ , and  $a_3 = 4$  plotted in reduced configuration space.

In the analysis of the 3-RPR platform, the plot of  $G(\Theta_i)$  in input joint space is termed the singularity locus [58, 62, 63]. The projected singularity curves divide the input joint space into regions having the same number of solutions to the forward kinematic problem (GIs) [58]. For the 3-RPR platform examined, each time the singularity curve is crossed, the number of geometric inversions changes by two [57, 58, 62, 63]. The singularity locus for the mechanism of Fig. 3.1 is shown in Fig. 3.6. The locus identifies the effect of the adjustment length of  $a_4$  on the number of singularities encountered and GI zones as the actuated variable ( $\theta_2$ ) moves.

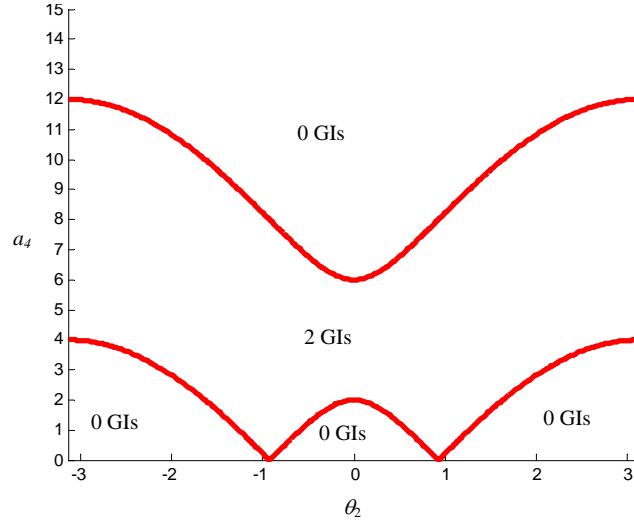


Figure 3.6: Singularity locus for an RRRPR mechanism with  $a_1 = 5$ ,  $a_2 = 3$ , and  $a_3 = 4$ .

### 3.5 Circuits

Assembly circuits are identified on an input/output plot as a disconnected continuous section of the curve [33]. If the choice of output is representative of all geometric inversions, the number of circuits can be observed from the input/output curve. If the Stephenson III mechanism shown in Fig. 3.7 is driven from within the four-bar loop with  $\theta_4$ , the output should be taken as either  $\theta_1$  or  $\theta_2$ . If  $\theta_o = \theta_5$  or  $\theta_6$ , the input/output plot will not represent all GIs as  $\theta_1$  and  $\theta_2$  can assume multiple positions for a specific location of the platform ( $\theta_6$ ).

The input/output plot in Fig. 3.2a has two circuits, that while in Fig. 3.2b has one. It is observed in Fig. 3.3 that the number of assembly circuits changes by one when the tangent plane of the manifold is parallel to the  $\theta_2 - \theta_4$  plane. Similarly, each local extreme point of the function in Eq. 3.7 is characterized by a change in the number of circuits. The singularity locus of Fig. 3.6

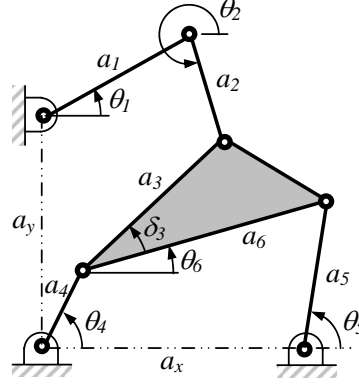


Figure 3.7: Choice of output should represent all geometric inversions.

is reproduced as Fig. 3.8 where the local extremes and the number of circuits for each zone are identified.

To determine the local extreme points of Fig. 3.8, the derivative is taken by identifying the actuated input as  $\theta_{act}$  and the adjustment input as  $\theta_{adj}$ ,

$$G'(\Theta_i) = \frac{\partial G / \partial \theta_{act}}{\partial G / \partial \theta_{adj}} = \frac{d\theta_{adj}}{d\theta_{act}} = 0. \quad (3.9)$$

The value of the adjustment input  $\theta_{adj}$  corresponding to the local extremes is obtained by combining Eqs. 3.7 and 3.9 to eliminate  $\theta_{act}$ . The resulting expressions identify the limits of  $\theta_{adj}$  as the boundary of mechanisms with different circuits.

For the RRRPR mechanism of Fig. 3.1,  $\theta_{act} = \theta_2$  and  $\theta_{adj} = a_4$ . Carrying out the process and solving for  $a_4$  at the change of number of circuits gives

$$\begin{aligned} a_4^{(1)} &= a_3 + a_2 - a_1, & a_4^{(2)} &= a_3 - a_2 - a_1, \\ a_4^{(3)} &= a_3 + a_2 + a_1, & a_4^{(4)} &= a_3 - a_2 + a_1, \\ a_4^{(5)} &= -a_3 + a_2 - a_1, & a_4^{(6)} &= -a_3 - a_2 - a_1, \end{aligned} \quad (3.10)$$

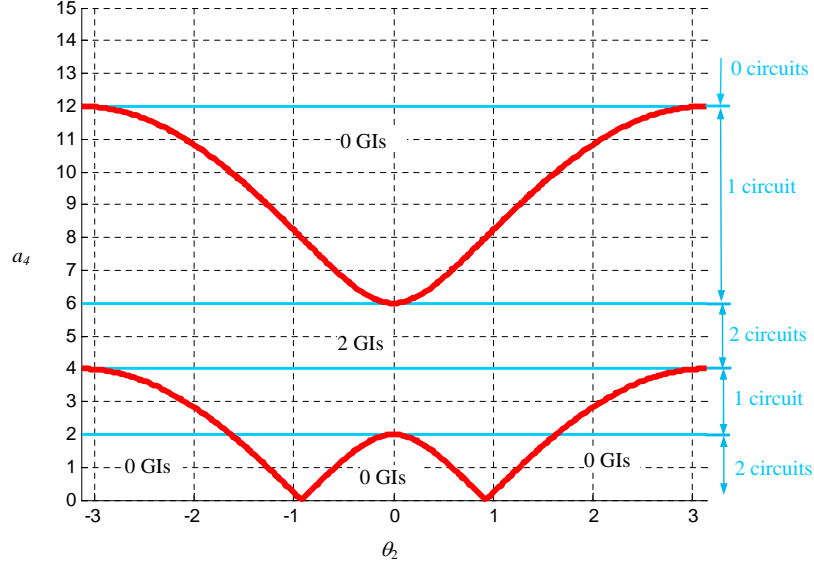


Figure 3.8: Singularity and circuit map for a five-bar mechanism with  $a_1 = 5$ ,  $a_2 = 3$ , and  $a_3 = 4$ .

$$a_4^{(7)} = -a_3 + a_2 + a_1, \quad a_4^{(8)} = -a_3 - a_2 + a_1.$$

Substituting  $a_1 = 5$ ,  $a_2 = 3$ , and  $a_3 = 4$  into Eq. 3.10 and considering only positive values gives  $a_4 = 2, 4, 6$  and  $12$ . These lengths serve as bounds between linkages with different numbers of circuits and can be clearly seen in Fig. 3.8.

### 3.6 Transition Functions

Murray et al. [53] developed a method to identify transition linkages that define boundaries where the behavior of the linkage changes. The transition conditions are determined as the non-square matrix of the derivative of the loop closure equations  $f_i$  with respect to all joint variables  $\theta_k$  loses rank. Thus,

$$\det \left[ \frac{\partial f_{2i-1}}{\partial \theta_k} \frac{\partial f_{2i}}{\partial \theta_k} \right] = 0. \quad (3.11)$$

Transition functions are generated by combining the set of equations from Eq. 3.11 and the loop equations to eliminate all joint variables. These transition functions contain only physical parameters and define boundary linkages between those with distinct motion characteristics. It is observed that the transition linkages coincide with the local extremes of Eq. 3.7. That is, transition conditions define mechanisms that border those with differing numbers of circuits. Implementing Eq. 3.11, the RRRPR mechanism generates expressions identical to Eq. 3.10.

It has also been found that

$$F = F'_{\theta_o} = F'_{\theta_i} = 0 \quad (3.12)$$

generate expressions identical to Eq. 3.10. Thus, any of the three Eqs. 3.9, 3.11, and 3.12 will yield adjustment expressions that define borders between linkages of differing number of circuits.

### 3.7 Motion Possibilities

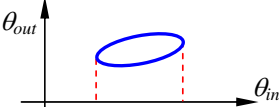
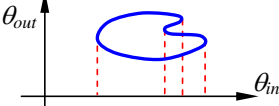
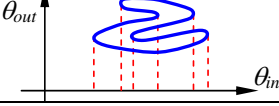
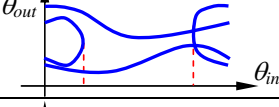
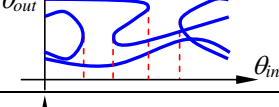
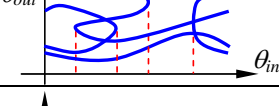
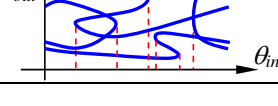
The singularity locus can be used to acquire the number of singularities, solutions and circuits associated with a specific adjustment variable. The motion possibilities were compiled for regions with one, two, three and four circuits, with up to 6 GI's and 6 singularities, and are shown in Tables 3.1, 3.2, 3.3, and 3.4, respectively. The order of the input/output function of a mechanism that can exhibit the motion is also given. A significant effort was undertaken to generate comprehensive tables, but a confirmation method is not yet available.

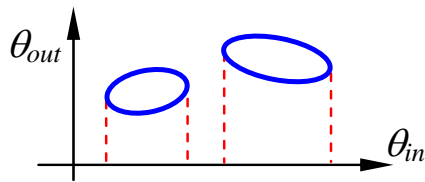
Whenever the motion possibility includes two circuits that each have two singularities, as shown in Fig. 3.9a, they can be replaced with the two circuits of Fig. 3.9b. Both input/output schemes exhibit the same number of circuits, GIs and singularities.

From Fig. 3.8, it is noticed that the zone between transition values of  $a_4 = 4$  and  $a_4 = 6$  has 2 solutions, 2 circuits and 0 singularities. This is described by Case 2d, indicating 2 circuits with

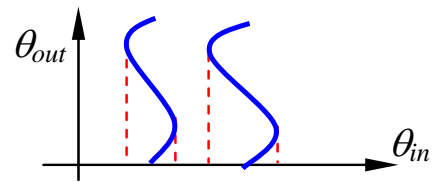


Table 3.1: One circuit motion possibilities.

Case	GI Zones	Number of Singularities	Input/Output Plot	Order		
				2	4	6
1a	0, 2	2		✓	✓	✓
1b	0, 2, 4	4			✓	✓
1c	0, 2, 4, 6	6				✓
1d	2, 4	2			✓	✓
1e	2, 4	4			✓	✓
1f	2, 4, 6	4				✓
1f	2, 4, 6	6				✓



(a)



(b)

Figure 3.9: 2 circuits with 2 GIs and 4 singularities.

Table 3.2: Two circuit motion possibilities.

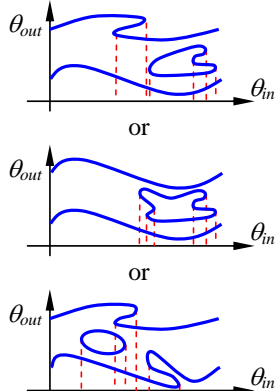
Case	GI Zones	Number of Singularities	Input/Output Plot	Order		
				2	4	6
2a	0, 2	4		✓	✓	✓
2b	0, 2, 4	4			✓	✓
2c	0, 2, 4	6				✓
2d	0, 2, 4, 6	6				✓
2e	2	0		✓	✓	✓
2f	2, 4	2			✓	✓
2g	2, 4	4			✓	✓
2h	2, 4, 6	4				✓

Table 3.3: Three circuit motion possibilities.

Case	GI Zones	Number of Singularities	Input/Output Plot	Order		
				2	4	6
3a	0, 2	6			✓	✓
3b	0, 2, 4	6			✓	✓
3c	0, 2, 4, 6	6		✓	✓	✓
3d	2, 4	2			✓	✓
3e	2, 4	4			✓	✓
3f	2, 4	6			✓	✓
3g	2, 4, 6	4				✓

a continuously rotating crank. Therefore, the adjustment variable positioned between these two transitions permits a fully rotatable  $\theta_2$ . This result can also be obtained from Grashof's criterion. Yet, the singularity locus is applicable to a variety of more complex mechanisms as demonstrated in the following examples.

Table 3.3: Three circuit motion possibilities (con't).

Case	GI Zones	Number of Singularities	Input/Output Plot	Order		
				2	4	6
3h	2, 4, 6	6				✓

### 3.8 Examples

#### 3.8.1 Example 3.1: Slider-Crank Mechanism

The process is applied to a slider-crank mechanism shown in Fig. 3.10 with  $a_1 = 2$  and  $a_2 = 4$ . The mechanism is actuated through link 2, driving  $\theta_2$ , and the output variable is taken as the position of the slider,  $a_4$ . The adjustment variable is  $a_3$ . For this case, the input/output relationship is  $2^{nd}$  order in  $a_4$ . The resulting singularity locus is shown as Fig. 3.11.

Using Eq 3.11, the transition functions are  $a_3 = a_1 + a_2 = 6$ ,  $a_3 = -a_1 + a_2 = 2$  [53]. The horizontal lines that separate the number of circuit regimes on Fig. 3.11 correspond exactly with these values. Geometrically, a slider-crank transition linkage will occur when links  $a_2$  and  $a_3$  become collinear with link  $a_1$ .

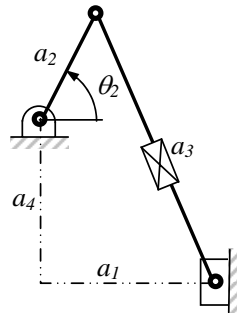


Figure 3.10: Slider-Crank Mechanism.

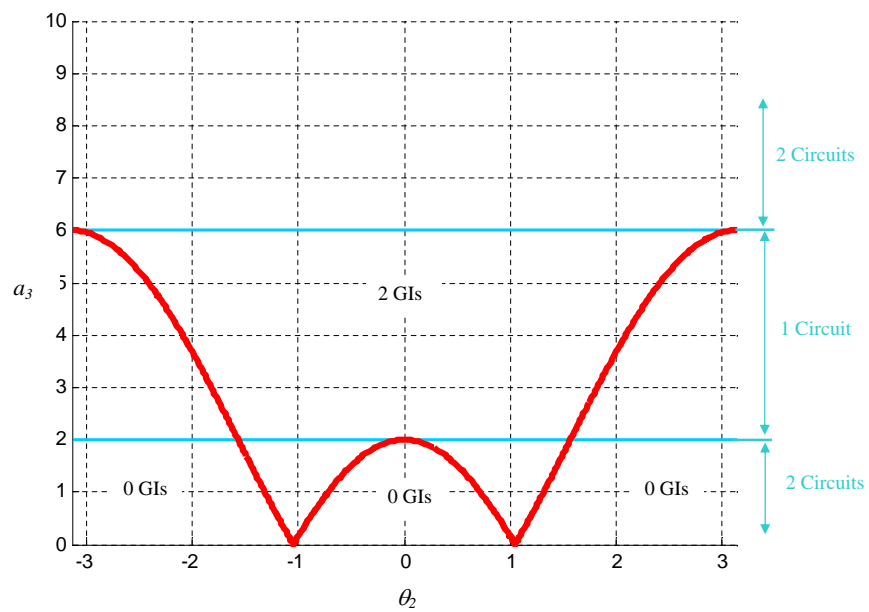


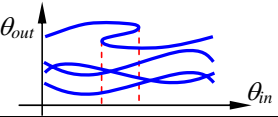
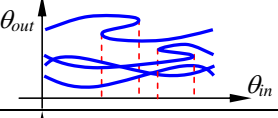
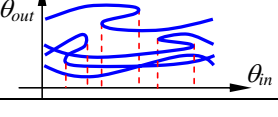
Figure 3.11: Design Map for a Slider-Crank Mechanism.

Table 3.4: Four circuit motion possibilities.

Case	GI Zones	Number of Singularities	Input/Output Plot	Order		
				2	4	6
3a	0, 2	6			✓	✓
3b	0, 2, 4	6			✓	✓
3c	0, 2, 4, 6	6		✓	✓	✓
3d	2, 4	2			✓	✓
3e	2, 4	4			✓	✓
3f	2, 4	6			✓	✓
3g	2, 4, 6	4				✓

With the aid of the locus, observations can be made such as selecting  $a_3 > 6$  ensures 2 geometric inversions, 2 circuits and 0 singularities. This is described by Case 2d, indicating two circuits with a continuously rotating crank.

Table 3.4: Four circuit motion possibilities (con't).

Case	GI Zones	Number of Singularities	Input/Output Plot	Order		
				2	4	6
4j	4, 6	2				✓
4k	4, 6	4				✓
4k	4, 6	6				✓

### 3.8.2 Example 3.2: Watt II Mechanism

The process is applied to a Watt II mechanism, shown in Fig. 3.12 with  $a_1 = 6$ ,  $a_2 = 3$ ,  $a_3 = 5$ ,  $a_4 = 5$ ,  $\delta = 40^\circ$ ,  $a_{6x} = 4$ ,  $a_{6y} = 1.5$ , and  $a_7 = 3$ . The mechanism is actuated through link 2, driving  $\theta_2$ , and the output variable was taken as the angle of link 8,  $\theta_8$ . The adjustment variable is  $a_8$ . For this case, the input/output relationship is 4<sup>th</sup> order in  $\theta_8$ . The resulting singularity locus is shown as Fig. 3.13.

The transition functions of a Watt II generated using Eq. 3.11 are more complex [53]. For this mechanism, transition values are calculated as  $a_8 = 1.6126, 3.6333, 4.8303, 5.2715, 7.6126, 9.6333, 10.8303, \text{ and } 11.2715$ . The horizontal lines that separate the number of circuit regimes on Fig. 3.13 correspond exactly with these values. Geometrically, a Watt II transition linkage will occur when links  $a_2$  and  $a_3$  become collinear while links  $a_7$  and  $a_8$  are collinear.

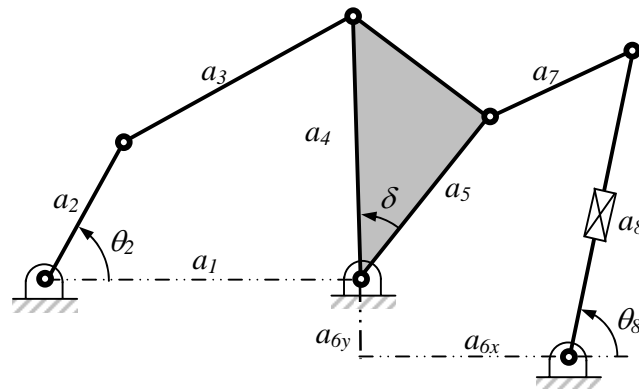


Figure 3.12: Watt II Mechanism.

With the aid of the locus, observations can be made such as selecting  $5.2715 < a_8 < 7.6126$  ensures 4 geometric inversions, 4 circuits and 0 singularities. This is described by Case 4i, indicating that all 4 circuits are associated with a continuously rotating crank. Further, setting  $4.8303 < a_8 < 5.2715$  or  $7.6126 < a_8 < 9.6333$  ensures 2 and 4 geometric inversions, 3 circuits and 2 singularities. This is described by Case 3d, indicating 2 geometric inversions will still be associated with a continuously rotating crank.

### 3.8.3 Example 3.3: Stephenson III Mechanism, Actuated through the Four-Bar Loop

The process is applied to a Stephenson III mechanism shown in Fig. 3.14, with  $a_x = 12$ ,  $a_y = 5.1$ ,  $a_1 = 2.930$ ,  $a_2 = 4.3012$ ,  $a_3 = 6.3738$ ,  $a_4 = 8.0623$ ,  $a_5 = 6.0208$  and  $\delta_3 = -30.32^\circ$ . The mechanism is actuated through link 4, driving  $\theta_4$ , and the output variable is taken as the angle of link  $a_1$  ( $\theta_1$ ). The adjustment variable is  $a_5$ . For this case, the input/output relationship is  $4^{th}$  order in  $\theta_1$ . The resulting singularity locus is shown as Fig. 3.15.



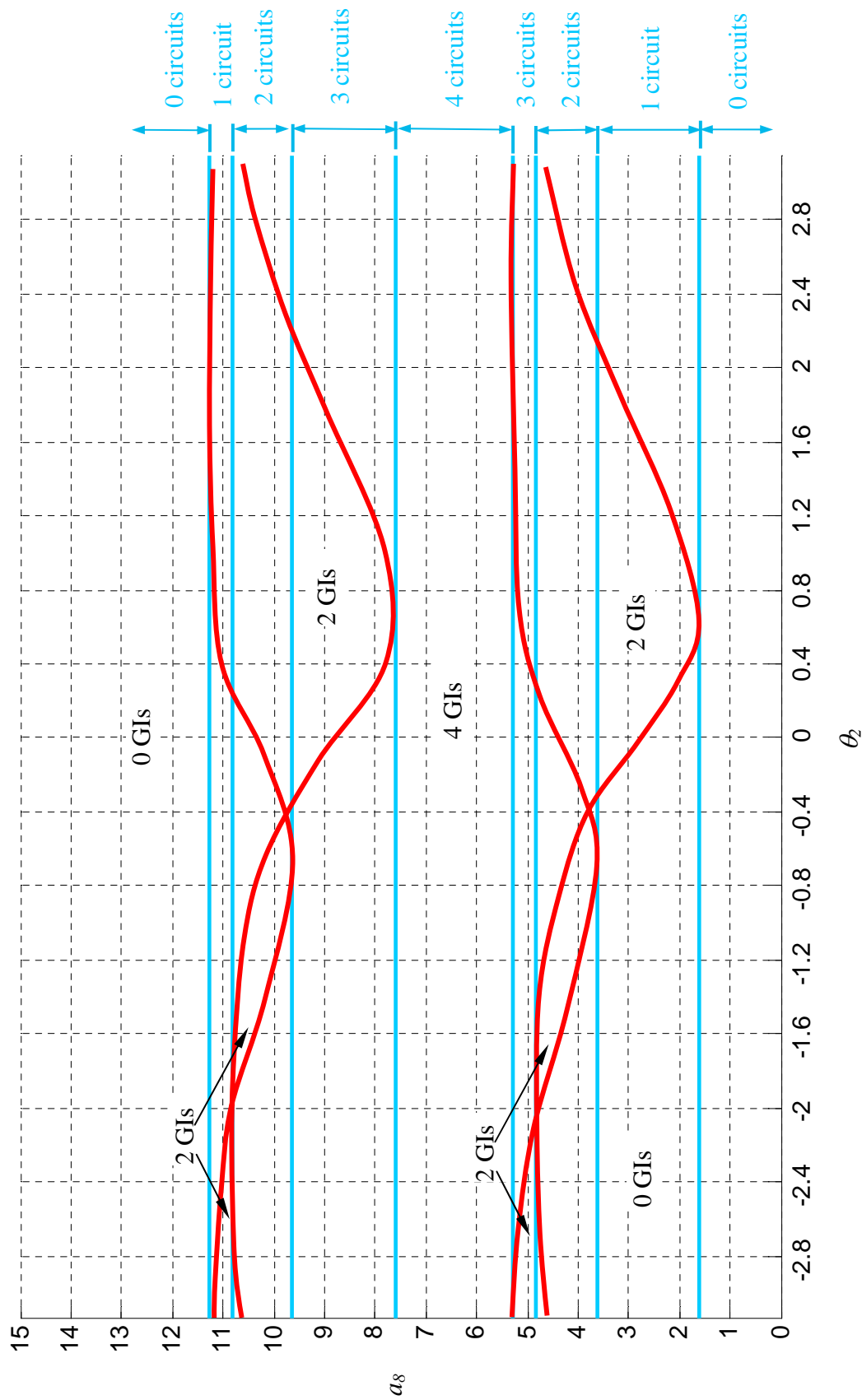


Figure 3.13: Design Map for a Watt II Mechanism.

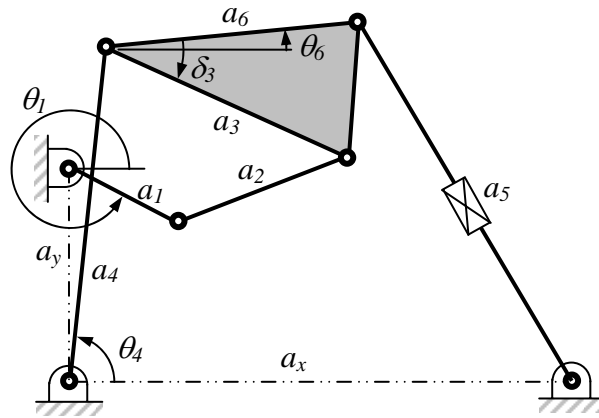


Figure 3.14: Stephenson III Mechanism.

Inspection of Fig. 3.15 reveals that no region of the locus corresponds to a continuously rotating crank. A peculiar occurrence is observed in that the number of GI's changes by 4 in the lower right portion of the plot. This reveals that two singularities are present at the same crank position. Due to complexity, expressions were not generated for the transition functions of the Stephenson III [53]. It is identified that a Stephenson III transition linkage will occur when links  $a_1$ ,  $a_4$  and  $a_5$  intersect at a common point, along with links  $a_1$  and  $a_2$  becoming collinear. In Murray's work, a numerical approach was used to generate acceptable design regions. Using the approach outlined in this chapter and Eq. 3.9, local extreme values are calculated as  $a_5 = 4.067, 8.162, 9.959, 10.165, 12.214, 13.329, 13.626, 15.115, 17.400, 18.421, \text{ and } 23.076$ . Figure 3.16 illustrates the orientation of the mechanism as transition conditions are satisfied.

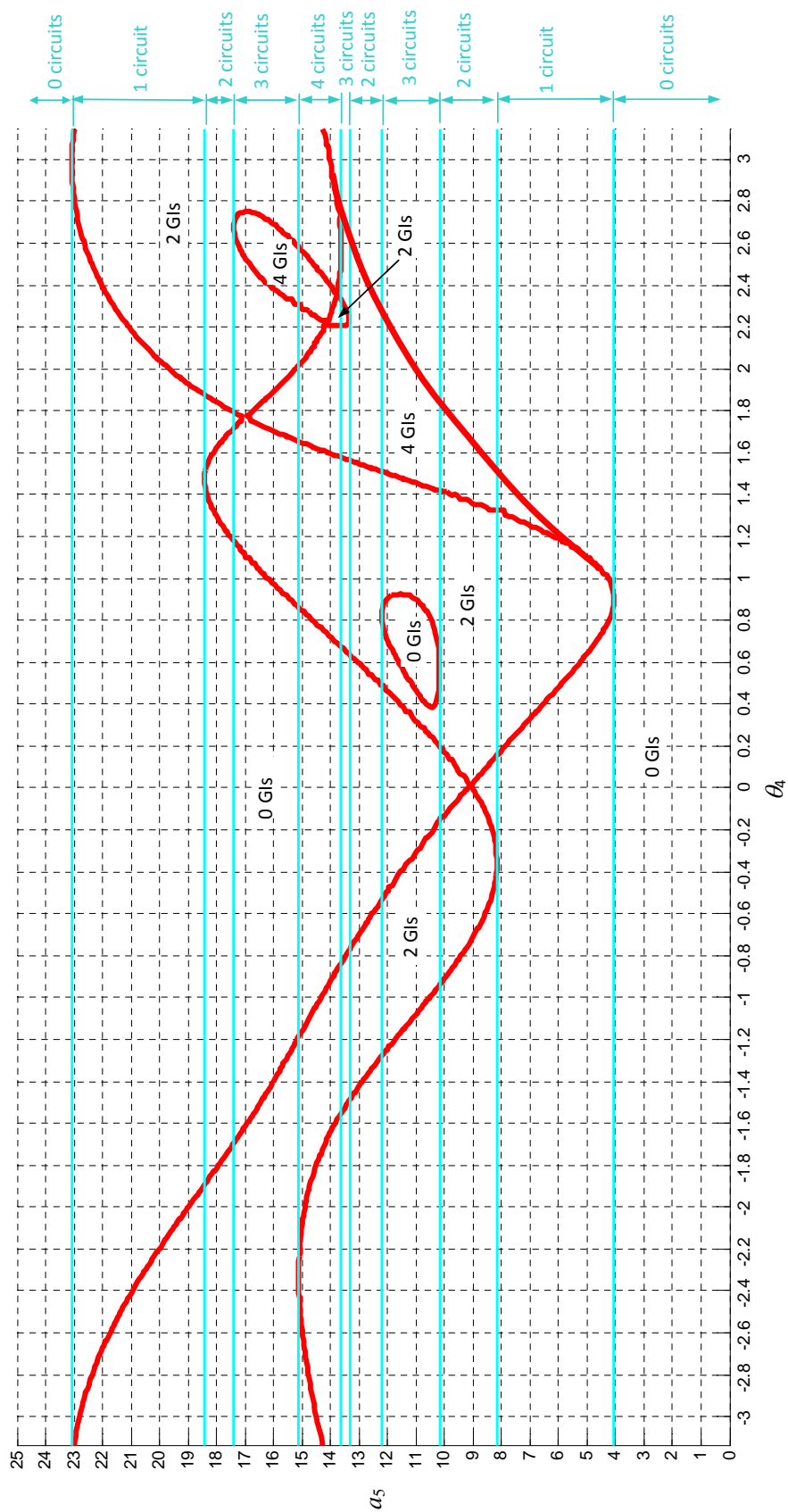


Figure 3.15: Singularity locus for a Stephenson III mechanism with  $\theta_4$  as input.

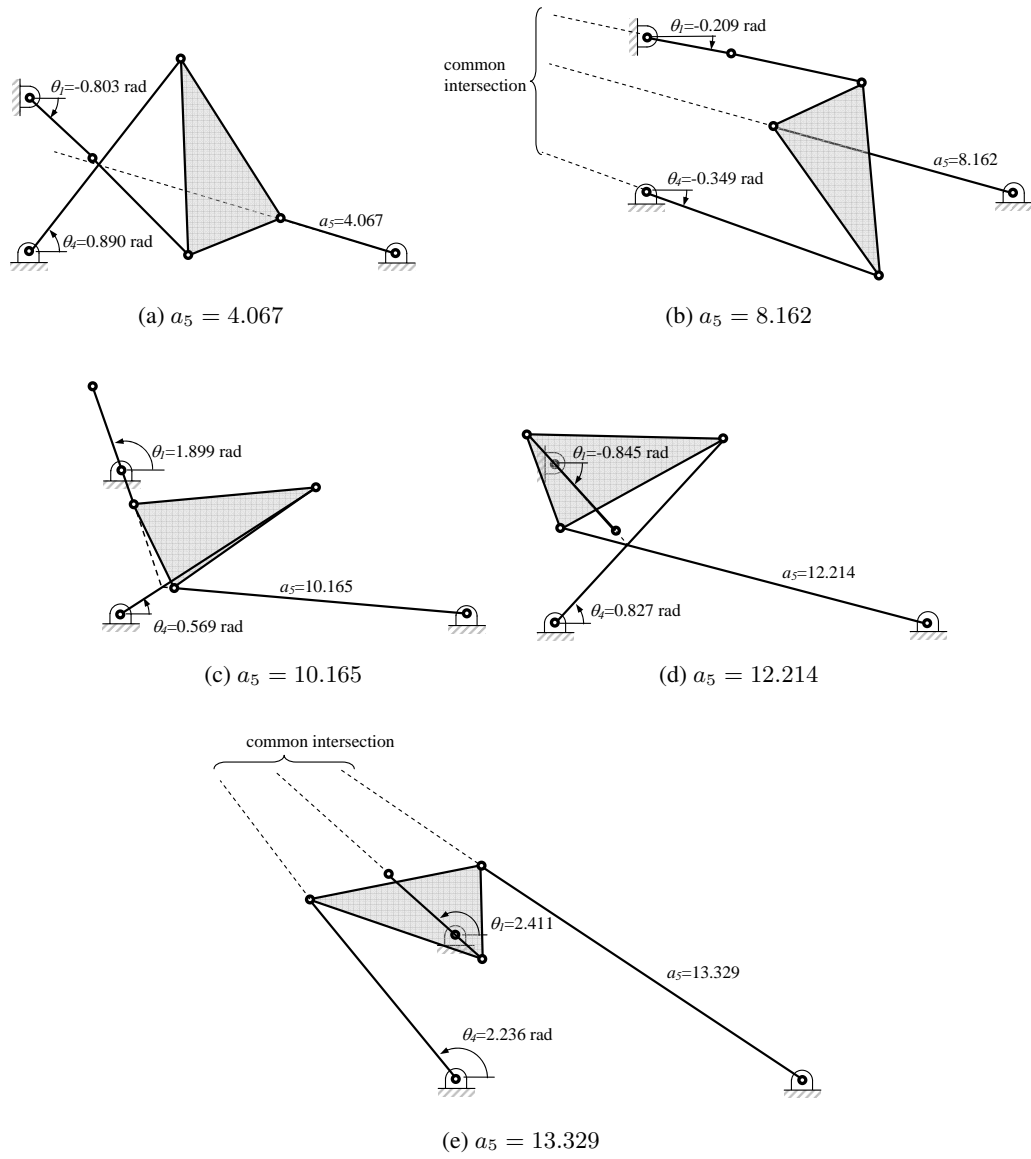


Figure 3.16: Transition configurations for Stephenson III of Fig. 3.14.

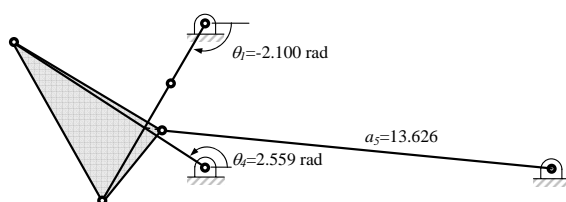
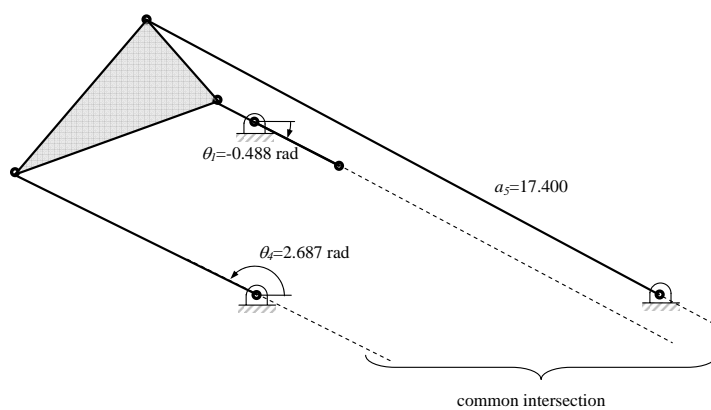
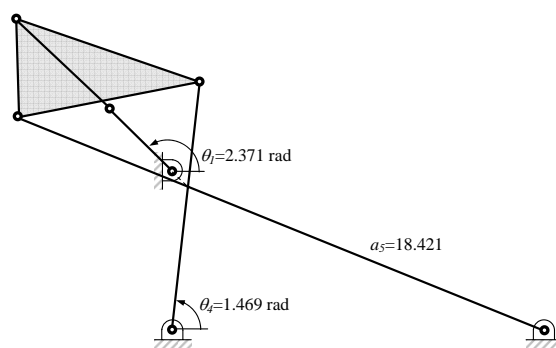
(f)  $a_5 = 13.626$ (g)  $a_5 = 17.400$ (h)  $a_5 = 18.421$ 

Figure 3.16: Transition configurations for Stephenson III of Fig. 3.14 (cont'd).

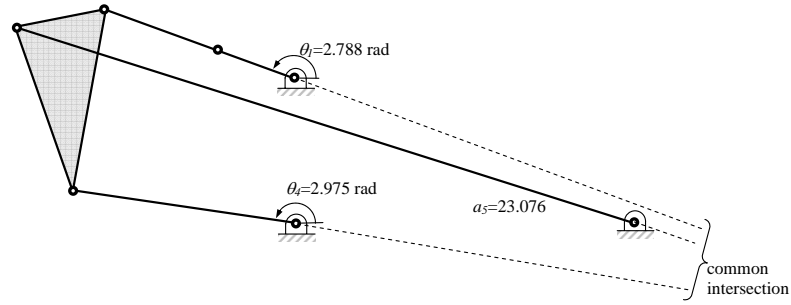
(i)  $a_5 = 23.076$ 

Figure 3.16: Transition configurations for Stephenson III of Fig. 3.14 (cont'd).

### 3.8.4 Example 3.4: Stephenson III Mechanism, Actuated through the Five-Bar Loop

The process is repeated on the Stephenson III mechanism shown in Fig. 3.14, but actuated through link 1, driving  $\theta_1$ . The output variable remains the angle of the platform,  $\theta_6$ , and the adjustment value remains  $a_5$ . This mechanism is identical to the mechanism studied by Chase and Mirth[33]. The input/output relationship is 6<sup>th</sup> order in  $\theta_6$ . The resulting singularity locus is shown as Fig. 3.17.

Again, local extremes are located as  $a_5 = 4.067, 8.162, 9.959, 10.165, 12.214, 13.329, 13.626, 15.115, 17.400, 18.421$ , and  $23.076$ . These values are identical to Fig. 3.15, which is consistent since the number of circuits is not a function of the input variable.

Many regions of a continuously rotating crank are revealed. The region bounded by  $16.000 \leq a_5 \leq 17.400$  exhibits 2 and 4 geometric inversions, 3 circuits, and 2 singularities. This corresponds with case 3d. Another continuously rotating crank is realized by setting  $13.626 \leq a_5 \leq 15.115$ . The singularity locus shows 2 and 4 geometric inversions, 4 circuits, and 4 singularities. This corresponds with case 4e.

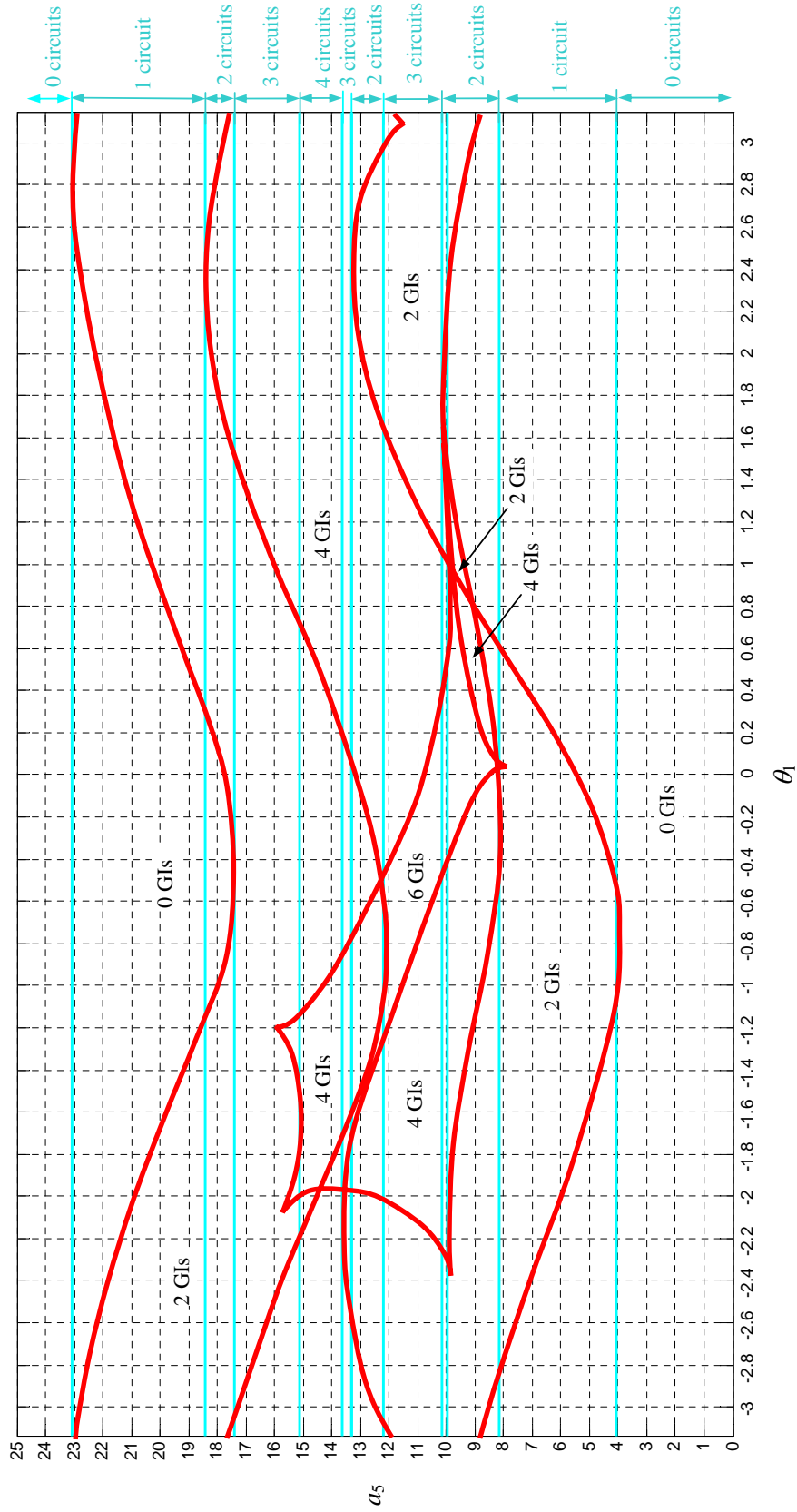


Figure 3.17: Singularity locus for a Stephenson III mechanism with  $\theta_1$  as input.

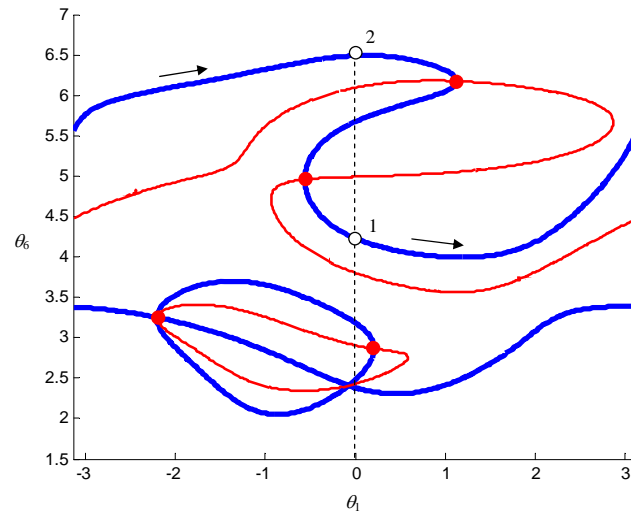
Chase and Mirth [33] cited that a value of  $a_5 = 11$  would generate a mechanism that contains a single branch with more than a full revolution of the input link. The singularity and circuit locus in Fig. 3.17 reveals this zone has 2, 4, and 6 solutions, 3 circuits and 4 singularities. This is described by Case 3g, indicating a possibility of a crank that travels greater than one revolution between singularities. The singularity locus shows that this motion scheme will exist for any  $10.165 \leq a_5 \leq 11.700$ . Figure 3.18a illustrates the input/output diagram for  $a_5 = 10.5$ . Notice that the blue curve extends greater than a full revolution without encountering a singularity. Figure 3.18b shows the two geometric inversions that lie on the same branch.

With aid of the singularity locus, another mechanism that contains a single branch with more than a full revolution of the input link is found. The region bounded by  $15.700 \leq a_5 \leq 16.000$  exhibits 2 and 4 geometric inversions, 3 circuits, and 4 singularities. This is described by Case 3e, indicating that the crank travel greater than one revolution between singularities. Figure 3.19a illustrates the input/output diagram for  $a_5 = 15.8$ . Notice that the blue curve extends just greater than a full revolution without encountering a singularity. Recall that a self-intersection on the input/output curve is not associated with a singularity. Figure 3.19b shows the two geometric inversions that lie on the same branch.

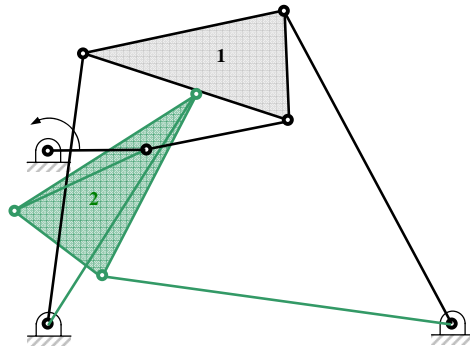
### 3.9 Summary

The work presented in this chapter extends the concepts used in the analysis of a 3-RPR platform to gain insight into single-actuated linkages. By generating a singularity locus, the number of singularities, geometric inversions, and circuit regimes are revealed. The input/output motion of the linkage can be inferred from the locus. The methodology to produce the singularity locus does not rely on geometrical conditions. By using the locus, desired operational features such as a





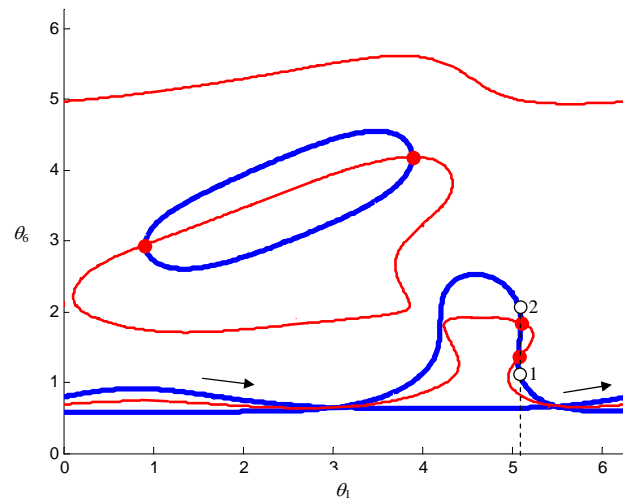
(a) Input/Output plot



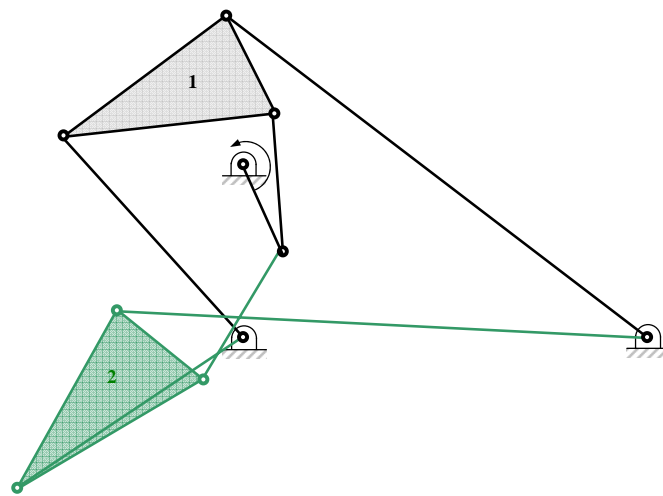
(b) Linkage Configurations

Figure 3.18: Stephenson III greater than one revolution, non-crank.

fully rotatable crank and unique motion characteristics, such as a greater than  $360^\circ$  non-rotatable crank can be identified. Further, it is observed that transition linkages serve as bounds between regions of different circuits. Examples presented include the Stephenson III linkage, actuated from within and outside the four-bar sub-chain. This linkage serves as the foundation for shape-changing mechanisms that approximate open curves.



(a) Input/Output plot



(b) Linkage Configurations

Figure 3.19: Stephenson III greater than one revolution, non-crank.

## CHAPTER IV

### SINGULARITY ANALYSIS OF AN EXTENSIBLE KINEMATIC ARCHITECTURE: ASSUR CLASS $N$ , ORDER $N - 1$

#### 4.1 Introduction

Branch defects and singularities were introduced in Section 1.3.2. This chapter presents a method to create a concise singularity equation for an Assur mechanism that contains a deformable closed contour [11]. Shape-changing mechanisms that approximate closed curves with  $N$  links in the “morphing contour” is classified as Assur Class  $N$ , Order  $N - 1$ . Significant difficulty has been experienced in locating an input link that rotates monotonically to drive among the desired shapes because the singular configurations are not intuitively identifiable. Generating the most concise statement of the singularities enables the designer to identify, and thus avoid, the special geometrical relationships that lead to singularities. This avoidance dramatically reduces the design space to be searched, speeding the synthesis process and enabling design optimization based upon more advanced criteria than simply singularity avoidance, such as force transmission.

The remainder of the chapter is organized as follows. The singularity condition is generated for a mechanism with three links in the closed contour in Section 4.3. Section 4.4 expands the analysis to an Assur IV/3 mechanism, while Section 4.5 deals with an Assur V/4. Section 4.6 utilizes these

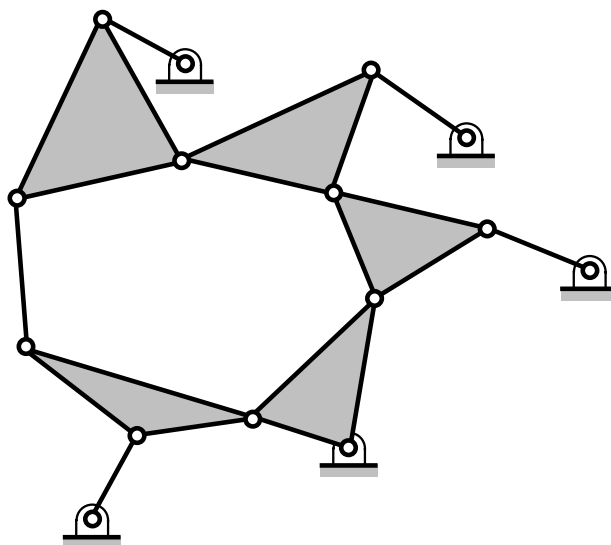
results to generalize the singularity condition for an Assur  $N/(N - 1)$ . Lastly, several illustrative examples are given in Section 4.9.

## 4.2 Assur Class Mechanisms

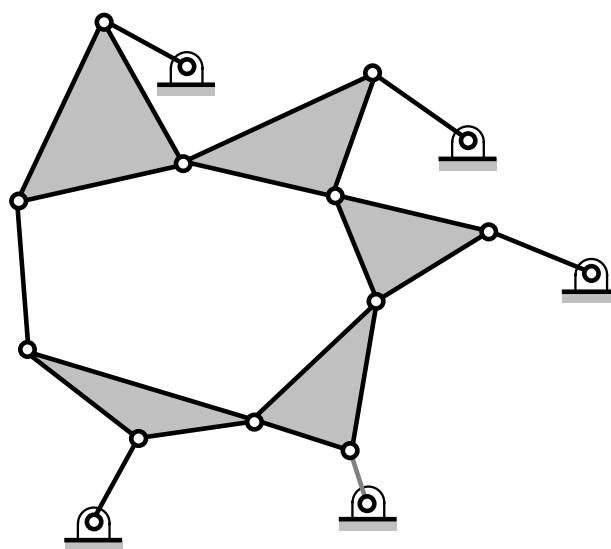
A classical approach for describing planar mechanism composition is with Assur groups. An Assur Kinematic Chain (AKC) is defined as the minimum arrangement of  $n$  links that creates a rigid structure [66]. That is, another rigid structure cannot be created by suppressing one or more links of an AKC. An AKC can be converted into a single-DOF mechanism by replacing one link in the structure by one pair of links. The mechanism shown in Fig. 4.1 is an Assur mechanism. If a dyad were removed, as indicated by the gray grounded pivot, an AKC structure would result. That is, no additional links could be suppressed to result in another structure.

Replacing a link of an existing mechanism with an AKC does not alter the number of degrees of freedom of the new mechanism. Thus, mechanisms of great complexity can be constructed by the sequential addition of AKCs to simpler chains [67]. The usefulness of AKCs arise in position analysis. Since an AKC is a structure, constraint equations can be readily generated to identify the position of all links in the chain. This approach allows a modularized approach to position analysis. Complex linkages can be analyzed by dividing them into a sequence of groups[68].

The class of an AKC is commonly referred to by the number of links contained in a deformable closed contour [69]. The order of an AKC refers to the number of external kinematic joints. Order, which is sometimes referred to as Series, can also be defined as the number binary links in the closed chain that are replaced with ternary, or quaternary links [70]. For example, if an Class IV AKC has two of the four links that comprise the closed chain as ternary, with the additional joints as free dyads, it is referred to as Order 2. This Assur mechanism is denoted as IV/2.



(a) Assur kinematic chain



(b) Assur mechanism

Figure 4.1: AKC that becomes an Assur Mechanism by adopting the pivot shown in gray.

The shape-changing mechanisms approximating closed curves described in Chapter 1 and shown in Fig. 1.3 are Assur Class  $N$ , Order  $N - 1$ . The Class arises because  $N$  links are incorporated in the shape-changing closed chain. The Order is because  $N - 1$  dyads are used to constrain the mechanism. The Order is also identified with  $N - 1$  ternary links included in the shape-changing loop. A general model of the Assur  $VI/5$  is illustrated in Fig. 4.1b.

### 4.3 Singularity Analysis of a Mechanism with Three Links in the Closed Contour

A mechanism with only three links defining the closed contour portion is shown in Fig. 4.2. The mechanism is composed of 6 moving links, 2 of which are ternary links, 7 revolute joints, and it has a single DOF. A closed kinematic chain of mobility 0 is obtained by suppressing one dyad,  $a_1$ . However, the resulting structure is not an AKC since additional links  $g_2$  and  $a_2$  can be subsequently suppressed to form another closed kinematic chain of mobility 0. Still, the mechanism is analogous to an Assur III/2.

It is noted that the mechanism in Fig. 4.2 is merely a four-bar linkage since the three links in the closed contour form a rigid structure. This trivial case is not a shape-changing mechanism, but is explored to develop singularity equations that provide a starting point for further generalizations.

The mechanism has 11 physical parameters ( $a_i, b_i, d_i, e_i, i = 1, 2$ , and  $f, g_{2x}, g_{2y}$ ) and 7 joint variables ( $\theta_1, \gamma_1, \psi_1, \theta_2, \phi_2, \psi_2, \beta$ ). The loop closure equations for the mechanism are

$$\begin{aligned}
 a_1 \cos \theta_1 + e_1 \cos \gamma_1 - g_{2x} - a_2 \cos \theta_2 - b_2 \cos \phi_2 &= 0, \\
 a_1 \sin \theta_1 + e_1 \sin \gamma_1 - g_{2y} - a_2 \sin \theta_2 - b_2 \sin \phi_2 &= 0, \\
 d_1 \cos \psi_1 + d_2 \cos \psi_2 + f \cos \beta &= 0, \\
 d_1 \sin \psi_1 + d_2 \sin \psi_2 + f \sin \beta &= 0,
 \end{aligned} \tag{4.1}$$

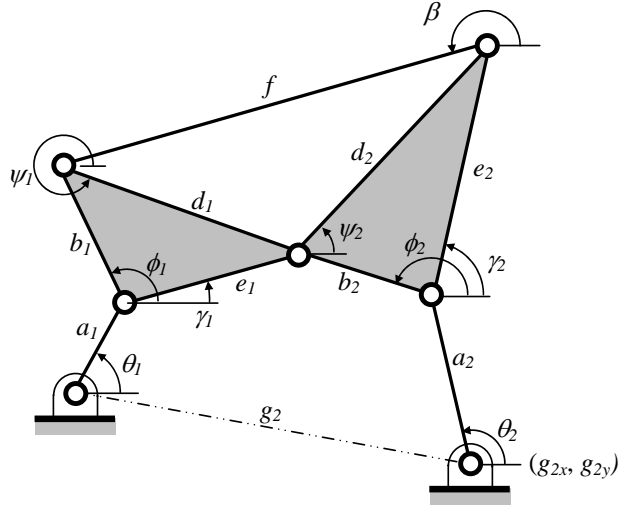


Figure 4.2: Mechanism with three links in the closed-contour.

$$\gamma_1 - \psi_1 - C_1 = 0, \quad \phi_2 - \psi_2 - C_2 = 0,$$

where  $C_1$  and  $C_2$  are constant interior angles within the rigid ternary links, noting that  $2b_1e_1 \cos C_1 = b_1^2 + e_1^2 - d_1^2$  and  $2b_2d_2 \cos C_2 = e_2^2 - b_2^2 - d_2^2$ . The time derivatives of the loop equations relate the velocities of the joint parameters, which is important in identifying the singular conditions. Being linear, the velocity equations can be written as

$$\vec{K}_3 \dot{\theta}_1 + M_3 \dot{v}_3 = 0, \quad (4.2)$$

where

$$\vec{K}_3 = \{-A_{1s}, A_{1c}, 0, 0, 0, 0\}^T, \quad (4.3)$$

$$M_3 = \begin{bmatrix} -E_{1s} & A_{2s} & B_{2s} & 0 & 0 & 0 \\ E_{1c} & -A_{2c} & -B_{2c} & 0 & 0 & 0 \\ 0 & 0 & 0 & -D_{1s} & -D_{2s} & -F_s \\ 0 & 0 & 0 & D_{1c} & D_{2c} & F_c \\ 1 & 0 & 0 & -1 & 0 & 0 \\ 0 & 0 & 1 & 0 & -1 & 0 \end{bmatrix}, \quad (4.4)$$

and

$$\vec{v}_3 = \left\{ \dot{\gamma}_1, \dot{\theta}_2, \dot{\phi}_2, \dot{\psi}_1, \dot{\psi}_2, \dot{\beta} \right\}^T \quad (4.5)$$

The nomenclature used in Eqs. 4.3 and 4.4 and continued through the remainder of this chapter paper is

$$\begin{aligned} A_{is} &= a_i \sin \theta_i, & A_{ic} &= a_i \cos \theta_i, & B_{is} &= b_i \sin \phi_i, & B_{ic} &= b_i \cos \phi_i, \\ D_{is} &= d_i \sin \psi_i, & D_{ic} &= d_i \cos \psi_i, & E_{is} &= e_i \sin \gamma_i, & E_{ic} &= e_i \cos \gamma_i, \end{aligned} \quad (4.6)$$

for  $1 \leq i \leq N - 1$ , and

$$F_s = f \sin \beta, \quad F_c = f \cos \beta. \quad (4.7)$$

When driving the mechanism with  $a_1$ , a singularity is encountered when the matrix  $M_3$  in Eq. 4.2 loses rank,

$$\det [M_3] = 0. \quad (4.8)$$

Taking the determinant generates the singularity equation

$$\begin{aligned} &A_{2s}B_{2c}D_{1c}F_s - A_{2c}B_{2s}D_{1c}F_s - A_{2s}B_{2c}D_{1s}F_c + A_{2c}B_{2s}D_{1s}F_s \\ &+ A_{2c}D_{2s}E_{1s}F_c - A_{2c}D_{2c}E_{1s}F_s - A_{2s}D_{2s}E_{1c}F_c + A_{2s}D_{2c}E_{1c}F_s = 0. \end{aligned} \quad (4.9)$$

Fully expanded, Eq. 4.9 contains 8 terms. With trigonometric substitutions, the singularity equation can be simplified to a concise form with 2 terms,

$$d_1 b_2 \sin(\phi_2 - \theta_2) \sin(\psi_1 - \beta) + e_1 d_2 \sin(\gamma_1 - \theta_2) \sin(\psi_2 - \beta) = 0. \quad (4.10)$$

Equation 4.10 presents the general singularity condition for a mechanism with 3 links in its closed contour, 2 of which are ternary links. That is, the mechanism driven by  $\theta_1$  will become stationary if Eq. 4.10 holds.



Written in the form of Eq. 4.10, special geometrical relationships that create the singularity are readily identified. For example, a singularity exists if links  $e_1$ ,  $b_2$ , and  $a_2$  are parallel, giving  $\gamma_1 = \phi_2(\pm\pi) = \theta_2(\pm\pi)$ . Note, however, that this creates two additional constraint equations on a single-DOF mechanism. Therefore, this case will not arbitrarily exist unless an additional relationship between the physical parameters in Eq. 4.1 is enforced. This situation is further explored in Section 4.6.

Starting from the determinant, Eq. 4.10 could not be produced using MATLAB's standard algebraic and trigonometric simplification tools without knowing the form of the equation a priori. Obtaining the most concise statement of the singularities enables the designer to identify, and thus avoid, the special geometrical relationships that lead to singularities. Without the benefit of mathematical software, another tool that generates the most concise statement is desired and presented in Section 4.5.

#### 4.4 Singularity Analysis of a Mechanism with a Four-Link Deformable Closed Contour: Assur IV/3

A mechanism with four links defining the deformable closed contour is shown in Fig. 4.3. This single-DOF mechanism is categorized as an Assur IV/3 which contains 7 moving links, 3 being ternary, and 10 revolute joints. It has 17 physical parameters ( $a_i, b_i, d_i, e_i, i = 1, 3$  and  $f, g_{2x}, g_{2y}, g_{3x}, g_{3y}$ ) and 11 joint variables ( $\theta_1, \gamma_1, \psi_1, \theta_2, \phi_2, \gamma_2, \psi_2, \theta_3, \phi_3, \psi_3, \beta$ ). The loop closure equations are

$$a_1 \cos \theta_1 + e_1 \cos \gamma_1 - g_{2x} - a_2 \cos \theta_2 - b_2 \cos \phi_2 = 0,$$

$$a_1 \sin \theta_1 + e_1 \sin \gamma_1 - g_{2y} - a_2 \sin \theta_2 - b_2 \sin \phi_2 = 0,$$

$$a_2 \cos \theta_2 + e_2 \cos \gamma_2 - g_{3x} - a_3 \cos \theta_3 - b_3 \cos \phi_3 = 0,$$

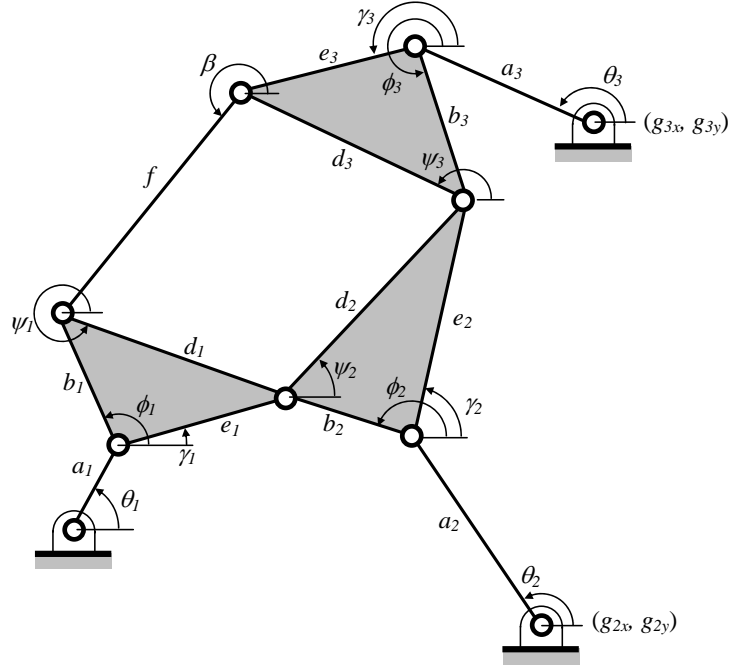


Figure 4.3: Assur IV/3 mechanism.

$$a_2 \sin \theta_2 + e_2 \sin \gamma_2 - g_{3y} - a_3 \sin \theta_3 - b_3 \sin \phi_3 = 0, \quad (4.11)$$

$$d_1 \cos \psi_1 + d_2 \cos \psi_2 + d_3 \cos \psi_3 + f \cos \beta = 0,$$

$$d_1 \sin \psi_1 + d_2 \sin \psi_2 + d_3 \sin \psi_3 + f \sin \beta = 0,$$

$$\gamma_1 - \psi_1 - C_1 = 0, \quad \phi_2 - \psi_2 - C_2 = 0,$$

$$\gamma_2 - \psi_2 - C_3 = 0, \quad \phi_3 - \psi_3 - C_4 = 0.$$

In addition to  $C_1$  and  $C_2$  defined in the previous case, constants  $C_3$  and  $C_4$  are used in the loop equations to ensure that the ternary links remain rigid. Again, the constants can be expressed in terms of the physical parameters,  $2d_2e_2 \cos C_3 = d_2^2 + e_2^2 - b_2^2$  and  $2b_3d_3 \cos C_4 = e_3^2 - b_3^2 - d_3^2$ .

Taking the time derivative of the loop equations and arranging into matrix form gives

$$\vec{K}_4 \dot{\theta}_1 + M_4 \dot{v}_4 = 0, \quad (4.12)$$

where

$$\vec{K}_4 = \{-A_{1s}, A_{1c}, 0, 0, 0, 0, 0, 0, 0, 0\}^T, \quad (4.13)$$

$$M_4 = \begin{bmatrix} -E_{1s} & -A_{2s} & B_{2s} & 0 & 0 & 0 & 0 & 0 & 0 & 0 \\ E_{1c} & A_{2c} & -B_{2c} & 0 & 0 & 0 & 0 & 0 & 0 & 0 \\ 0 & -A_{2s} & 0 & -E_{2s} & A_{3s} & B_{3s} & 0 & 0 & 0 & 0 \\ 0 & A_{2c} & 0 & E_{2c} & -A_{3c} & -B_{3c} & 0 & 0 & 0 & 0 \\ 0 & 0 & 0 & 0 & 0 & 0 & -D_{1s} & -D_{2s} & -D_{3s} & -f_s \\ 0 & 0 & 0 & 0 & 0 & 0 & D_{1c} & D_{2c} & D_{3c} & f_c \\ 1 & 0 & 0 & 0 & 0 & 0 & -1 & 0 & 0 & 0 \\ 0 & 0 & 1 & 0 & 0 & 0 & 0 & -1 & 0 & 0 \\ 0 & 0 & 0 & 1 & 0 & 0 & 0 & -1 & 0 & 0 \\ 0 & 0 & 0 & 0 & 0 & 1 & 0 & 0 & -1 & 0 \end{bmatrix}, \quad (4.14)$$

and

$$\dot{v}_4 = \{\dot{\gamma}_1, \dot{\theta}_2, \dot{\phi}_2, \dot{\gamma}_2, \dot{\theta}_3, \dot{\phi}_3, \dot{\psi}_1, \dot{\psi}_2, \dot{\psi}_3, \dot{\beta}\}^T. \quad (4.15)$$

When driving the mechanism with  $a_1$ , a singularity will be encountered when

$$\det[M_4] = 0. \quad (4.16)$$

Taking the determinant generates the singularity equation

$$\begin{aligned} & A_{2c}A_{3s}F_cE_{1s}D_{2s}B_{3s} + A_{2c}A_{3s}F_sE_{1s}D_{2c}B_{3c} + A_{2s}A_{3s}F_sE_{1c}D_{2s}B_{3c} \\ & + A_{2s}A_{3c}F_sE_{1c}D_{2c}B_{3s} - A_{2c}A_{3c}F_sE_{1s}D_{2c}B_{3s} - A_{2c}A_{3s}F_cE_{1s}D_{2s}B_{3c} \\ & - A_{2s}A_{3c}F_cE_{1c}D_{2s}B_{3s} - A_{2s}A_{3s}F_sE_{1c}D_{2c}B_{3c} + A_{2c}A_{3c}F_cE_{1s}E_{2s}D_{3s} \\ & + A_{2c}A_{3s}F_sE_{1s}E_{2c}D_{3c} + A_{2s}A_{3c}F_sE_{1c}E_{2s}D_{3c} + A_{2s}A_{3s}F_cE_{1c}E_{2c}D_{3s} \\ & - A_{2s}A_{3s}F_sE_{1c}E_{2c}D_{3c} - A_{2c}A_{3c}F_sE_{1s}E_{2s}D_{3c} - A_{2c}A_{3s}F_cE_{1s}E_{2c}D_{3s} \end{aligned} \quad (4.17)$$

$$\begin{aligned}
& -A_{2s}A_{3c}F_cE_{1c}E_{2s}D_{3s} + A_{2s}A_{3c}F_sE_{1s}B_{2c}D_{3c} + A_{2c}A_{3s}F_cE_{1s}B_{2c}D_{3s} \\
& + A_{2c}A_{3s}F_sE_{1c}B_{2s}D_{3c} + A_{2s}A_{3c}F_cE_{1c}B_{2s}D_{3s} - A_{2c}A_{3s}F_sE_{1s}B_{2c}D_{3c} \\
& - A_{2s}A_{3c}F_cE_{1s}B_{2c}D_{3s} - A_{2s}A_{3c}F_sE_{1c}B_{2s}D_{3c} - A_{2c}A_{3s}F_cE_{1c}B_{2s}D_{3s} \\
& + A_{2s}A_{3s}F_cD_{1s}B_{2c}B_{3c} + A_{2c}A_{3s}F_cD_{1c}B_{2c}B_{3s} + A_{2c}A_{3s}F_sD_{1c}B_{2s}B_{3c} \\
& + A_{2c}A_{3c}F_cD_{1s}B_{2s}B_{3s} - A_{2s}A_{3c}F_cD_{1s}B_{2c}B_{3s} - A_{2c}A_{3s}F_cD_{1s}B_{2s}B_{3c} \\
& - A_{2s}A_{3s}F_sD_{1c}B_{2c}B_{3c} - A_{2c}A_{3c}F_sD_{1c}B_{2s}B_{3s} = 0.
\end{aligned}$$

After factoring and substituting the appropriate trigonometric relationships, the singularity equation for an Assur IV/3 mechanism, driven with  $a_1$ , reduces to

$$\begin{aligned}
& d_1b_2b_3 \sin(\phi_2 - \theta_2) \sin(\phi_3 - \theta_3) \sin(\psi_1 - \beta) \\
& + e_1d_2b_3 \sin(\gamma_1 - \theta_2) \sin(\phi_3 - \theta_3) \sin(\psi_2 - \beta) \\
& + e_1b_2d_3 \sin(\gamma_1 - \phi_2) \sin(\theta_3 - \theta_2) \sin(\psi_3 - \beta) \\
& + e_1e_2d_3 \sin(\gamma_1 - \theta_2) \sin(\gamma_2 - \theta_3) \sin(\psi_3 - \beta) = 0.
\end{aligned} \tag{4.18}$$

The 32 terms in Eq. 4.17 reduce to 4 terms in Eq. 4.18, and again, specialized geometrical relationships can be more readily detected with the reduced version. For example, a singularity exists if links  $e_1$ ,  $a_2$ ,  $a_3$ , and  $b_3$  are parallel, giving  $\gamma_1 = \theta_2(\pm\pi) = \theta_3(\pm\pi) = \phi_3(\pm\pi)$ . Note, however, that this creates three additional constraint equations on a single-DOF mechanism. Therefore, this case will not arbitrarily exist unless two additional relationships between the physical parameters in Eq. 4.11 are enforced.

With a judicious change in definition of the variables, these results can be utilized for mechanisms driven with the other outer dyad  $a_3$ . Note that Eq. 4.12 can be regrouped with the middle dyad  $a_2$  as the driving link (resulting in a different  $\vec{K}$  and  $M_4$ ). Following the process outlined

above, a singularity equation with 24 terms is generated. A reduced singularity condition with only 3 terms is

$$\begin{aligned}
 & d_1 b_2 b_3 \sin(\phi_2 - \theta_1) \sin(\phi_3 - \theta_3) \sin(\psi_1 - \beta) \\
 & + e_1 d_2 b_3 \sin(\gamma_1 - \theta_1) \sin(\phi_3 - \theta_3) \sin(\psi_2 - \beta) \\
 & + e_1 e_2 d_3 \sin(\gamma_1 - \theta_1) \sin(\gamma_2 - \theta_3) \sin(\psi_3 - \beta) = 0.
 \end{aligned} \tag{4.19}$$

#### 4.5 Singularity Analysis of a Mechanism with a Five-Link Deformable Closed Contour: Assur V/4

A mechanism with five links defining the deformable closed contour is shown in Fig. 4.4. This single-DOF mechanism is categorized as an Assur V/4 with 9 moving links, 4 of which are ternary, and 13 revolute joints. Completing an analysis identical to those leading to Eqs. 4.10 and 4.18, the following singularity condition applies to the Assur V/4.

$$\begin{aligned}
 & d_1 b_2 b_3 b_4 \sin(\phi_2 - \theta_2) \sin(\phi_3 - \theta_3) \sin(\phi_4 - \theta_4) \sin(\psi_1 - \beta) \\
 & + e_1 d_2 b_3 b_4 \sin(\gamma_1 - \theta_2) \sin(\phi_3 - \theta_3) \sin(\phi_4 - \theta_4) \sin(\psi_2 - \beta) \\
 & + e_1 e_2 d_3 b_4 \sin(\gamma_1 - \theta_2) \sin(\gamma_2 - \theta_3) \sin(\phi_4 - \theta_4) \sin(\psi_3 - \beta) \\
 & + e_1 b_2 d_3 b_4 \sin(\gamma_1 - \phi_2) \sin(\theta_3 - \theta_2) \sin(\phi_4 - \theta_4) \sin(\psi_3 - \beta) \\
 & + e_1 e_2 b_3 d_4 \sin(\gamma_1 - \theta_2) \sin(\gamma_2 - \phi_3) \sin(\theta_4 - \theta_3) \sin(\psi_4 - \beta) \\
 & + e_1 b_2 b_3 d_4 \sin(\gamma_1 - \phi_2) \sin(\phi_3 - \theta_2) \sin(\theta_4 - \theta_3) \sin(\psi_4 - \beta) \\
 & + e_1 e_2 e_3 d_4 \sin(\gamma_1 - \theta_2) \sin(\gamma_2 - \theta_3) \sin(\gamma_3 - \theta_4) \sin(\psi_4 - \beta) \\
 & + e_1 b_2 e_3 d_4 \sin(\gamma_1 - \phi_2) \sin(\theta_3 - \theta_2) \sin(\gamma_3 - \theta_4) \sin(\psi_4 - \beta) = 0
 \end{aligned} \tag{4.20}$$

The general equation of 64 terms reduces to the 8 terms of Eq. 4.20. By judiciously redefining the parameters, the condition can be utilized for mechanisms driven with the other outer dyad  $a_4$ .

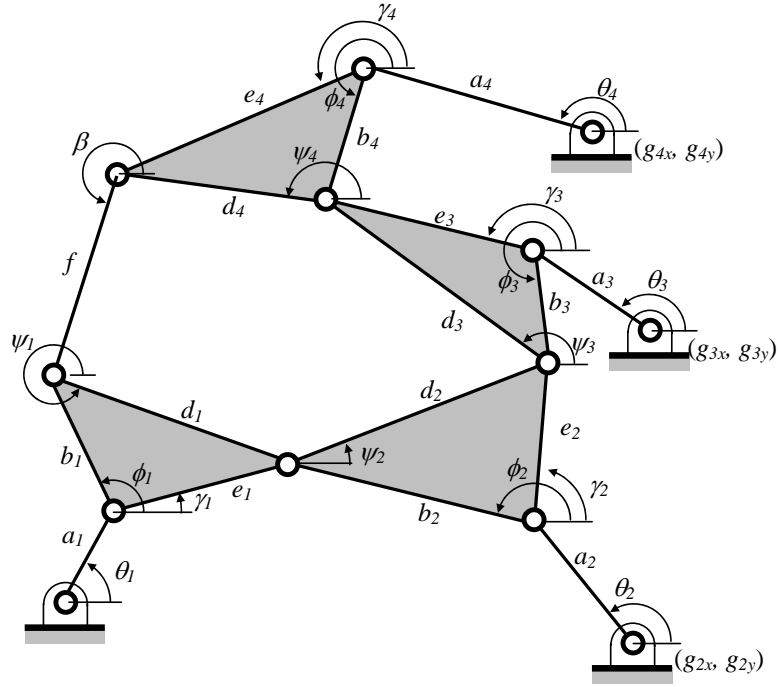


Figure 4.4: Assur V/4 mechanism.

As in the Assur IV/3 case, the singularity analysis can be completed with  $a_2$  as the driving link.

The reduced singularity condition is

$$\begin{aligned}
 & d_1 b_2 b_3 b_4 \sin(\phi_2 - \theta_1) \sin(\phi_3 - \theta_3) \sin(\phi_4 - \theta_4) \sin(\psi_1 - \beta) \\
 & + e_1 d_2 b_3 b_4 \sin(\gamma_1 - \theta_1) \sin(\phi_3 - \theta_3) \sin(\phi_4 - \theta_4) \sin(\psi_2 - \beta) \\
 & + e_1 e_2 d_3 b_4 \sin(\gamma_1 - \theta_1) \sin(\gamma_2 - \theta_3) \sin(\phi_4 - \theta_4) \sin(\psi_3 - \beta) \\
 & + e_1 e_2 b_3 d_4 \sin(\gamma_1 - \theta_1) \sin(\gamma_2 - \phi_3) \sin(\theta_4 - \theta_3) \sin(\psi_4 - \beta) \\
 & + e_1 e_2 e_3 d_4 \sin(\gamma_1 - \theta_1) \sin(\gamma_2 - \theta_3) \sin(\gamma_3 - \theta_4) \sin(\psi_4 - \beta) = 0.
 \end{aligned} \tag{4.21}$$

The general equation of 40 terms reduces to the 5 terms of Eq. 4.21, which more clearly reveals geometric relationships. As before, by redefining parameters, the condition can be utilized for mechanisms driven with  $a_3$ .

#### 4.6 Singularity Analysis of a Mechanism with an $N$ -Link Deformable Closed Contour: Assur $N/(N - 1)$

When extending the Assur Class of the mechanism, it became apparent that the new singularity condition built upon the condition associated with the lower class mechanism. A series of rules were formulated that allows construction of the higher class mechanism. A general model of the Assur  $N/(N - 1)$  is illustrated in Figure 4.5. The singularity condition for Class  $N - 1$ , when driving with  $\theta_1$ , can be used to generate the Class  $N$  singularity condition by making the following modifications:

1. Each of the initial  $2^{N-3}$  terms is multiplied by  $b_{N-1} \sin(\phi_{N-1} - \theta_{N-1})$ .
2.  $2^{N-3}$  new terms are created, each including the product  $e_1 d_{N-1} \sin(\psi_{N-1} - \beta)$ .
3. Each of the  $2^{N-3}$  terms identified in step 2 are multiplied by the product of  $b_2$  or  $e_2$  and  $b_3$  or  $e_3$  up to  $b_{n-2}$  or  $e_{n-2}$ . For example, the four new terms generated when  $N = 5$  are multiplied by  $b_2 b_3$ ,  $b_2 e_3$ ,  $e_2 b_3$ , and  $e_2 e_3$ .
4. Each new term from step 3 that contains a  $b_2$  is multiplied by  $\sin(\gamma_1 - \phi_2)$ .
5. Each new term from step 3 that contains an  $e_2$  is multiplied by  $\sin(\gamma_1 - \theta_2)$ .
6. Each new term from step 3 that contains a  $b_{N-2}$  is multiplied  $\sin(\theta_{N-1} - \theta_{N-2})$ .
7. Each new term from step 3 that contains an  $e_{N-2}$  is multiplied by  $\sin(\gamma_{N-2} - \theta_{N-1})$ .

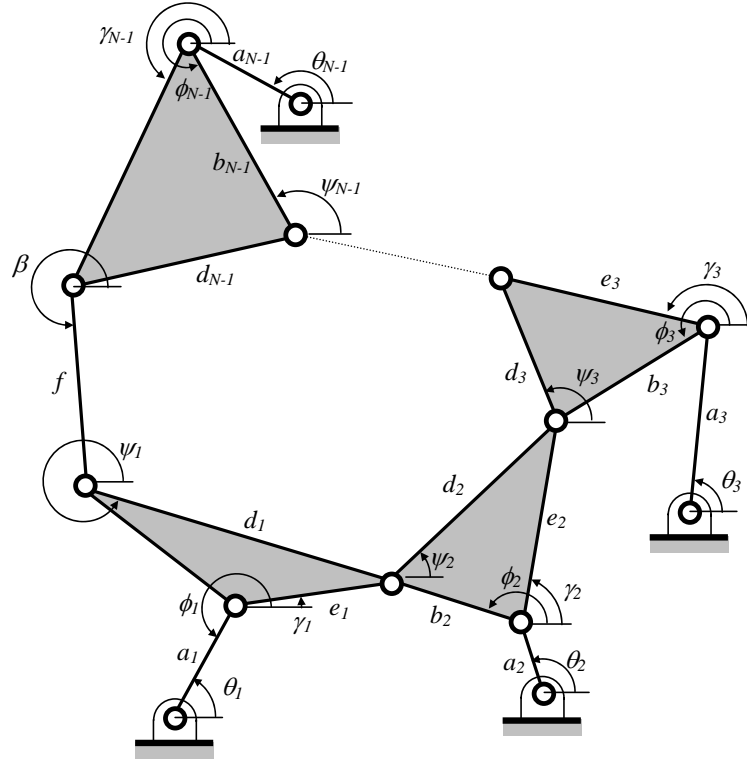


Figure 4.5: Assur  $N/(N - 1)$  mechanism.

8. If  $N > 4$ , the physical parameters of the  $2^{N-3}$  new terms created in step 3 are reviewed in pairs. Each new term that contains a  $b_i b_{i+1}$  is multiplied by  $\sin(\phi_{i+1} - \theta_i)$ . Each new term that contains a  $b_i e_{i+1}$  is multiplied by  $\sin(\theta_{i+1} - \theta_i)$ . Each new term that contains an  $e_i b_{i+1}$  is multiplied by  $\sin(\gamma_i - \phi_{i+1})$ . Each new term that contains an  $e_i e_{i+1}$  is multiplied by  $\sin(\gamma_i - \theta_{i+1})$ .

The final equation contains  $2^{N-2}$  terms.

The singularity condition for Class  $N$ , when driving with  $a_2$ , can be generated from the condition when driving with  $a_1$  by making the following modifications:



1. Each term that begins with  $e_1 b_2$  is eliminated.
2. In all instances,  $\theta_1$  is substituted for  $\theta_2$ .

The new equation will have  $2^{N-3} + 1$  terms.

#### 4.7 Singularity Equation of a Mechanism with a Six-Link Deformable Closed Contour: Assur VI/5

Using the method outlined, the reduced singularity equation for an Assur VI/5, when driven with  $a_1$  is

$$\begin{aligned}
& d_1 b_2 b_3 b_4 b_5 \sin(\phi_2 - \theta_2) \sin(\phi_3 - \theta_3) \sin(\phi_4 - \theta_4) \sin(\phi_5 - \theta_5) \sin(\psi_1 - \beta) \\
& + e_1 d_2 b_3 b_4 b_5 \sin(\gamma_1 - \theta_2) \sin(\phi_3 - \theta_3) \sin(\phi_4 - \theta_4) \sin(\phi_5 - \theta_5) \sin(\psi_2 - \beta) \\
& + e_1 b_2 d_3 b_4 b_5 \sin(\gamma_1 - \phi_2) \sin(\theta_3 - \theta_2) \sin(\phi_4 - \theta_4) \sin(\phi_5 - \theta_5) \sin(\psi_3 - \beta) \\
& + e_1 e_2 d_3 b_4 b_5 \sin(\gamma_1 - \theta_2) \sin(\gamma_2 - \theta_3) \sin(\phi_4 - \theta_4) \sin(\phi_5 - \theta_5) \sin(\psi_3 - \beta) \\
& + e_1 b_2 b_3 d_4 b_5 \sin(\gamma_1 - \phi_2) \sin(\phi_3 - \theta_2) \sin(\theta_4 - \theta_3) \sin(\phi_5 - \theta_5) \sin(\psi_4 - \beta) \\
& + e_1 b_2 e_3 d_4 b_5 \sin(\gamma_1 - \phi_2) \sin(\theta_3 - \theta_2) \sin(\gamma_3 - \theta_4) \sin(\phi_5 - \theta_5) \sin(\psi_4 - \beta) \\
& + e_1 e_2 b_3 d_4 b_5 \sin(\gamma_1 - \theta_2) \sin(\gamma_2 - \phi_3) \sin(\theta_4 - \theta_3) \sin(\phi_5 - \theta_5) \sin(\psi_4 - \beta) \\
& + e_1 e_2 e_3 d_4 b_5 \sin(\gamma_1 - \theta_2) \sin(\gamma_2 - \theta_3) \sin(\gamma_3 - \theta_4) \sin(\phi_5 - \theta_5) \sin(\psi_4 - \beta) \\
& + e_1 b_2 b_3 b_4 d_5 \sin(\gamma_1 - \phi_2) \sin(\phi_3 - \theta_2) \sin(\phi_4 - \theta_3) \sin(\theta_5 - \theta_4) \sin(\psi_5 - \beta) \\
& + e_1 b_2 b_3 e_4 d_5 \sin(\gamma_1 - \phi_2) \sin(\phi_3 - \theta_2) \sin(\theta_4 - \theta_3) \sin(\gamma_4 - \theta_5) \sin(\psi_5 - \beta) \\
& + e_1 b_2 e_3 b_4 d_5 \sin(\gamma_1 - \phi_2) \sin(\theta_3 - \theta_2) \sin(\gamma_3 - \phi_4) \sin(\theta_5 - \theta_4) \sin(\psi_5 - \beta) \\
& + e_1 b_2 e_3 e_4 d_5 \sin(\gamma_1 - \phi_2) \sin(\theta_3 - \theta_2) \sin(\gamma_3 - \theta_4) \sin(\gamma_4 - \theta_5) \sin(\psi_5 - \beta) \\
& + e_1 e_2 b_3 b_4 d_5 \sin(\gamma_1 - \theta_2) \sin(\gamma_2 - \phi_3) \sin(\phi_4 - \theta_3) \sin(\theta_5 - \theta_4) \sin(\psi_5 - \beta)
\end{aligned}$$

$$\begin{aligned}
& +e_1e_2b_3e_4d_5 \sin(\gamma_1 - \theta_2) \sin(\gamma_2 - \phi_3) \sin(\theta_4 - \theta_3) \sin(\gamma_4 - \theta_5) \sin(\psi_5 - \beta) \\
& +e_1e_2e_3b_4d_5 \sin(\gamma_1 - \theta_2) \sin(\gamma_2 - \theta_3) \sin(\gamma_3 - \phi_4) \sin(\theta_5 - \theta_4) \sin(\psi_5 - \beta) \\
& +e_1e_2e_3e_4d_5 \sin(\gamma_1 - \theta_2) \sin(\gamma_2 - \theta_3) \sin(\gamma_3 - \theta_4) \sin(\gamma_4 - \theta_5) \sin(\psi_5 - \beta) = 0.
\end{aligned}$$

The reduced singularity equation for an Assur VI/5, when driven with  $a_2$  is

$$\begin{aligned}
& d_1b_2b_3b_4b_5 \sin(\phi_2 - \theta_1) \sin(\phi_3 - \theta_3) \sin(\phi_4 - \theta_4) \sin(\phi_5 - \theta_5) \sin(\psi_1 - \beta) \\
& +e_1d_2b_3b_4b_5 \sin(\gamma_1 - \theta_1) \sin(\phi_3 - \theta_3) \sin(\phi_4 - \theta_4) \sin(\phi_5 - \theta_5) \sin(\psi_2 - \beta) \\
& +e_1e_2d_3b_4b_5 \sin(\gamma_1 - \theta_1) \sin(\gamma_2 - \theta_3) \sin(\phi_4 - \theta_4) \sin(\phi_5 - \theta_5) \sin(\psi_3 - \beta) \\
& +e_1e_2b_3d_4b_5 \sin(\gamma_1 - \theta_1) \sin(\gamma_2 - \phi_3) \sin(\theta_4 - \theta_3) \sin(\phi_5 - \theta_5) \sin(\psi_4 - \beta) \\
& +e_1e_2e_3d_4b_5 \sin(\gamma_1 - \theta_1) \sin(\gamma_2 - \theta_3) \sin(\gamma_3 - \theta_4) \sin(\phi_5 - \theta_5) \sin(\psi_4 - \beta) \\
& +e_1e_2b_3b_4d_5 \sin(\gamma_1 - \theta_1) \sin(\gamma_2 - \phi_3) \sin(\phi_4 - \theta_3) \sin(\theta_5 - \theta_4) \sin(\psi_5 - \beta) \\
& +e_1e_2b_3e_4d_5 \sin(\gamma_1 - \theta_1) \sin(\gamma_2 - \phi_3) \sin(\theta_4 - \theta_3) \sin(\gamma_4 - \theta_5) \sin(\psi_5 - \beta) \\
& +e_1e_2e_3b_4d_5 \sin(\gamma_1 - \theta_1) \sin(\gamma_2 - \theta_3) \sin(\gamma_3 - \phi_4) \sin(\theta_5 - \theta_4) \sin(\psi_5 - \beta) \\
& +e_1e_2e_3e_4d_5 \sin(\gamma_1 - \theta_1) \sin(\gamma_2 - \theta_3) \sin(\gamma_3 - \theta_4) \sin(\gamma_4 - \theta_5) \sin(\psi_5 - \beta) = 0.
\end{aligned}$$

#### 4.8 Singularity Equation of a Mechanism with a Seven-Link Deformable Closed Contour: Assur VII/6

Using the method outlined, the reduced singularity equation for an Assur VII/6, when driven with  $a_1$  is

$$\begin{aligned}
& d_1b_2b_3b_4b_5b_6 \sin(\phi_2 - \theta_2) \sin(\phi_3 - \theta_3) \sin(\phi_4 - \theta_4) \sin(\phi_5 - \theta_5) \sin(\phi_6 - \theta_6) \sin(\psi_1 - \beta) \\
& +e_1d_2b_3b_4b_5b_6 \sin(\gamma_1 - \theta_2) \sin(\phi_3 - \theta_3) \sin(\phi_4 - \theta_4) \sin(\phi_5 - \theta_5) \sin(\phi_6 - \theta_6) \sin(\psi_2 - \beta)
\end{aligned}$$

$$\begin{aligned}
& +e_1 b_2 d_3 b_4 b_5 b_6 \sin(\gamma_1 - \phi_2) \sin(\theta_3 - \theta_2) \sin(\phi_4 - \theta_4) \sin(\phi_5 - \theta_5) \sin(\phi_6 - \theta_6) \sin(\psi_3 - \beta) \\
& +e_1 e_2 d_3 b_4 b_5 b_6 \sin(\gamma_1 - \theta_2) \sin(\gamma_2 - \theta_3) \sin(\phi_4 - \theta_4) \sin(\phi_5 - \theta_5) \sin(\phi_6 - \theta_6) \sin(\psi_3 - \beta) \\
& +e_1 b_2 b_3 d_4 b_5 b_6 \sin(\gamma_1 - \phi_2) \sin(\phi_3 - \theta_2) \sin(\theta_4 - \theta_3) \sin(\phi_5 - \theta_5) \sin(\phi_6 - \theta_6) \sin(\psi_4 - \beta) \\
& +e_1 b_2 e_3 d_4 b_5 b_6 \sin(\gamma_1 - \phi_2) \sin(\theta_3 - \theta_2) \sin(\gamma_3 - \theta_4) \sin(\phi_5 - \theta_5) \sin(\phi_6 - \theta_6) \sin(\psi_4 - \beta) \\
& +e_1 e_2 b_3 d_4 b_5 b_6 \sin(\gamma_1 - \theta_2) \sin(\gamma_2 - \phi_3) \sin(\theta_4 - \theta_3) \sin(\phi_5 - \theta_5) \sin(\phi_6 - \theta_6) \sin(\psi_4 - \beta) \\
& +e_1 e_2 e_3 d_4 b_5 b_6 \sin(\gamma_1 - \theta_2) \sin(\gamma_2 - \theta_3) \sin(\gamma_3 - \theta_4) \sin(\phi_5 - \theta_5) \sin(\phi_6 - \theta_6) \sin(\psi_4 - \beta) \\
& +e_1 b_2 b_3 b_4 d_5 b_6 \sin(\gamma_1 - \phi_2) \sin(\phi_3 - \theta_2) \sin(\phi_4 - \theta_3) \sin(\theta_5 - \theta_4) \sin(\phi_6 - \theta_6) \sin(\psi_5 - \beta) \\
& +e_1 b_2 b_3 e_4 d_5 b_6 \sin(\gamma_1 - \phi_2) \sin(\phi_3 - \theta_2) \sin(\theta_4 - \theta_3) \sin(\gamma_4 - \theta_5) \sin(\phi_6 - \theta_6) \sin(\psi_5 - \beta) \\
& +e_1 b_2 e_3 b_4 d_5 b_6 \sin(\gamma_1 - \phi_2) \sin(\theta_3 - \theta_2) \sin(\gamma_3 - \phi_4) \sin(\theta_5 - \theta_4) \sin(\phi_6 - \theta_6) \sin(\psi_5 - \beta) \\
& +e_1 b_2 e_3 e_4 d_5 b_6 \sin(\gamma_1 - \phi_2) \sin(\theta_3 - \theta_2) \sin(\gamma_3 - \theta_4) \sin(\gamma_4 - \theta_5) \sin(\phi_6 - \theta_6) \sin(\psi_5 - \beta) \\
& +e_1 e_2 b_3 b_4 d_5 b_6 \sin(\gamma_1 - \theta_2) \sin(\gamma_2 - \phi_3) \sin(\phi_4 - \theta_3) \sin(\theta_5 - \theta_4) \sin(\phi_6 - \theta_6) \sin(\psi_5 - \beta) \\
& +e_1 e_2 b_3 e_4 d_5 b_6 \sin(\gamma_1 - \theta_2) \sin(\gamma_2 - \phi_3) \sin(\theta_4 - \theta_3) \sin(\gamma_4 - \theta_5) \sin(\phi_6 - \theta_6) \sin(\psi_5 - \beta) \\
& +e_1 e_2 e_3 b_4 d_5 b_6 \sin(\gamma_1 - \theta_2) \sin(\gamma_2 - \theta_3) \sin(\gamma_3 - \phi_4) \sin(\theta_5 - \theta_4) \sin(\phi_6 - \theta_6) \sin(\psi_5 - \beta) \\
& +e_1 e_2 e_3 e_4 d_5 b_6 \sin(\gamma_1 - \theta_2) \sin(\gamma_2 - \theta_3) \sin(\gamma_3 - \theta_4) \sin(\gamma_4 - \theta_5) \sin(\phi_6 - \theta_6) \sin(\psi_5 - \beta) \\
& +e_1 b_2 b_3 b_4 b_5 d_6 \sin(\gamma_1 - \phi_2) \sin(\phi_3 - \theta_2) \sin(\phi_4 - \theta_3) \sin(\phi_5 - \theta_4) \sin(\theta_6 - \theta_5) \sin(\psi_6 - \beta) \\
& +e_1 b_2 b_3 b_4 e_5 d_6 \sin(\gamma_1 - \phi_2) \sin(\phi_3 - \theta_2) \sin(\phi_4 - \theta_3) \sin(\theta_5 - \theta_4) \sin(\gamma_5 - \theta_6) \sin(\psi_6 - \beta) \\
& +e_1 b_2 b_3 e_4 b_5 d_6 \sin(\gamma_1 - \phi_2) \sin(\phi_3 - \theta_2) \sin(\theta_4 - \theta_3) \sin(\gamma_4 - \phi_5) \sin(\theta_6 - \theta_5) \sin(\psi_6 - \beta) \\
& +e_1 b_2 b_3 e_4 e_5 d_6 \sin(\gamma_1 - \phi_2) \sin(\phi_3 - \theta_2) \sin(\theta_4 - \theta_3) \sin(\gamma_4 - \theta_5) \sin(\gamma_5 - \theta_6) \sin(\psi_6 - \beta) \\
& +e_1 b_2 e_3 b_4 b_5 d_6 \sin(\gamma_1 - \phi_2) \sin(\theta_3 - \theta_2) \sin(\gamma_3 - \phi_4) \sin(\phi_5 - \theta_4) \sin(\theta_6 - \theta_5) \sin(\psi_6 - \beta) \\
& +e_1 b_2 e_3 b_4 e_5 d_6 \sin(\gamma_1 - \phi_2) \sin(\theta_3 - \theta_2) \sin(\gamma_3 - \phi_4) \sin(\theta_5 - \theta_4) \sin(\gamma_5 - \theta_6) \sin(\psi_6 - \beta) \\
& +e_1 b_2 e_3 e_4 b_5 d_6 \sin(\gamma_1 - \phi_2) \sin(\theta_3 - \theta_2) \sin(\gamma_3 - \theta_4) \sin(\gamma_4 - \phi_5) \sin(\theta_6 - \theta_5) \sin(\psi_6 - \beta)
\end{aligned}$$

$$\begin{aligned}
& +e_1 b_2 e_3 e_4 e_5 d_6 \sin(\gamma_1 - \phi_2) \sin(\theta_3 - \theta_2) \sin(\gamma_3 - \theta_4) \sin(\gamma_4 - \theta_5) \sin(\gamma_5 - \theta_6) \sin(\psi_6 - \beta) \\
& +e_1 e_2 b_3 b_4 b_5 d_6 \sin(\gamma_1 - \theta_2) \sin(\gamma_2 - \phi_3) \sin(\phi_4 - \theta_3) \sin(\phi_5 - \theta_4) \sin(\theta_6 - \theta_5) \sin(\psi_6 - \beta) \\
& +e_1 e_2 b_3 b_4 e_5 d_6 \sin(\gamma_1 - \theta_2) \sin(\gamma_2 - \phi_3) \sin(\phi_4 - \theta_3) \sin(\theta_5 - \theta_4) \sin(\gamma_5 - \theta_6) \sin(\psi_6 - \beta) \\
& +e_1 e_2 b_3 e_4 b_5 d_6 \sin(\gamma_1 - \theta_2) \sin(\gamma_2 - \phi_3) \sin(\theta_4 - \theta_3) \sin(\gamma_4 - \phi_5) \sin(\theta_6 - \theta_5) \sin(\psi_6 - \beta) \\
& +e_1 e_2 b_3 e_4 e_5 d_6 \sin(\gamma_1 - \theta_2) \sin(\gamma_2 - \phi_3) \sin(\theta_4 - \theta_3) \sin(\gamma_4 - \theta_5) \sin(\gamma_5 - \theta_6) \sin(\psi_6 - \beta) \\
& +e_1 e_2 e_3 b_4 b_5 d_6 \sin(\gamma_1 - \theta_2) \sin(\gamma_2 - \theta_3) \sin(\gamma_3 - \phi_4) \sin(\phi_5 - \theta_4) \sin(\theta_6 - \theta_5) \sin(\psi_6 - \beta) \\
& +e_1 e_2 e_3 b_4 e_5 d_6 \sin(\gamma_1 - \theta_2) \sin(\gamma_2 - \theta_3) \sin(\gamma_3 - \phi_4) \sin(\theta_5 - \theta_4) \sin(\gamma_5 - \theta_6) \sin(\psi_6 - \beta) \\
& +e_1 e_2 e_3 e_4 b_5 d_6 \sin(\gamma_1 - \theta_2) \sin(\gamma_2 - \theta_3) \sin(\gamma_3 - \theta_4) \sin(\gamma_4 - \phi_5) \sin(\theta_6 - \theta_5) \sin(\psi_6 - \beta) \\
& +e_1 e_2 e_3 e_4 e_5 d_6 \sin(\gamma_1 - \theta_2) \sin(\gamma_2 - \theta_3) \sin(\gamma_3 - \theta_4) \sin(\gamma_4 - \theta_5) \sin(\gamma_5 - \theta_6) \sin(\psi_6 - \beta) \\
& = 0.
\end{aligned} \tag{4.22}$$

The reduced singularity equation for an Assur VII/6, when driven with  $a_2$  is

$$\begin{aligned}
& d_1 b_2 b_3 b_4 b_5 b_6 \sin(\phi_2 - \theta_1) \sin(\phi_3 - \theta_3) \sin(\phi_4 - \theta_4) \sin(\phi_5 - \theta_5) \sin(\phi_6 - \theta_6) \sin(\psi_1 - \beta) \\
& +e_1 d_2 b_3 b_4 b_5 b_6 \sin(\gamma_1 - \theta_1) \sin(\phi_3 - \theta_3) \sin(\phi_4 - \theta_4) \sin(\phi_5 - \theta_5) \sin(\phi_6 - \theta_6) \sin(\psi_2 - \beta) \\
& +e_1 e_2 d_3 b_4 b_5 b_6 \sin(\gamma_1 - \theta_1) \sin(\gamma_2 - \theta_3) \sin(\phi_4 - \theta_4) \sin(\phi_5 - \theta_5) \sin(\phi_6 - \theta_6) \sin(\psi_3 - \beta) \\
& +e_1 e_2 b_3 d_4 b_5 b_6 \sin(\gamma_1 - \theta_1) \sin(\gamma_2 - \phi_3) \sin(\theta_4 - \theta_3) \sin(\phi_5 - \theta_5) \sin(\phi_6 - \theta_6) \sin(\psi_4 - \beta) \\
& +e_1 e_2 e_3 d_4 b_5 b_6 \sin(\gamma_1 - \theta_1) \sin(\gamma_2 - \theta_3) \sin(\gamma_3 - \theta_4) \sin(\phi_5 - \theta_5) \sin(\phi_6 - \theta_6) \sin(\psi_4 - \beta) \\
& +e_1 e_2 b_3 b_4 d_5 b_6 \sin(\gamma_1 - \theta_1) \sin(\gamma_2 - \phi_3) \sin(\phi_4 - \theta_3) \sin(\theta_5 - \theta_4) \sin(\phi_6 - \theta_6) \sin(\psi_5 - \beta) \\
& +e_1 e_2 b_3 e_4 d_5 b_6 \sin(\gamma_1 - \theta_1) \sin(\gamma_2 - \phi_3) \sin(\theta_4 - \theta_3) \sin(\gamma_4 - \theta_5) \sin(\phi_6 - \theta_6) \sin(\psi_5 - \beta) \\
& +e_1 e_2 e_3 b_4 d_5 b_6 \sin(\gamma_1 - \theta_1) \sin(\gamma_2 - \theta_3) \sin(\gamma_3 - \phi_4) \sin(\theta_5 - \theta_4) \sin(\phi_6 - \theta_6) \sin(\psi_5 - \beta) \\
& +e_1 e_2 e_3 e_4 d_5 b_6 \sin(\gamma_1 - \theta_1) \sin(\gamma_2 - \theta_3) \sin(\gamma_3 - \theta_4) \sin(\gamma_4 - \theta_5) \sin(\phi_6 - \theta_6) \sin(\psi_5 - \beta) \\
& +e_1 e_2 b_3 b_4 b_5 d_6 \sin(\gamma_1 - \theta_1) \sin(\gamma_2 - \phi_3) \sin(\phi_4 - \theta_3) \sin(\phi_5 - \theta_4) \sin(\theta_6 - \theta_5) \sin(\psi_6 - \beta)
\end{aligned}$$

Table 4.1: Mechanism parameters for Example 4.1,  $\beta = 223^\circ$  and  $f = 2.3865$ .

$i$	$\theta_i$	$\gamma_i$	$\phi_i$	$\psi_i$	$a_i$	$b_i$	$d_i$	$e_i$	$g_{ix}$	$g_{iy}$
1	$62^\circ$	$47^\circ$	$88^\circ$	$308^\circ$	2.6406	3.0553	2.0179	2.0000	0.0000	0.0000
2	$105^\circ$	$65^\circ$	$147^\circ$	$20^\circ$	2.3981	2.7134	3.8000	3.0646	5.5000	0.0000
3	$152^\circ$	$208^\circ$	$257^\circ$	$148^\circ$	1.2000	4.1000	3.6183	4.4992	8.1563	8.5254

$$\begin{aligned}
& +e_1e_2b_3b_4e_5d_6 \sin(\gamma_1 - \theta_1) \sin(\gamma_2 - \phi_3) \sin(\phi_4 - \theta_3) \sin(\theta_5 - \theta_4) \sin(\gamma_5 - \theta_6) \sin(\psi_6 - \beta) \\
& +e_1e_2b_3b_4b_5d_6 \sin(\gamma_1 - \theta_1) \sin(\gamma_2 - \phi_3) \sin(\theta_4 - \theta_3) \sin(\gamma_4 - \phi_5) \sin(\theta_6 - \theta_5) \sin(\psi_6 - \beta) \\
& +e_1e_2b_3e_4e_5d_6 \sin(\gamma_1 - \theta_1) \sin(\gamma_2 - \phi_3) \sin(\theta_4 - \theta_3) \sin(\gamma_4 - \theta_5) \sin(\gamma_5 - \theta_6) \sin(\psi_6 - \beta) \\
& +e_1e_2e_3b_4b_5d_6 \sin(\gamma_1 - \theta_1) \sin(\gamma_2 - \theta_3) \sin(\gamma_3 - \phi_4) \sin(\phi_5 - \theta_4) \sin(\theta_6 - \theta_5) \sin(\psi_6 - \beta) \\
& +e_1e_2e_3b_4e_5d_6 \sin(\gamma_1 - \theta_1) \sin(\gamma_2 - \theta_3) \sin(\gamma_3 - \phi_4) \sin(\theta_5 - \theta_4) \sin(\gamma_5 - \theta_6) \sin(\psi_6 - \beta) \\
& +e_1e_2e_3e_4b_5d_6 \sin(\gamma_1 - \theta_1) \sin(\gamma_2 - \theta_3) \sin(\gamma_3 - \theta_4) \sin(\gamma_4 - \phi_5) \sin(\theta_6 - \theta_5) \sin(\psi_6 - \beta) \\
& +e_1e_2e_3e_4e_5d_6 \sin(\gamma_1 - \theta_1) \sin(\gamma_2 - \theta_3) \sin(\gamma_3 - \theta_4) \sin(\gamma_4 - \theta_5) \sin(\gamma_5 - \theta_6) \sin(\psi_6 - \beta) \\
& = 0.
\end{aligned} \tag{4.23}$$

## 4.9 Examples

### 4.9.1 Example 4.1: Combination of physical and joint parameters resulting in a singularity

A singular configuration for an Assur IV/3 mechanism, with the properties identified in Table 4.1, is shown in Fig. 4.6. No two links are parallel. Additionally, lines along the links have been extended to assist an inspection for any special relationships such as three lines intersecting at a single point, and none exist. The singularity is attributed to a combination of physical and joint parameters that satisfy Eq. 4.18.

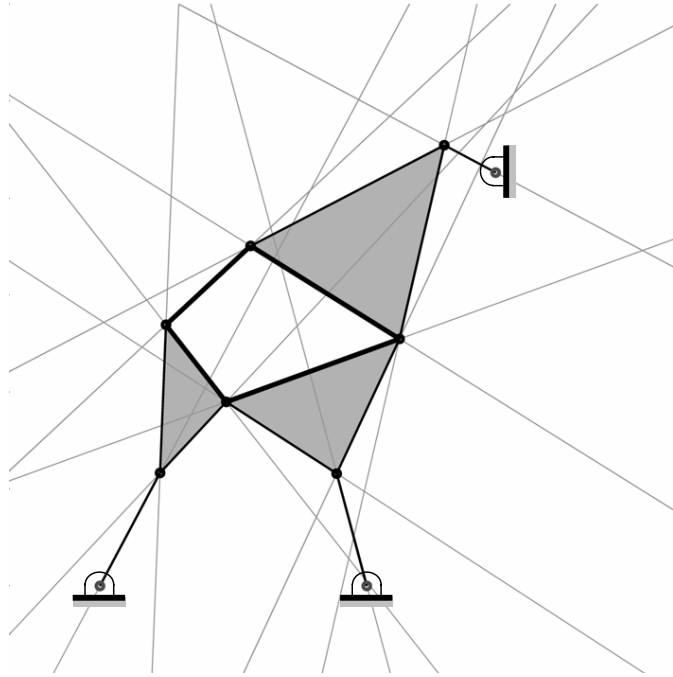


Figure 4.6: Singularity discussed in Example 4.1.

#### 4.9.2 Example 4.2: Singularity with adjacent parallel links

By inspecting Eq. 4.18, it is clear that an Assur IV/3 mechanism will encounter a singularity if the adjacent links  $e_1$ ,  $b_2$  and  $a_2$  are parallel. As noted earlier, this singularity condition presents two additional constraints:

$$\phi_2 = \gamma_1 - \pi, \quad (4.24)$$

$$\theta_2 = \gamma_1 - \pi. \quad (4.25)$$

Since the mechanism has a single DOF, one physical parameter is dependent upon the others.

Consider a mechanism with the arbitrary physical parameters given in the first section of Table 4.2. For that mechanism to reach a singularity with links  $e_1$ ,  $b_2$  and  $a_2$  being parallel, the final

Table 4.2: Mechanism parameters for Example 4.2,  $\beta = 221^\circ$ .

$i$	$a_i$	$b_i$	$d_i$	$e_i$	$g_{ix}$	$g_{iy}$	$\theta_i$	$\gamma_i$	$\phi_i$	$\psi_i$
1	1.0000	1.5000	2.2695	1.1261	0.0000	0.0000	$60^\circ$	$346^\circ$	$105^\circ$	$311^\circ$
2	1.3434	1.1361	4.1342	3.4830	4.0000	0.0000	$166^\circ$	$49^\circ$	$166^\circ$	$34^\circ$
3	1.7500	2.0000	3.0000	1.9249	6.9514	3.3900	$129^\circ$	$149^\circ$	$244^\circ$	$106^\circ$

physical parameter  $f$  can be determined by substituting Eqs. 4.24 and 4.25 into the Assur IV/3 loop equations in Eq. 4.11. Solving,  $f = 5.3771$ . The resulting mechanism with these physical parameters is shown in an arbitrary configuration in Fig. 4.7a. The joint values consistent with the singularity are given in the second section of Table 4.2, and the resulting mechanism at the singularity is shown in Fig. 4.7b.

#### 4.9.3 Example 4.3: Singularity with isolated parallel links

By inspecting Eq. 4.18, an additional relationship that will induce a singularity in an Assur IV/3 mechanism is when the isolated links  $e_1$ ,  $a_2$ ,  $a_3$  and  $b_3$  are parallel. This singularity condition presents three additional constraints:

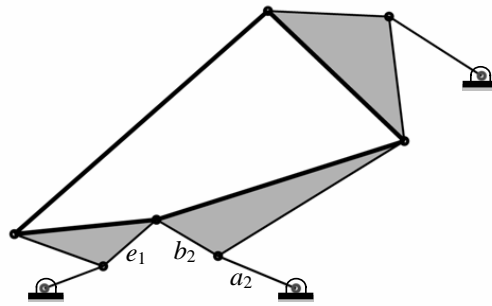
$$\theta_2 = \gamma_1 - \pi, \quad (4.26)$$

$$\phi_3 = \gamma_1 - \pi, \quad (4.27)$$

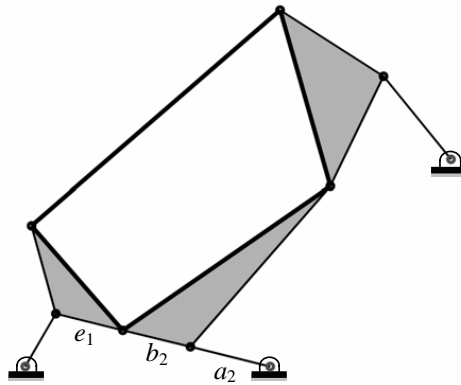
$$\theta_3 = \gamma_1 - \pi. \quad (4.28)$$

Since the mechanism has a single DOF, two physical parameters will be dependent upon the others.

Consider a mechanism with the arbitrary physical parameters given in the first section of Table 4.3. For that mechanism to reach a singularity with links  $e_1$ ,  $a_2$ ,  $a_3$  and  $b_3$  being parallel, the two remaining physical parameters,  $a_1$  and  $f$ , can be determined by substituting Eqs. 4.26, 4.27 and 4.28 into the Assur IV/3 loop equations given in Eq. 4.11. Solving,  $a_1 = 1.0048$ , and  $f = 2.6493$ .



(a) Assur IV/3 from Example 4.2



(b) Assur IV/3 from Example 4.2 at singularity

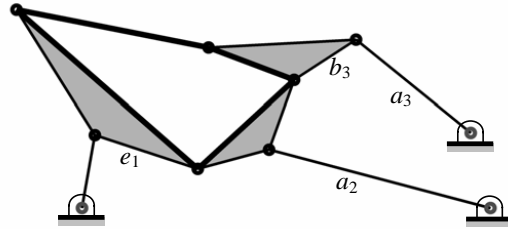
Figure 4.7: Singularity discussed in Example 4.2.

The resulting mechanism with these physical parameters is shown in an arbitrary configuration in Fig. 4.8a. The joint values consistent with the singularity are given in the second section of Table 4.3, and the resulting mechanism at the singularity is shown in Fig. 4.8b.

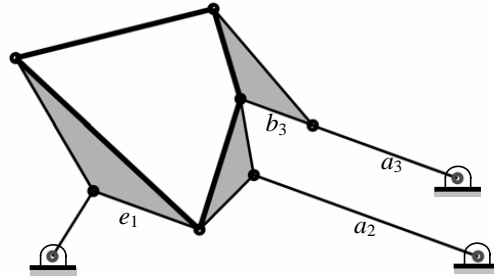


Table 4.3: Mechanism parameters for Example 4.3,  $\beta = 194^\circ$ .

$i$	$a_i$	$b_i$	$d_i$	$e_i$	$g_{ix}$	$g_{iy}$	$\theta_i$	$\gamma_i$	$\phi_i$	$\psi_i$
1		2.0000	3.2652	1.4668	0.0000	0.0000	$58^\circ$	$340^\circ$	$120^\circ$	$317^\circ$
2	3.0995	1.0000	1.7740	1.0000	5.5293	0.0000	$160^\circ$	$100^\circ$	$225^\circ$	$73^\circ$
3	2.0000	1.0000	1.2393	2.0000	5.2621	1.0188	$160^\circ$	$130^\circ$	$160^\circ$	$106^\circ$



(a) Assur IV/3 from Example 4.3



(b) Assur IV/3 from Example 4.3 at singularity

Figure 4.8: Singularity discussed in Example 4.3.

## 4.10 Summary

This chapter presented an analysis to create the singularity condition of an Assur mechanism, which is commonly used in shape-changing mechanisms that approximate closed curves. The general singularity equation was reduced to a condensed form, which allows geometric relationships

to be readily detected. The identification of singularities of this extensible kinematic architecture is particularly relevant to rigid-link, shape-changing mechanisms. A procedure for generating the reduced form of the singularity condition for an Assur Class  $N$  mechanism, knowing the condition for a Class  $N - 1$ , is presented. Additionally, a procedure for producing the singularity condition with an alternate driving dyad is presented. This approach was illustrated with several examples.

## **CHAPTER V**

### **ASSESSING POSITION ORDER IN RIGID BODY GUIDANCE: AN INTUITIVE APPROACH TO FIXED PIVOT SELECTION**

#### **5.1 Introduction**

The order defect was introduced in Section 1.3.3. This chapter extends the work of Prentis [46] and presents an organized and concise method to detect whether a single dyad will achieve the task positions in order. The method can be used to assess the suitability of a candidate fixed pivot location by determining whether an ordered dyad will be generated. This evaluation can be performed prior to the actual process of dimensional synthesis. Similar to the other rectification work, this paper does not address the synthesis process, but focuses on a method that provides a necessary condition for order of an individual dyad. As with the work of Waldron [43, 44, 45] and Prentis, the method presented here is not sufficient since a branch point can appear between the ordered positions as two dyads are coupled to form a four-bar linkage. The benefit of this assessment process is that linkage designers can limit the work of dimensional synthesis to evaluating only viable fixed pivot locations.

The chapter is organized as follows. Crank angles are defined and necessary conditions for an ordered dyad are presented in Section 5.2. The “Center Point Theorem” of McCarthy [23] described in Section 5.3 is used in Sections 5.4 and 5.5 to establish necessary and sufficient conditions for the relative location of the poles to a fixed pivot for an ordered dyad. From these concepts, Section

5.6 develops a “propeller method” for determining the order that is associated with a fixed pivot location. Lastly, several illustrative examples are given in Section 5.7.

## 5.2 Ordered Dyads

A typical desire for machine design is operation by a constantly rotating actuator, so in planar linkages, the actuated crank of the driving RR dyad most commonly rotates in a unidirectional fashion. Throughout the development of the order assessment method, a counter-clockwise crank rotation is assumed and taken to be positive. All crank angles are measured such that

$$0 \leq \beta_{ij} < 2\pi \quad \forall i, j, \quad (5.1)$$

where  $\beta_{ij}$  is the change in crank angle from position  $i$  to position  $j$ . For an RR chain to achieve the task positions in a specific order, the driving crank angle  $\beta$  measured counter-clockwise from the first position must monotonically increase as each task position is reached. Therefore, a dyad does not exhibit an order defect if

$$0 < \beta_{12} < \beta_{13} < \dots < \beta_{1N} < 2\pi. \quad (5.2)$$

Equation 5.2 assumes that the task positions are numbered in the order in which they are to be achieved.

## 5.3 Center-Point Theorem

Figure 5.1 illustrates the floating link of an RR chain displaced from position  $M_i$  to position  $M_j$  under a crank rotation of  $\beta_{ij}$ . The pair of triangles formed by the pole  $\mathbf{P}_{ij}$ , the fixed pivot  $\mathbf{G}$ , and the moving pivot  $\mathbf{W}$  are termed dyad triangles by McCarthy [23]. By definition, the pole  $\mathbf{P}_{ij}$  lies on the perpendicular bisector of  $\mathbf{W}_i$  and  $\mathbf{W}_j$ . Therefore, the interior angle of each dyad triangle at

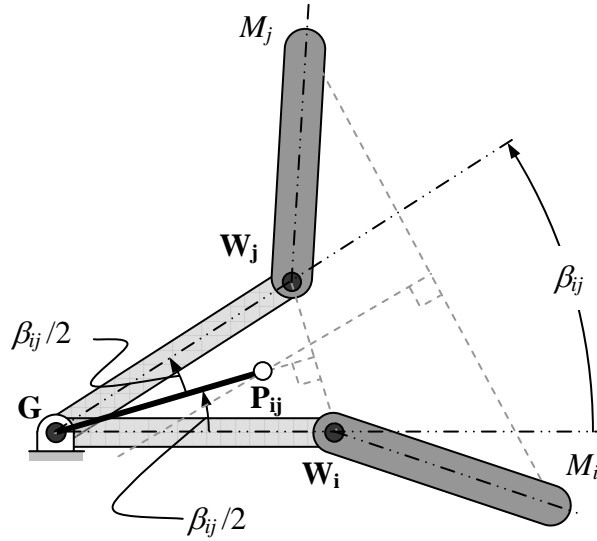


Figure 5.1: The relationship between the fixed pivot of two positions, the pole and the crank angle.

$G$  is half of the crank angle  $\beta_{ij}$ ,

$$\angle W_i G P_{ij} = \angle P_{ij} G W_j = \frac{\beta_{ij}}{2}. \quad (5.3)$$

The displacement of the floating link could also be such that the pole is located on the opposite side of the fixed pivot. That situation is depicted in Fig. 5.2 wherein

$$\angle W_i G P_{ij} = \angle P_{ij} G W_j = \frac{\beta_{ij}}{2} + \pi. \quad (5.4)$$

Summarizing the two cases in Eqs. 5.3 and 5.4,

$$\angle W_i G P_{ij} = \angle P_{ij} G W_j = \frac{\beta_{ij}}{2} \text{ or } \frac{\beta_{ij}}{2} + \pi. \quad (5.5)$$

Figure 5.3 examines the geometry as a third position  $M_k$  is included. The angles between the circle points  $W$  and the pole as viewed from the fixed pivot are combined, and

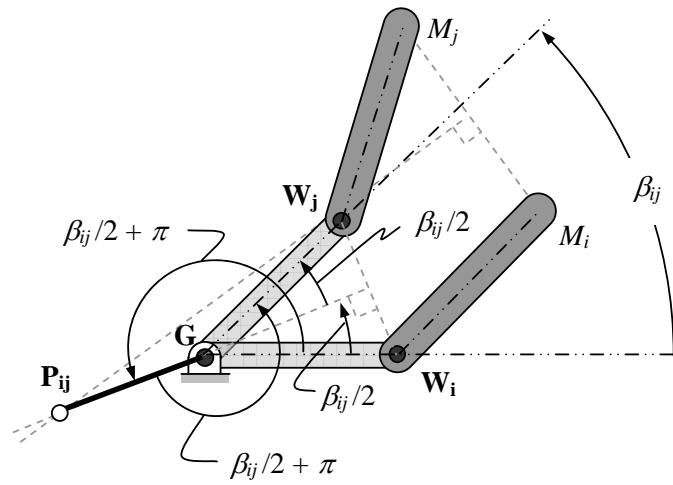


Figure 5.2: An alternative relationship between the fixed pivot of two positions, the pole and the crank angle.

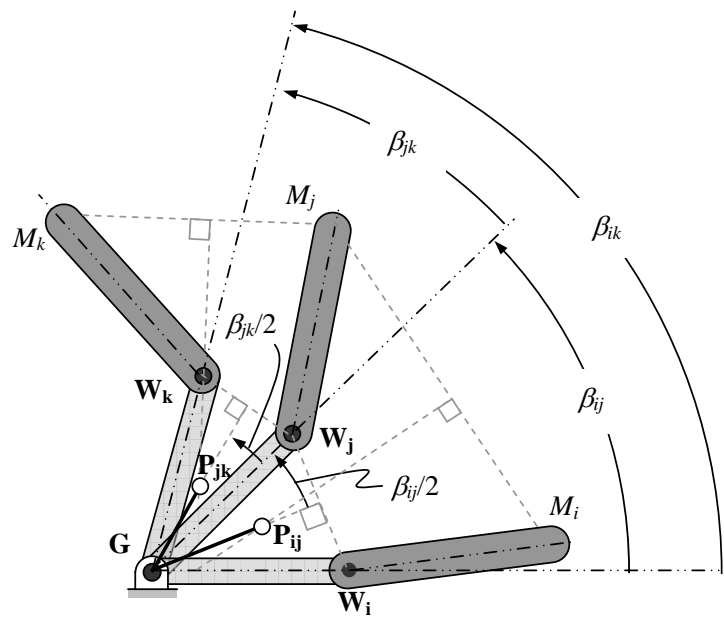


Figure 5.3: The relationship between the fixed pivot, the poles and three positions.

$$\angle \mathbf{P}_{ij} \mathbf{G} \mathbf{P}_{jk} = \angle \mathbf{P}_{ij} \mathbf{G} \mathbf{W}_j + \angle \mathbf{W}_j \mathbf{G} \mathbf{P}_{jk}. \quad (5.6)$$

Maintaining a consistent angle measure, such as counter-clockwise being positive, Equation 5.6 generalizes for any arbitrary arrangement of positions  $M_i$ ,  $M_j$ , and  $M_k$ . Substituting Eq. 5.5 into Eq. 5.6,

$$\angle \mathbf{P}_{ij} \mathbf{G} \mathbf{P}_{jk} = \frac{\beta_{ij}}{2} + \frac{\beta_{jk}}{2} \text{ or } \frac{\beta_{ij}}{2} + \frac{\beta_{jk}}{2} + \pi. \quad (5.7)$$

The addition of crank angles  $\beta_{ij} + \beta_{jk} = \beta_{ik}$  results in the center point theorem, as stated by McCarthy [23],

$$\angle \mathbf{P}_{ij} \mathbf{G} \mathbf{P}_{jk} = \frac{\beta_{ik}}{2} \text{ or } \frac{\beta_{ik}}{2} + \pi, \quad (5.8)$$

recalling that either crank angle value is positive counter-clockwise.

Equation 5.8 expresses a relationship between the crank angle, the poles, and the fixed pivot location. In the case of two parallel positions,  $M_q$  and  $M_r$ , pole  $\mathbf{P}_{qr}$  is at infinity in the direction of the perpendicular bisector. A line through the fixed pivot and parallel to the perpendicular bisector represents the line segment  $\overrightarrow{\mathbf{G} \mathbf{P}_{qr}}$ . For this special situation with a pole at infinity, Equation 5.8 is still valid. In the following sections, Equations 5.2 and 5.8 are combined to generate a method for determining the position order of a synthesized dyad.

#### 5.4 Necessary Pole Condition

Figure 5.4 illustrates two poles and a fixed pivot. Note that the angle of rotation about  $\mathbf{G}$  from the line segment  $\overrightarrow{\mathbf{G} \mathbf{P}_{ij}}$  to the line segment  $\overrightarrow{\mathbf{G} \mathbf{P}_{jk}}$  is  $\beta_{ik}/2 + \pi$ . Defining  $\overline{\mathbf{G} \mathbf{P}_{ij}}$  to be a line through points  $\mathbf{G}$  and  $\mathbf{P}_{ij}$ , extending infinitely in both directions, the angle of rotation about  $\mathbf{G}$  from the line  $\overline{\mathbf{G} \mathbf{P}_{ij}}$  to the line  $\overline{\mathbf{G} \mathbf{P}_{jk}}$  is  $\beta_{ik}/2$ , and

$$\angle \overline{\mathbf{G} \mathbf{P}_{ij}} \overline{\mathbf{G} \mathbf{P}_{jk}} = \frac{\beta_{ik}}{2} < \pi. \quad (5.9)$$

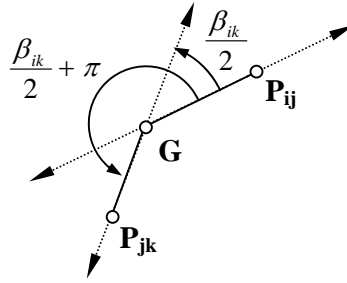


Figure 5.4: The angle between line  $\overline{GP_{ij}}$  and  $\overline{GP_{jk}}$  is  $\beta_{ik}/2$ .

Note that if  $G$ ,  $P_{ij}$  and  $P_{jk}$  are collinear, the resulting dyad will exhibit a zero crank angle from position  $M_i$  to  $M_k$  and  $\beta_{ik}/2 = 0$ .

From Equation 5.2, a dyad does not exhibit an order defect if

$$0 < \frac{\beta_{12}}{2} < \frac{\beta_{13}}{2} < \dots < \frac{\beta_{1N}}{2} < \pi. \quad (5.10)$$

Combining Equations 5.9 and 5.10, a dyad does not exhibit an order defect if

$$0 < \angle \overline{GP_{1k}} \overline{GP_{2k}} < \angle \overline{GP_{1k}} \overline{GP_{3k}} < \dots < \angle \overline{GP_{1k}} \overline{GP_{Nk}} < \pi. \quad (5.11)$$

Interpreted graphically, line  $\overline{GP_{1k}}$  rotates counter-clockwise about  $G$  analogous to a propeller with infinitely long blades rotating about a fixed pivot. A necessary condition for an ordered dyad with a fixed pivot at  $G$  is that the line begins at  $P_{1k}$  and sweeps through the poles  $P_{2k}, P_{3k}, \dots, P_{N,k}$  in order within a rotation of  $\pi$  radians.



### 5.5 Sufficient Pole Condition

The condition in Eq. 5.11 is necessary, but not sufficient. Consider the poles relative to position  $k$ ,

$$\dots < \angle \overline{\mathbf{GP}_{1k}} \overline{\mathbf{GP}_{k-1,k}} < \angle \overline{\mathbf{GP}_{1k}} \overline{\mathbf{GP}_{kk}} < \angle \overline{\mathbf{GP}_{1k}} \overline{\mathbf{GP}_{k,k+1}} < \dots < \pi, \quad (5.12)$$

which includes the undefined quantity  $\mathbf{P}_{kk}$ . Therefore, Equation 5.11 contains no information that confirms the location of position  $k$  within the order of the other positions. Observe, however, that Equation 5.11 will be true for all  $k$ . Hence, a sufficient condition for an ordered dyad is

$$k = 1 : \quad 0 < \angle \overline{\mathbf{GP}_{12}} \overline{\mathbf{GP}_{13}} < \angle \overline{\mathbf{GP}_{12}} \overline{\mathbf{GP}_{14}} < \dots < \angle \overline{\mathbf{GP}_{12}} \overline{\mathbf{GP}_{1N}} < \pi, \quad (5.13)$$

$$k = 2 : \quad 0 < \angle \overline{\mathbf{GP}_{12}} \overline{\mathbf{GP}_{23}} < \angle \overline{\mathbf{GP}_{12}} \overline{\mathbf{GP}_{24}} < \dots < \angle \overline{\mathbf{GP}_{12}} \overline{\mathbf{GP}_{2N}} < \pi, \quad (5.14)$$

$$k = 3 : \quad 0 < \angle \overline{\mathbf{GP}_{13}} \overline{\mathbf{GP}_{23}} < \angle \overline{\mathbf{GP}_{13}} \overline{\mathbf{GP}_{34}} < \dots < \angle \overline{\mathbf{GP}_{13}} \overline{\mathbf{GP}_{3N}} < \pi, \quad (5.15)$$

$$\vdots$$

$$\vdots$$

$$k = N : \quad 0 < \angle \overline{\mathbf{GP}_{1N}} \overline{\mathbf{GP}_{2N}} < \angle \overline{\mathbf{GP}_{1N}} \overline{\mathbf{GP}_{3N}} < \dots < \angle \overline{\mathbf{GP}_{1N}} \overline{\mathbf{GP}_{N-1,N}} < \pi. \quad (5.16)$$

The following may be observed. As a line, infinitely extending in both directions, rotates about  $\mathbf{G}$ , starting at  $\mathbf{P}_{1k}$ , it will sweep through every pole in a counter-clockwise rotation of  $\pi$  radians. If every other pole involving position  $k$  is encountered in ascending order, and this is true for all  $k$ , the positions are ordered for that choice of fixed pivot  $\mathbf{G}$ . This rotating line is analogous to a propeller, with infinitely long blades, rotating about  $\mathbf{G}$  and sweeping through the poles. Inspecting the poles to assess order in this fashion is termed the propeller method.

For an ordered solution to a three-position problem with a counter-clockwise crank, the line starting at  $\overline{\mathbf{GP}_{12}}$  intersects, in order,  $\mathbf{P}_{13}$  and  $\mathbf{P}_{23}$  as it is rotated counter-clockwise. This is

represented with the notation  $P_{12} P_{13} P_{23}$ , meaning that if the line intersects the poles in that order as it rotates over a counter-clockwise turn of  $\pi$  radians, the crank is ordered.

For an ordered solution to a four-position problem with a counter-clockwise crank, the line starting at  $\overline{GP_{12}}$  must intersect  $P_{13}$  before  $P_{14}$  ( $P_{12}P_{13}P_{14}$ ) and likewise  $P_{23}$  before  $P_{24}$  ( $P_{12}P_{23}P_{24}$ ). When starting at  $\overline{GP_{13}}$ , the line must intersect  $P_{23}$  before  $P_{34}$  ( $P_{13} P_{23} P_{34}$ ). Finally, when starting at  $\overline{GP_{14}}$ , it must intersect  $P_{24}$  before  $P_{34}$  ( $P_{14}P_{24}P_{34}$ ). The combination of these statements yields  $P_{12}P_{13}P_{14}P_{23}P_{24}P_{34}$ ,  $P_{12}P_{13}P_{23}P_{14}P_{24}P_{34}$ ,  $P_{12}P_{34}P_{13}P_{14}P_{23}P_{24}$ , and  $P_{12}P_{34}P_{13}P_{23}P_{14}P_{24}$  as acceptable orders for a four-position synthesis problem in a single propeller turn of  $\pi$ .

For an ordered solution to a five-position problem, the line sweeps through the poles in the following orders:  $P_{12}P_{13}P_{14}P_{15}$ ,  $P_{12}P_{23}P_{24}P_{25}$ ,  $P_{13}P_{23}P_{34}P_{35}$ ,  $P_{14}P_{24}P_{34}P_{45}$ , and  $P_{15}P_{25}P_{35}P_{45}$ . Combining these propeller results generates 82 possible sequences that characterize an ordered dyad for five positions.

## 5.6 Propeller Theorem

From Equation 5.13 alone, positions 2 through  $N$  can be confirmed to be ordered for a crank. That is, the crank angle relationship shown in Fig. 5.5,

$$0 < \beta_{23} < \beta_{24} < \dots < \beta_{2N} < 2\pi, \quad (5.17)$$

is established if the poles are encountered in the following order for a rotation of  $\pi$  radians of a line about  $G$ :

$$P_{12}P_{13}P_{14} \dots P_{1N}. \quad (5.18)$$

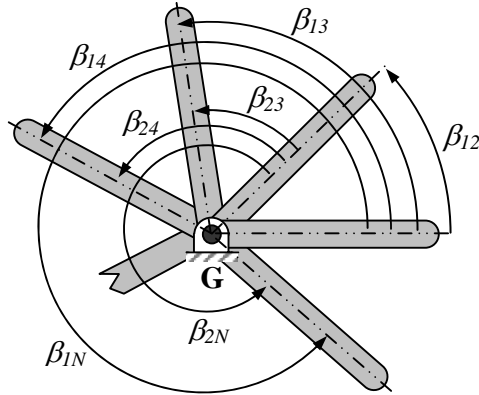


Figure 5.5: Equations 5.18 and 5.20 ensure the order of all  $N$  positions.

An ordered solution is confirmed if position 1 occurs after position  $N$ , and before position 2. This is verified if

$$0 < \beta_{12} < \beta_{1N} < 2\pi. \quad (5.19)$$

Equation 5.19 can be established if the poles are encountered in the following order for a  $\pi$ -radian rotation of a line about  $G$ :

$$\mathbf{P}_{12}\mathbf{P}_{1N}\mathbf{P}_{2N}. \quad (5.20)$$

Thus, Equations 5.17 and 5.19, expressed as relationships among poles in Equations 5.18 and 5.20, offer proof of the following.

**Theorem :** As a line, infinitely extending in both directions, rotates about  $G$ , it sweeps through every pole in the plane in a counter-clockwise (clockwise) turn of  $\pi$  radians. Starting when the line passes through  $\mathbf{P}_{12}$ , if it intersects  $\mathbf{P}_{13}\mathbf{P}_{14} \dots \mathbf{P}_{1N}\mathbf{P}_{2N}$  in order, the positions are ordered for that choice of fixed pivot  $G$  with a counter-clockwise (clockwise) rotation. Moreover, if the poles are

not encountered in the order  $P_{12} \dots P_{1N}P_{2N}$ , the positions will not be ordered for that choice of fixed pivot.

The entire development of this theorem assumed a counter-clockwise rotation. The derivation may be readily performed by considering the crank rotating clockwise, arriving at a clockwise version of the theorem. Moreover, for four positions, the order check reduces to  $P_{12}P_{13}P_{14}P_{24}$ . For five positions, the order check reduces to  $P_{12}P_{13}P_{14}P_{15}P_{25}$ .

For a set of positions defining a unique set of poles (no two poles are coincident), the theorem is true even if the fixed pivot is located at a pole. In addition, if the fixed pivot is selected as one of the poles in the necessary sequence ( $P_{12}P_{13} \dots P_{1N}P_{2N}$ ), then only the remaining poles in the sequence must be checked for satisfaction of the theorem. The authors recognize that degenerate cases exist in which the fixed pivot may be selected at coincident poles. In such cases, the theorem is inconclusive, as discussed in Section 5.7.2.

The derivation of the propeller method was phrased in terms of RR dyads, but applies to RP and PR dyads as well. For RP dyads, the check proceeds with no modification. For PR dyads, the propeller's center is located at infinity in the direction perpendicular to the path of sliding. Checking order reduces to starting at  $P_{12}$  and "sliding" the propeller along the prismatic joint in the direction that order is desired. Order is confirmed if the poles are encountered in the sequence identified in the aforementioned theorem. Therefore, the propeller method can be used to assess order for any dyad.

## 5.7 Examples

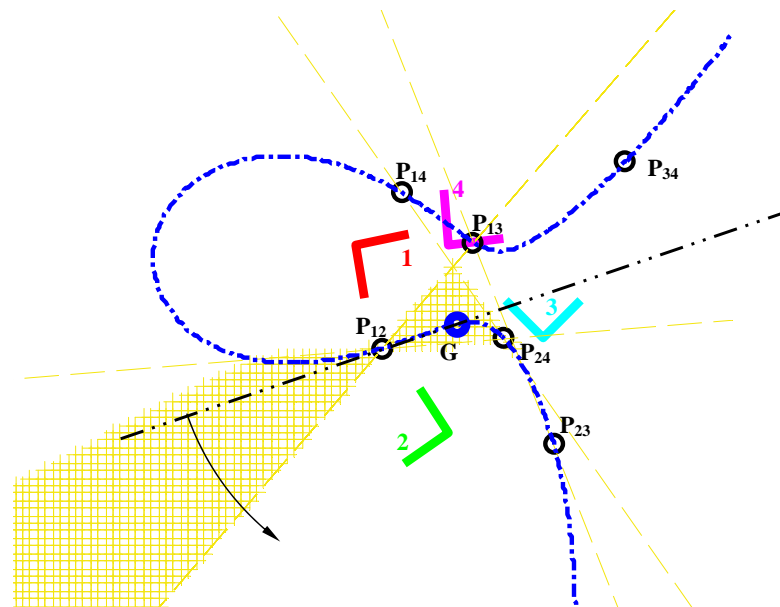
Examples 1 and 2 present applications of the theorem to four task positions. Examples 3 and 4 offer five task position scenarios.

### 5.7.1 Example 5-1

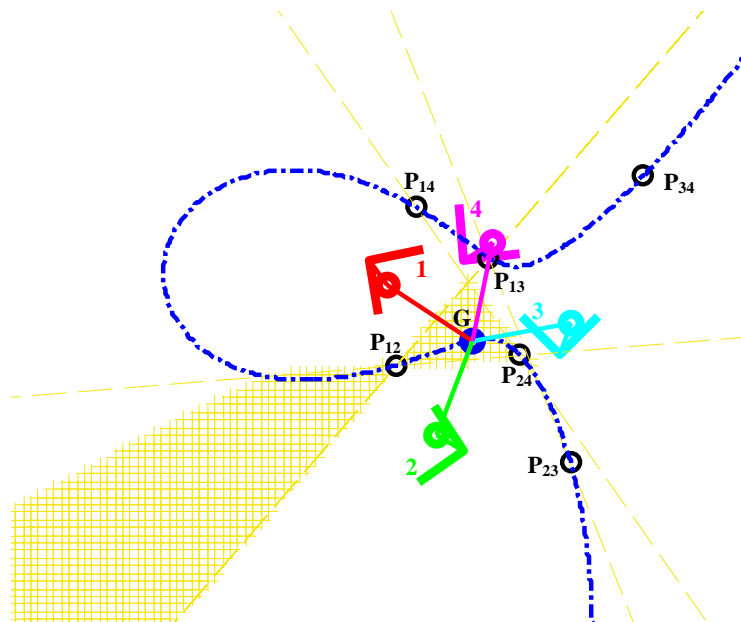
Figure 5.6a illustrates four task positions with the following coordinates and orientations:  $\mathbf{d}_1 = [0, 0]^T$ ,  $\theta_1 = -80^\circ$ ,  $\mathbf{d}_2 = [1, -2]^T$ ,  $\theta_2 = 124^\circ$ ,  $\mathbf{d}_3 = [2, -1]^T$ ,  $\theta_3 = 45^\circ$ ,  $\mathbf{d}_4 = [1, 0]^T$ ,  $\theta_4 = 5^\circ$ . Also shown are the associated displacement poles, the center-point curve, and crosshatched regions that satisfy the propeller theorem. In addition, a fixed pivot location is selected in a crosshatched region. A line is shown, extending in both directions from the fixed pivot and directed through  $\mathbf{P}_{12}$ . As the line is rotated counter-clockwise, it sweeps through  $\mathbf{P}_{34}$  and  $\mathbf{P}_{13}$  (with the section of the line located on the side opposite  $\mathbf{P}_{12}$ ), then  $\mathbf{P}_{23}$  (on the same side as  $\mathbf{P}_{12}$ ),  $\mathbf{P}_{14}$ , and finally  $\mathbf{P}_{24}$ . With this pole ordering, the propeller theorem states that the crank of a synthesized dyad will achieve the four positions in proper order. The resulting dyad is shown in Fig. 5.6b, and as the crank rotates monotonically in a counter-clockwise direction, the task positions are achieved in order.

### 5.7.2 Example 5-2

Figure 5.7a illustrates a second case of four task positions with the following coordinates and orientations:  $\mathbf{d}_1 = [2, 0]^T$ ,  $\theta_1 = 0^\circ$ ,  $\mathbf{d}_2 = [3, 2]^T$ ,  $\theta_2 = 45^\circ$ ,  $\mathbf{d}_3 = [1, 1]^T$ ,  $\theta_3 = 90^\circ$ ,  $\mathbf{d}_4 = [-1, 2]^T$ ,  $\theta_4 = 135^\circ$ . The poles and center-point curve are also shown. In this example, two poles,  $\mathbf{P}_{13}$  and  $\mathbf{P}_{24}$ , are coincident. The propeller method makes apparent the problem associated with this case. When the rotating line strikes  $\mathbf{P}_{13}$ , it also intersects  $\mathbf{P}_{24}$ , but the propeller theorem dictates that  $\mathbf{P}_{14}$  must fall between  $\mathbf{P}_{13}$  and  $\mathbf{P}_{24}$ . Therefore, the only valid fixed pivots must be placed along the line defined by  $\mathbf{P}_{13}$ ,  $\mathbf{P}_{24}$ , and  $\mathbf{P}_{14}$ . That way, all three poles are swept at the same time by the rotating line. Figure 5.7b shows a dyad where  $\mathbf{P}_{23}$  is selected as the fixed pivot. A crank rotation of zero is generated between two positions, producing an unordered solution. It was previously identified that since two poles and the fixed pivot are collinear, a zero crank rotation will

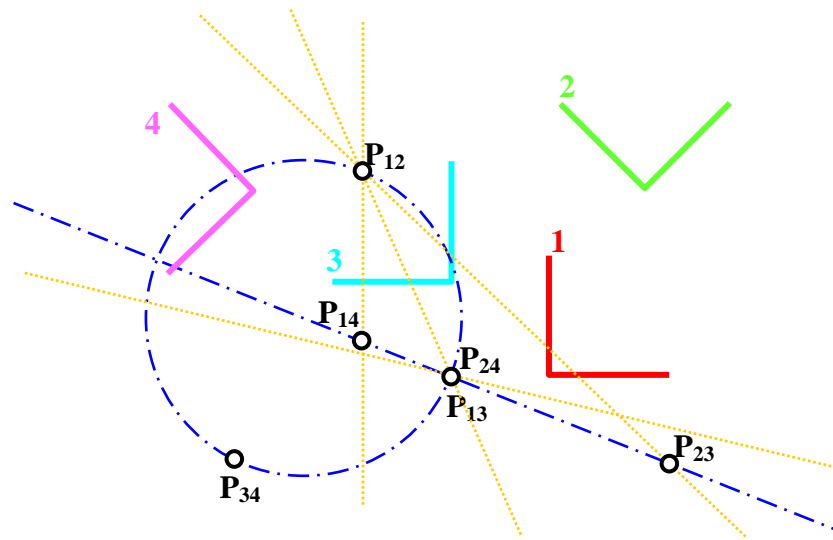


(a) Propeller in start position

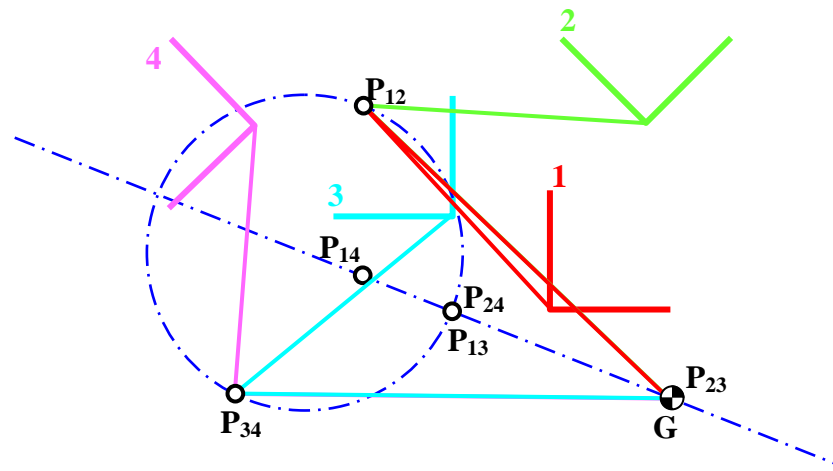


(b) Synthesized dyad

Figure 5.6: The four-position application of the propeller method in Example 5-1, with the regions that satisfy the theorem crosshatched.

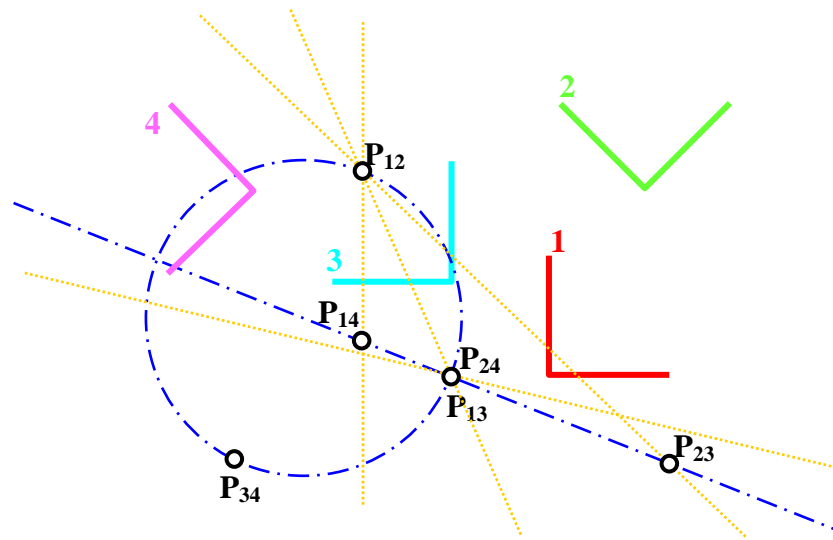


(a) Positions generate coincident poles

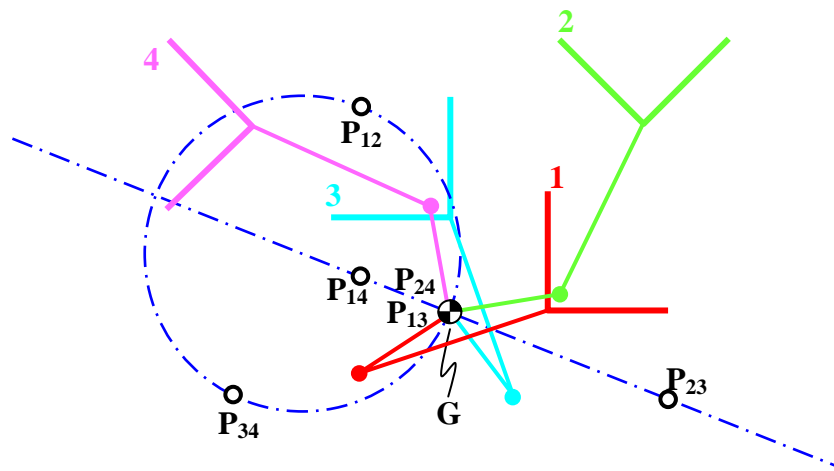


(b) Synthesized dyad with a crank rotation of zero.

Figure 5.7: The special four-position application of the propeller method in Example 5-2.



(c) An ordered dyad solution.



(d) An unordered dyad solution.

Figure 5.7: The special four-position application of the propeller method in Example 5-2 (con't).



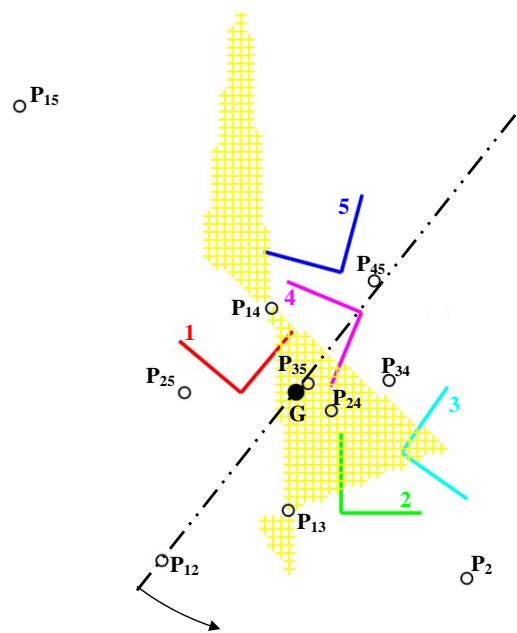
result. Notice that selecting a fixed pivot anywhere along the straight portion of the center-point curve, excluding  $P_{13}/P_{24}$ , will generate a “zero crank rotation” solution similar to the one shown in Fig. 5.7b. When  $P_{13}/P_{24}$  is selected as a fixed pivot, a corresponding moving pivot location is not unique. Thus, multiple dyad solutions are possible, some ordered and others not. This is common in degenerate task positions when placing a fixed pivot at coincident poles. Figure 5.7c shows a dyad that generates an ordered solution, while Fig. 5.7d shows another dyad from the same fixed pivot that produces an unordered solution. This example demonstrates that the propeller method can readily identify situations with highly restricted possibilities for ordered dyads.

### 5.7.3 Example 5-3

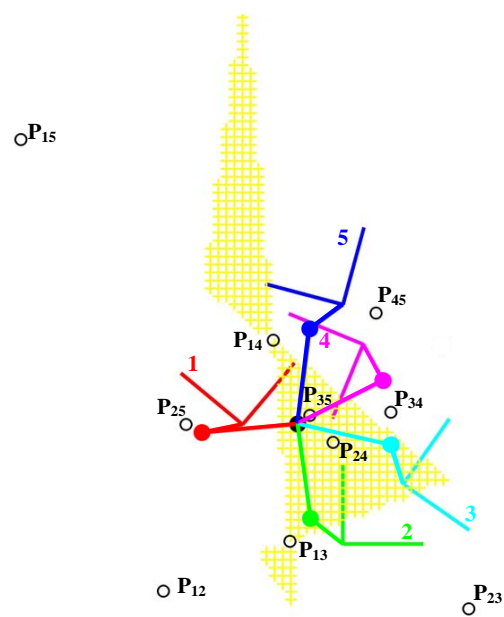
Figure 4.26 illustrates five precision points with the following coordinates and orientations:  $\mathbf{d}_1 = [-2, -2]^T$ ,  $\theta_1 = 50^\circ$ ,  $\mathbf{d}_2 = [3, -8]^T$ ,  $\theta_2 = 0^\circ$ ,  $\mathbf{d}_3 = [6, -5]^T$ ,  $\theta_3 = -35^\circ$ ,  $\mathbf{d}_4 = [4, 2]^T$ ,  $\theta_4 = 105^\circ$ ,  $\mathbf{d}_5 = [3, 4]^T$ ,  $\theta_5 = 75^\circ$ . The displacement poles and crosshatched regions that satisfy the propeller method are also shown. A feasible fixed pivot location is shown, consistent with five-position synthesis techniques. Also, a line is shown extending in both directions through the fixed pivot and directed through  $P_{12}$ . As the line is rotated counter-clockwise, it sweeps through  $P_{45}P_{13}P_{14}P_{23}P_{24}P_{15}P_{25}P_{34}P_{35}$ . The propeller method indicates that the crank of a dyad will achieve the five positions in proper order. The resulting dyad is shown in Fig. 4.27.

### 5.7.4 Example 5-4

Sets of five task positions have been identified for which no fixed pivots are able to satisfy the propeller method. Thus, no ordered solutions exist on the entire plane. Figure 5.9 illustrates a set of five such task positions with the following coordinates and orientations:  $\mathbf{d}_1 = [0, 0]^T$ ,  $\theta_1 = 10^\circ$ ,  $\mathbf{d}_2$



(a) Propeller in start position



(b) Synthesized dyad

Figure 5.8: The five-position application of the propeller method from Example 5-3, with ordered regions crosshatched.

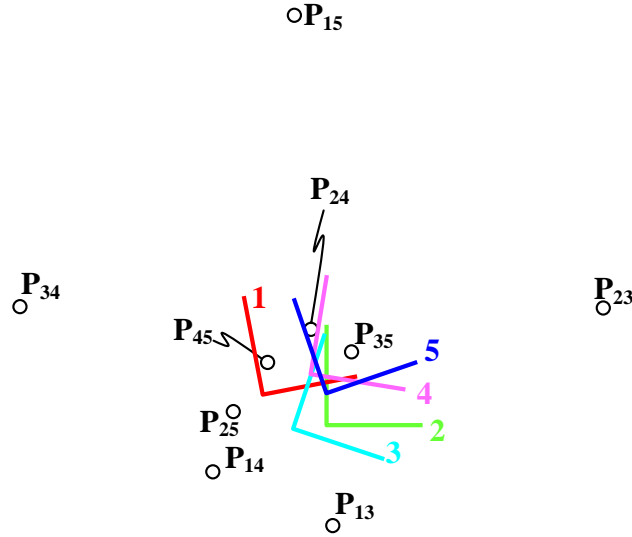


Figure 5.9: The five-position problem from Example 5-4, without any ordered regions.

$$= [2, -2]^T, \theta_2 = 0^\circ, \mathbf{d}_3 = [1, 1]^T, \theta_3 = -10^\circ, \mathbf{d}_4 = [0, -2]^T, \theta_4 = -20^\circ, \mathbf{d}_5 = [2, 0]^T, \theta_5 = 20^\circ.$$

This scenario is readily identified using the propeller method.

## 5.8 Summary

The order in which any number of design positions are reached with an RR dyad depends solely on the relative location of the fixed pivot and the displacement poles. This chapter presents the propeller method, a straightforward check of whether finitely separated positions will be reached in order, developed from fundamental relationships of displacement poles. Necessary and sufficient conditions for an ordered solution are developed, reducing the complexity of the order check. The method assumes a counter-clockwise rotation of a line that passes through the fixed pivot, but is equally applicable to a clockwise rotation. The line, or propeller, must encounter the displacement

poles in a specific order to ensure that the positions will be reached in order with a counter-clockwise rotation of the crank.

## **CHAPTER VI**

### **CONCLUSIONS AND FUTURE WORK**

#### **6.1 Contributions of the Dissertation**

This dissertation builds upon many existing techniques of rigid-body guidance to develop new methods of synthesis and analysis. Many practical rigid-body guidance design problems can benefit from the developments of this study. One specific application is planar, rigid-body, shape-changing mechanisms.

Chapter 2 presents a study that outlines a procedure to identify four finitely separated positions that create distinctive shapes of the center-point curve. This study is unique in determining a set of design positions that arrange the poles in specific shapes resulting in these center-point curves. Shapes explored include open and closed forms of a rhombus, kite, parallelogram, and quadrilaterals with the sum of the lengths of two sides is equal to that of the other two. Further, the association between these distinctive compatibility linkages and the unusual center-point curves is noted. The process is expanded to generate distinctive pole arrangements in three- and five-position cases.

Four- and five-position pole configurations for which the associated center-point curve(s) includes the line at infinity are identified. With a center-point line at infinity, a PR dyad with line of slide in any direction can be synthesized to achieve the design positions. Further, four- and five-position pole configurations for which the associated circle-point curve(s) includes the line at

infinity are identified. With a circle-point curve that includes a line at infinity, an RP dyad originating anywhere on a center-point curve can be synthesized to achieve the design positions. If the rigid-body guidance problem is approximate, small changes to the positions may result in the introduction of a one-parameter family of dyads including a prismatic joint.

It was also discovered that a slider-crank mechanism serves as a compatibility linkage. A study explored the implications as a vertex of the compatibility linkage is selected at infinity. The resulting linkage is a slider-crank. A procedure is outlined to generate slider cranks that serve as compatibility linkages. Further, a parameterization of the center-point curve by the crank angle of the slider-crank is given. This study is presented in Appendix A.

Chapter 3 extended the concepts used in the analysis of a 3-RPR platform to gain insight into single-actuated linkages. By generating a singularity locus, the number of singularities, geometric inversions, and circuit regimes are revealed. The input/output motion of the linkage can be inferred from the locus. The process is unique in that the methodology to produce the singularity locus does not rely on geometrical conditions. By using the locus, desired operational features such as a fully rotatable crank, or unique motion characteristics, such as a greater than  $360^\circ$  non-rotatable crank can be identified. Further, it is observed that transition linkages serve as bounds between regions of different circuits. Examples presented include the Stephenson III linkage, actuated from within and outside the four-bar sub-chain. This linkage serves as the foundation for shape-changing mechanisms that approximate open curves.

Chapter 4 presented an analysis to create the singularity condition of an Assur mechanism. This extensible kinematic architecture is particularly relevant to shape-changing mechanisms that approximate closed curves. The general singularity equation was reduced to a condensed form, which allows geometric relationships to be readily detected. A procedure for generating the reduced

form of the singularity condition for an Assur Class  $N$  mechanism, knowing the condition for a Class  $N - 1$ , is presented. Additionally, a procedure for producing the singularity condition with an alternate driving dyad is presented. This approach is illustrated with several examples.

The order in which any number of design positions are reached with an RR dyad depends solely on the relative location of the fixed pivot and the displacement poles. Chapter 5 presents the propeller method, a straightforward check of whether finitely separated positions will be reached in order, developed from fundamental relationships of displacement poles. Necessary and sufficient conditions for an ordered solution are developed, reducing the complexity of the order check. The method rotates a line, or propeller, that passes through the fixed pivot in the direction consistent with the crank. The line must encounter the displacement poles in a specific order to ensure that the positions will be reached in order.

## 6.2 Directions for Future Work

The developments presented in Chapter 2 require movement of the poles to realize the benefits. The corresponding displacement of the task positions introduce structural errors into the synthesis process. In order to evaluate the advantages of introducing prismatic joints, the amount of error introduced must be understood. A study relating the movement of the poles into a desired arrangement and the subsequent change in task positions is necessary.

In similar a vein, the singularity locus of Chapter 3 is used to determine the changes required in the length of an adjustment link to produce a desired motion scheme or number of circuits of a given mechanism. If the intention of the mechanism is rigid body guidance, structural errors are produced as link lengths are adjusted. A study on the deviation of the task positions as a select link length is altered is necessary

Several different metrics have been developed to assess the quality of approximate motion synthesis. One includes measures of the closeness of the actual positions achieved by a synthesized mechanism and the original task positions. Others involve the proximity to singularities, the actuation forces required, the sensitivity to manufacturing tolerances of link lengths, and other practical considerations. A study that generates a composite metric for several applications is appropriate. Once a metric is formulated, it should be incorporated into the studies identified in the previous paragraphs.

Specific to the mechanization of shape-changing linkages, several improvements can be made that require further research. Currently, approximate guidance techniques are used when more than 3 design profiles are specified. Assessing precision-point possibilities for 4 and 5 positions should be included. This could lead to integrating the developments presented in Chapter 2 of this dissertation.



## APPENDIX A

### SLIDER CRANKS AS COMPATIBILITY LINKAGES FOR PARAMETERIZING CENTER POINT CURVES

#### A-1 Introduction

This chapter explores the implications as a vertex of the compatibility linkage is selected at infinity. The resulting linkage becomes a slider-crank. Sections A-2 and A-3 review existing results that will be used to develop a procedure to generate a slider-crank that serves as a compatibility linkage. The center-point curve is then parameterized by the crank angle of the slider crank. The final section illustrates examples with different center-point curve types and the generating slider-crank compatibility linkage.

#### A-2 Compatibility Linkage

As presented in Chapter 2, an opposite pole quadrilateral is defined by four poles, such that the poles along the diagonal do not share an index. For the four position case, three different opposite pole quadrilaterals can be formed with vertices  $P_{12}P_{23}P_{34}P_{14}$ ,  $P_{12}P_{24}P_{34}P_{13}$ , and  $P_{13}P_{23}P_{24}P_{14}$ . An opposite pole quadrilateral can serve as a compatibility linkage [48].

The compatibility linkage can be used to graphically construct a center-point curve. As the crank of the compatibility linkage is displaced an arbitrary amount, a feasible center point can be located by determining the pole of the coupler displacement as shown in Fig. A-1. The center-point

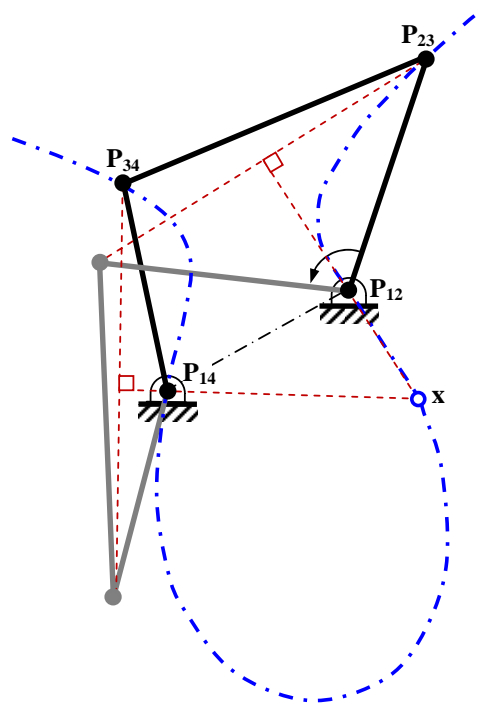


Figure A-1: Compatibility linkage used to generate a feasible center point.

curve is generated by tracking the coupler displacement pole between the original compatibility linkage and numerous assembly configurations.

The intersection of lines along opposite sides of an opposite pole quadrilateral are designated as  $Q_{ij}$ -points, where the subscript designates the uncommon positions defining the two poles. For example, the intersection of  $P_{12}P_{14}$  and  $P_{23}P_{34}$  is designated as  $Q_{24}$ . Along with the six poles, the center-point curve passes through the six  $Q_{ij}$  points as shown in Fig. A-2.

Cubic curves have a principal focus  $F$  defined as the intersection of its tangents at the isotropic points. Bottema and Roth [20] state that the focus of the center-point curve is on the curve itself, which is not a general requirement of circular cubic curves. They present a formulation for

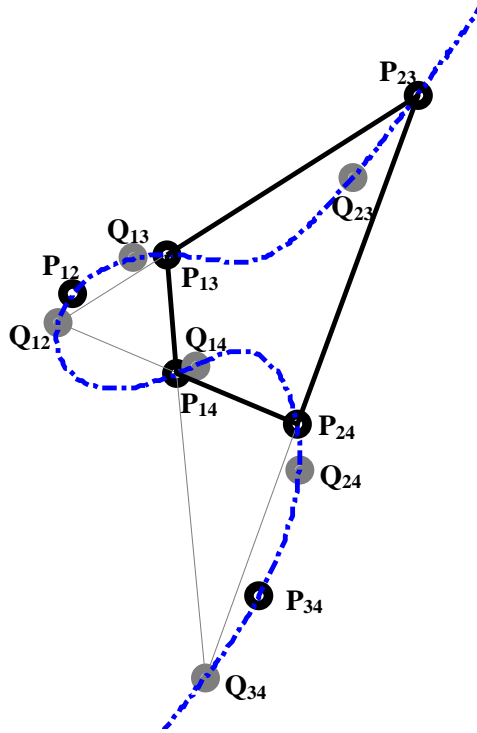


Figure A-2: Q Points are on the center-point curve.

**F** using specialized coordinates. Beyer [18] describes a geometric construction to locate the focus. Three circumscribed circles  $\bar{J}$ ,  $\bar{J}'$ , and  $\bar{J}''$  are constructed from  $P_{23}P_{24}Q_{12}$ ,  $P_{13}P_{14}Q_{12}$  and  $P_{13}P_{23}Q_{34}$ , respectively. The intersection of  $\bar{J}$ ,  $\bar{J}'$ , and  $\bar{J}''$  locates **F**. The construction is illustrated in Fig. A-3

### A-3 Algebraic form of Center-point Curves

Burmester showed that every point on a center-point curve must view opposite sides of a compatibility linkage in equal or supplementary angles, as shown in Fig. A-4. Vertices of the compatibility linkage are designated as points  $P_i = (p_i, q_i)^T$ ,  $i = 1, 2, 3, 4$ . The condition that a point **x** on

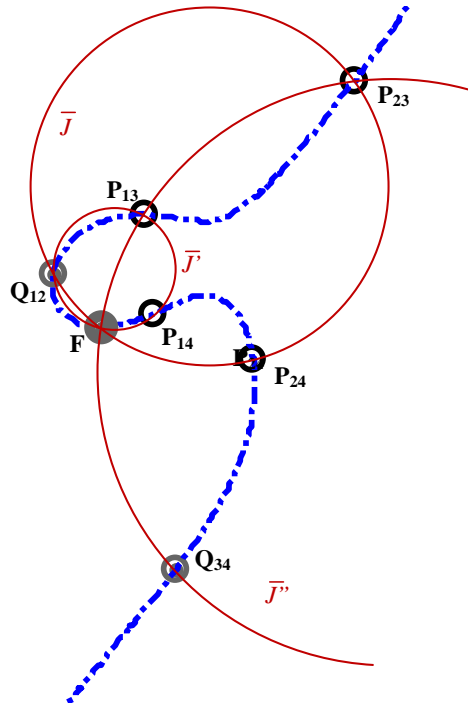


Figure A-3: Graphical construction of the principal focus.

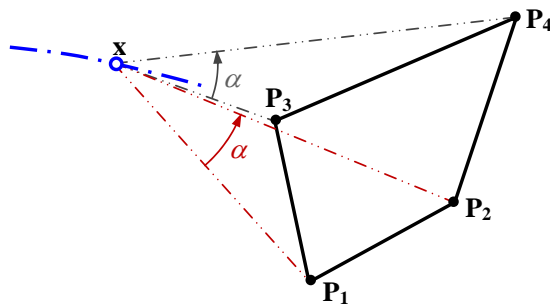


Figure A-4: Feasible center-point views opposite sides in equal, or supplementary, angles.

the center-point curve views sides  $\mathbf{P}_1\mathbf{P}_2$  and  $\mathbf{P}_3\mathbf{P}_4$  in the angle  $\alpha$  is

$$\begin{aligned}\alpha &= \frac{|(\mathbf{P}_1 - \mathbf{x}), (\mathbf{P}_2 - \mathbf{x})|}{|(\mathbf{P}_1 - \mathbf{x}) \cdot (\mathbf{P}_2 - \mathbf{x})|} \\ &= \frac{|(\mathbf{P}_3 - \mathbf{x}), (\mathbf{P}_4 - \mathbf{x})|}{|(\mathbf{P}_3 - \mathbf{x}) \cdot (\mathbf{P}_4 - \mathbf{x})|}.\end{aligned}\tag{A-1}$$

The vertical bars denote the  $2 \times 2$  determinant of the matrix formed by the coordinates. Expanding Eq. A-1 produces

$$\begin{aligned}(C_1x + C_2y)(x^2 + y^2) + C_3x^2 + C_4y^2 + C_5xy \\ + C_6x + C_7y + C_8 = 0.\end{aligned}\tag{A-2}$$

The coefficients  $C_i$  are in terms of the vertices  $\mathbf{P}_i$  :

$$C_1 = q_1 - q_2 - q_3 + q_4,\tag{A-3}$$

$$C_2 = -p_1 + p_2 + p_3 - p_4,\tag{A-4}$$

$$\begin{aligned}C_3 &= -p_2q_1 - (p_3 + p_4)(q_1 - q_2) + p_1q_2 + p_4q_3 \\ &\quad + (p_1 + p_2)(q_3 - q_4) - p_3q_4,\end{aligned}\tag{A-5}$$

$$\begin{aligned}C_4 &= -p_2q_1 + p_1q_2 + (p_4 - p_3)(q_1 + q_2) + p_4q_3 \\ &\quad - p_3q_4 - (p_2 - p_1)(q_3 + q_4),\end{aligned}\tag{A-6}$$

$$C_5 = 2(p_1p_4 - p_2p_3 - q_1q_4 + q_2q_3),\tag{A-7}$$

$$\begin{aligned}C_6 &= p_2(p_3 + p_4)q_1 + p_3p_4(q_1 - q_2) - p_1(p_3 + p_4)q_2 \\ &\quad - (p_1 + p_2)p_4q_3 - p_1p_2(q_3 - q_4) \\ &\quad - q_1q_2(q_3 - q_4) + (p_1 + p_2)p_3q_4 + (q_1 - q_2)q_3q_4,\end{aligned}\tag{A-8}$$

$$\begin{aligned}C_7 &= (p_2 - p_1)p_3p_4 - p_1p_2(p_4 - p_3) - (p_4 - p_3)q_1q_2 \\ &\quad - p_4(q_1 + q_2)q_3 + p_3(q_1 + q_2)q_4 + (p_2 - p_1)q_3q_4\end{aligned}$$

$$+p_2q_1(q_3 + q_4) - p_1q_2(q_3 + q_4), \quad (\text{A-9})$$

$$\begin{aligned} C_8 &= -p_2p_3p_4q_1 + p_1p_3p_4q_2 + p_1p_2p_4q_3 + p_4q_1q_2q_3 \\ &\quad -p_1p_2p_3q_4 - p_3q_1q_2q_4 - p_2q_1q_3q_4 + p_1q_2q_3q_4. \end{aligned} \quad (\text{A-10})$$

Since the center-point equation is homogeneous, any set of coefficients  $(KC_i)$ , where  $i = 1, 2, \dots, 8$ , and  $K$  is constant, defines the same curve. Murray and McCarthy [49] state that any four vertices that produce a set of coefficients  $(KC_i)$  consistent with Eq. A-2 serves as a compatibility linkage. Using the opposite pole quadrilateral as the compatibility linkage,  $\mathbf{P}_1 = \mathbf{P}_{12}$ ,  $\mathbf{P}_2 = \mathbf{P}_{14}$ ,  $\mathbf{P}_3 = \mathbf{P}_{23}$  and  $\mathbf{P}_4 = \mathbf{P}_{34}$ . Equations A-3 through A-10 can be used to determine values for the coefficients of the center-point curve.

As the center-point curve approaches infinity, the highest order terms in Eq. A-2 dominate. The equation of the asymptote is

$$C_1x + C_2y = 0, \quad (\text{A-11})$$

which has a slope

$$m = y/x = -C_1/C_2. \quad (\text{A-12})$$

#### A-4 Alternative Compatibility Linkages

Given a center-point curve, Murray and McCarthy [49] outline a method to determine  $\mathbf{P}_3$  and  $\mathbf{P}_4$  for any  $\mathbf{P}_1$  and  $\mathbf{P}_2$  selected on the curve. Using that procedure, it is observed that only the opposite vertices are dependent on each other. That is, selecting a new  $\mathbf{P}_1$ , but leaving  $\mathbf{P}_2$  unchanged, corresponds to a change only in  $\mathbf{P}_4$ . Likewise, selecting a new  $\mathbf{P}_2$ , but leaving  $\mathbf{P}_1$  unchanged, corresponds to a change only in  $\mathbf{P}_3$ .

Equations A-3 through A-10 can be written as a linear combination of the components of a single vertex  $\mathbf{P}_j$

$$f_i = R_i p_j + S_i q_j + T_i - K C_i = 0, \quad (\text{A-13})$$

where  $i = 1, 2, \dots, 8$  and  $R_i, S_i, T_i = f(p_k, q_k), k \neq j$ .

Starting with the opposite pole quadrilateral, an alternative compatibility vertex  $\mathbf{P}_{1A}$  can be selected as any point on the center-point curve, and the corresponding vertex  $\mathbf{P}_{4A}$  can be readily found. Values for  $p_{1A}, q_{1A}, p_2, q_2, p_3$  and  $q_3$  can be substituted into any three Eqs. A-3 through A-10. By factoring  $p_{4A}$  and  $q_{4A}$ , the coefficients  $R_i, S_i$ , and  $T_i$  of Eq. A-13 are determined. Written in matrix form,

$$\begin{bmatrix} R_{i_1} & S_{i_1} & C_{i_1} \\ R_{i_2} & S_{i_2} & C_{i_2} \\ R_{i_3} & S_{i_3} & C_{i_3} \end{bmatrix} \begin{Bmatrix} p_{4A} \\ q_{4A} \\ K \end{Bmatrix} = \begin{bmatrix} -T_{i_1} \\ -T_{i_2} \\ -T_{i_3} \end{bmatrix} \quad (\text{A-14})$$

is used to solve for the corresponding vertex  $\mathbf{P}_{4A}$ . In the same manner, this procedure applies to selecting an alternative  $\mathbf{P}_{2A}$  on the center-point curve and solving for the corresponding  $\mathbf{P}_{3A}$ .

As an example, design positions are given as  $\mathbf{d}_1 = (5, -10)^T, \theta_1 = 200^\circ, \mathbf{d}_2 = (0, 0)^T, \theta_2 = -100^\circ, \mathbf{d}_3 = (5, 0)^T, \theta_3 = 50^\circ$  and  $\mathbf{d}_4 = (10, -5)^T, \theta_4 = 100^\circ$ . Poles comprising a compatibility linkage are calculated as  $\mathbf{P}_{12} = \mathbf{P}_1 = (-6.1603, -9.3301)^T, \mathbf{P}_{23} = \mathbf{P}_3 = (2.5000, 0.6699)^T, \mathbf{P}_{34} = \mathbf{P}_4 = (12.8613, 2.8613)^T$ , and  $\mathbf{P}_{14} = \mathbf{P}_2 = (9.5977, -9.5977)^T$ . Moving  $\mathbf{P}_1$  to an arbitrary point on the curve  $\mathbf{P}_{1A} = (-0.4094, -7.2907)^T$ , Eq. A-14 is used with  $i_1 = 3, i_2 = 5$ , and  $i_3 = 8$  to determine the corresponding  $\mathbf{P}_{4A} = (10.0216, -0.5047)^T$ . The two remaining vertices  $\mathbf{P}_2$  and  $\mathbf{P}_3$  remain unaffected. The resulting alternative compatibility linkage is shown in Fig. A-5.

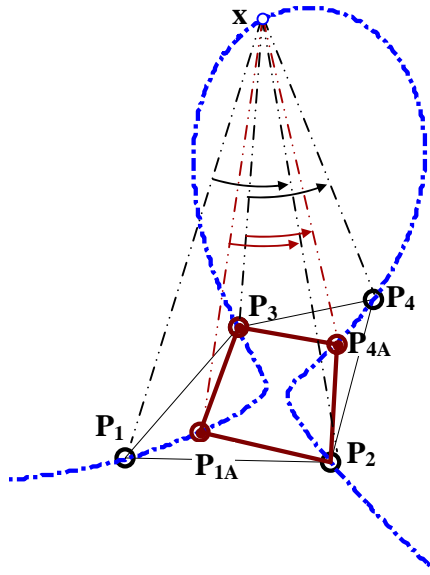


Figure A-5: Compatibility linkage with alternate vertices.

### A-5 Slider-Crank Compatibility Linkages

By selecting an alternative vertex of the compatibility linkage at infinity along the asymptote of the center-point curve, the compatibility linkage becomes a slider-crank mechanism as shown in Fig. A-6. If vertex  $P_{1A}$  is moved to infinity and  $P_2$  is considered the fixed pivot, vertex  $P_3$  becomes a revolute joint attached to a prismatic, where the line of slide is perpendicular to the asymptote of the center-point curve. Substituting the point  $(p_{1A}, q_{1A})$  into Eq. A-12 and rearranging gives

$$n = -1/m = -p_{1A}/q_{1A}. \quad (\text{A-15})$$

As  $p_{1A}$  and  $q_{1A}$  become large, so do the coefficients in Eqs. A-3 through A-10. Therefore, the center-point equation will be normalized to deal with the numerical issues. If  $C_1 \neq 0$ , Eq. A-2 is



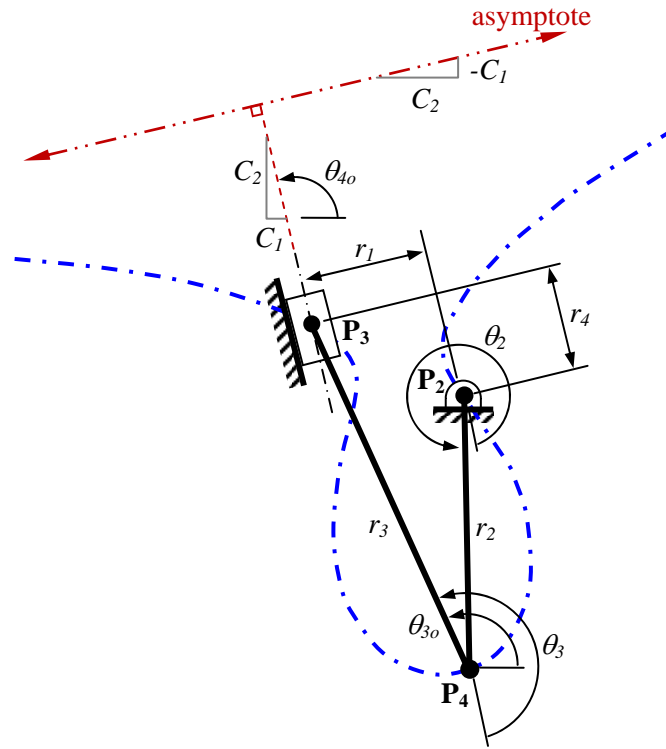


Figure A-6: Slider-crank compatibility linkage.

divided by  $C_1$  throughout, producing

$$\begin{aligned} (x + \frac{C_2}{C_1}y)(x^2 + y^2) + \frac{C_3}{C_1}x^2 + \frac{C_4}{C_1}y^2 + \frac{C_5}{C_1}xy \\ + \frac{C_6}{C_1}x + \frac{C_7}{C_1}y + \frac{C_8}{C_1} = 0, \end{aligned} \quad (\text{A-16})$$

observing that

$$\begin{aligned} \frac{C_2}{C_1} &= \frac{-p_{1A} + p_2 + p_3 - p_{4A}}{q_{1A} - q_2 - q_3 + q_{4A}} \\ &= \frac{-p_{1A} + p_2 + p_3 - p_{4A}}{q_{1A} - q_2 - q_3 + q_{4A}} \left( \frac{1/q_{1A}}{1/q_{1A}} \right) \\ &= \frac{-p_{1A}/q_{1A} + p_2/q_{1A} + p_3/q_{1A} - p_{4A}/q_{1A}}{q_{1A}/q_{1A} - q_2/q_{1A} - q_3/q_{1A} + q_{4A}/q_{1A}} \end{aligned} \quad (\text{A-17})$$

$$= \frac{-p_{1A}/q_{1A} + (p_2 + p_3 - p_{4A})/q_{1A}}{1 + (-q_2 - q_3 + q_{4A})/q_{1A}}.$$

When  $q_{1A} \rightarrow \infty$ , Eq. A-17 states  $C_2/C_1 = -p_{1A}/q_{1A} = n$ . Repeating this process on Eqs. A-5 through A-10 produces a set of  $C_i/C_1$ 's consistent with Eq. A-16. Specifically, using Eqs. A-5 and A-7,

$$-p_2 - p_3 - p_{4A} + (p_{1A}/q_{1A})q_2 + (p_{1A}/q_{1A})q_3 - (p_{1A}/q_{1A})q_{4A} = C_3/C_1, \quad (\text{A-18})$$

$$2(p_{1A}/q_{1A})p_{4A} - 2q_{4A} = C_5/C_1. \quad (\text{A-19})$$

Rewriting Eqs. A-18 and A-19 gives

$$\begin{aligned} & \begin{bmatrix} -1 & (C_2/C_1) \\ 2(C_2/C_1) & 2 \end{bmatrix} \begin{Bmatrix} p_{4A} \\ q_{4A} \end{Bmatrix} \\ &= \begin{bmatrix} p_2 + p_3 + (C_2/C_1)q_2 + (C_2/C_1)q_3 + C_3/C_1 \\ -C_5/C_1 \end{bmatrix}, \end{aligned} \quad (\text{A-20})$$

which can be solved for the corresponding vertex  $\mathbf{P}_{4A}$  associated with  $\mathbf{P}_{1A}$  at infinity. It is observed that this vertex  $\mathbf{P}_{4A}$  coincides with the focus of the center-point curve. Thus, Eq. A-20 becomes a direct calculation for the focus of a center-point curve to complement the construction shown in Fig.A-3.

Up to this point, the fixed pivot of the slider-crank compatibility linkage is  $\mathbf{P}_2 = \mathbf{P}_{14}$ . An alternative  $\mathbf{P}_{2A}$  can be placed anywhere on the curve. However, Eq. A-13 cannot be used with  $\mathbf{P}_{1A}$  at infinity. Using a process similar to generating Eq. A-20, Eqs. A-6 and A-10 can be divided by  $q_{1A} \rightarrow \infty$  and rewritten factoring  $p_{3A}$ , and  $q_{3A}$ , giving

$$\begin{aligned} & (-1)p_{3A} - (C_2/C_1)q_{3A} \\ & + [-C_4/C_1 - p_2 - p_4 - (C_2/C_1)(q_2 + q_4)] = 0, \end{aligned} \quad (\text{A-21})$$

and

$$[p_{2A}p_{4A} + (C_2/C_1)p_{4A}q_{2A} - (C_2/C_1)p_{2A}q_{4A} + q_{2A}q_{4A}]p_{3A}$$

$$\begin{aligned}
& + [(C_2/C_1)p_{2A}p_{4A} - p_{4A}q_{2A} + p_{2A}q_{4A} + (C_2/C_1)q_{2A}q_{4A}] q_{3A} \\
& + (C_8/C_1) = 0,
\end{aligned} \tag{A-22}$$

which can be used to determine the corresponding  $\mathbf{P}_{3A}$ . Thus, there is a one-dimensional set of slider-crank compatibility linkages that define a center-point curve. Additionally, kinematic inversion allows  $\mathbf{P}_{3A}$  to be considered the fixed pivot and  $\mathbf{P}_{2A}$  to be the revolute attached to the prismatic. Both forms of the slider-crank will generate identical center-point curves.

As an example, design positions are given as  $\mathbf{d}_1 = (0, 0)^T$ ,  $\theta_1 = 0^\circ$ ,  $\mathbf{d}_2 = (1, 0)^T$ ,  $\theta_2 = 5^\circ$ ,  $\mathbf{d}_3 = (2, -1)^T$ ,  $\theta_3 = 10^\circ$  and  $\mathbf{d}_4 = (1, -2)^T$ ,  $\theta_4 = 20^\circ$ . Poles comprising the opposite pole quadrilateral are calculated as  $\mathbf{P}_{12} = \mathbf{P}_1 = (0.5000, 11.4519)^T$ ,  $\mathbf{P}_{23} = \mathbf{P}_3 = (12.9519, 10.9519)^T$ ,  $\mathbf{P}_{34} = \mathbf{P}_4 = (7.2150, -7.2150)^T$ , and  $\mathbf{P}_{14} = \mathbf{P}_2 = (6.1713, 1.8356)^T$ . The first two coefficients of the center-point curve, calculated from Eqs. A-3 and A-4, are  $C_1 = -8.5507$  and  $C_2 = 11.4081$ . The slope of the asymptote, calculated from Eq. A-12, is  $m = -C_1/C_2 = 1.3342$ . Moving  $\mathbf{P}_1$  to infinity, Eq. A-20 is used to determine the corresponding  $\mathbf{P}_4 = (-0.9628, 0.8037)^T$ . The two remaining vertices can be held as is, and the line of slide for  $\mathbf{P}_3$  will be perpendicular to the asymptote, having a slope  $n = C_2/C_1 = -0.7495$ . The resulting compatibility linkage is given in Fig. A-7.

## A-6 Parameterizing the Center-point Curve with the Slider-Crank Linkage

The link lengths of the compatibility slider-crank linkage as shown in Fig. A-6 are

$$r_2 = |\mathbf{P}_2 - \mathbf{P}_4|, \tag{A-23}$$

$$r_3 = |\mathbf{P}_3 - \mathbf{P}_4|. \tag{A-24}$$

The angle for the original configuration of link 3 and the angle of the slide direction of link 4 are

$$\theta_{3o} = \tan^{-1} \left( \frac{q_3 - q_4}{p_3 - p_4} \right), \tag{A-25}$$

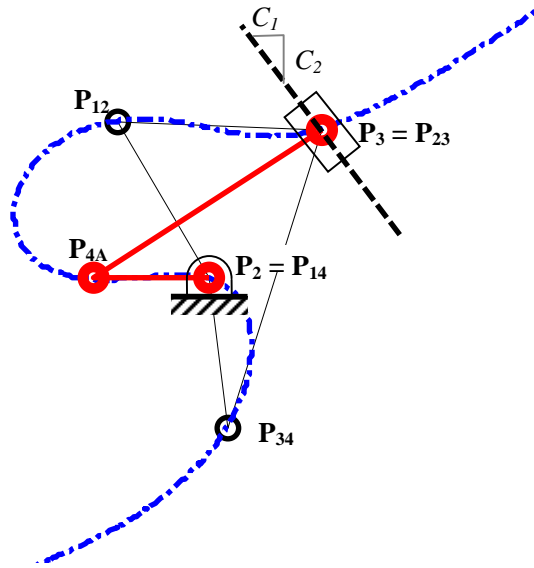


Figure A-7: Slider-crank compatibility linkage from example A-1.

$$\theta_{4o} = \tan^{-1} \left( \frac{C_2}{C_1} \right). \quad (\text{A-26})$$

In practice, a four-quadrant arctangent function should be used to ensure the proper angle. The offset distance is calculated as

$$r_1 = |\mathbf{P}_3 - \mathbf{P}_2| \sin \left[ \tan^{-1} \left( \frac{q_3 - q_2}{p_3 - p_2} \right) - \theta_{4o} \right]. \quad (\text{A-27})$$

The loop closure equations for a slider-crank linkage can be reduced to a well known equation for the coupler angle [2, 21, 22] as

$$\theta_3 = \sin^{-1} \left( \frac{r_1 - r_2 \sin \theta_2}{r_3} \right). \quad (\text{A-28})$$

The two angles resulting from the inverse sine function pertain to the two assembly circuits of the slider-crank linkage. Both configurations must be used to generate the center-point curve. The pole

for the displacement of the coupler from its initial position to an arbitrary position defined by  $\theta_2$  is

$$C(\theta_2) = A_\theta[A_\theta - A_o](\mathbf{P}_4 - \mathbf{d}_\theta) + \mathbf{d}_\theta, \quad (\text{A-29})$$

where

$$\mathbf{d}_\theta = \mathbf{P}_3 + r_2 \begin{bmatrix} \cos(\theta_2 + \theta_{4o}) \\ \sin(\theta_2 + \theta_{4o}) \end{bmatrix}, \quad (\text{A-30})$$

and  $A_o$  and  $A_\theta$  are determined by substituting  $\theta_{3o}$  and  $(\theta_3 + \theta_{4o})$  into Eq. 2.2, respectively.

Once all substitutions are made, Eq. A-29 defines a point on the center-point curve for every value of the crank angle  $\theta_2$ . Thus, the center-point curve is parameterized based on the crank angle of a slider-crank linkage. Using complex vector notation, Eq. A-29 can be rewritten into a form similar to McCarthy's 4R compatibility parameterization [48]. A benefit of this formulation is that a center-point curve can be classified by linkage type of the slider-crank that generates it, as will be discussed in the following section.

Parameterization by crank angle was applied to the example presented in Fig. A-7 with an angular increment of  $5^\circ$ . The resulting center-point curve is shown in Fig. A-8.

### A-7 Curve Types and the Generating Slider-Crank

Consistent with Chase, et al. [52], if a link in the generating linkage is able to fully rotate, the center-point curve will have a two circuits (bicursal). Conversely, if no link in the generating linkage is able to fully rotate, the center-point curve will have a single circuit (unicursal). The condition [23] that a slider-crank will have a link that fully rotates is

$$|r_3 - r_2| > r_1. \quad (\text{A-31})$$

A slider-crank that produces an equality of Eq. A-31 is considered a transition linkage by Murray [53].

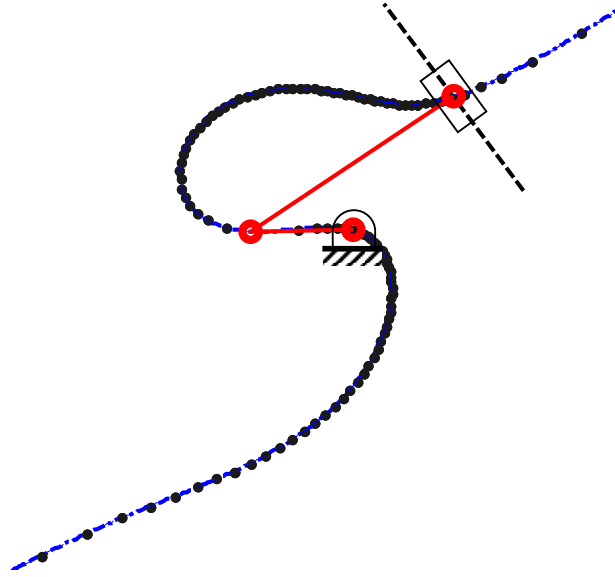


Figure A-8: Center-point curve generated from a slider-crank compatibility linkage.

### A-7.1 Example A-1: Unicursal, Center-point Curve

For the example presented at the end of Sec. A-5,  $r_1 = 13.1691$ ,  $r_2 = 2.2791$ , and  $r_3 = 15.2520$ . With these values, Eq. A-31 is not satisfied, and no link in the generating slider-crank is able to fully rotate resulting in a unicursal center-point curve (Fig. A-7).

### A-7.2 Example A-2: Bicursal, Center-point Curve

Design positions are given as  $\mathbf{d}_1 = (-2, 0)^T$ ,  $\theta_1 = 260^\circ$ ,  $\mathbf{d}_2 = (-2, 2)^T$ ,  $\theta_2 = 120^\circ$ ,  $\mathbf{d}_3 = (2, 4)^T$ ,  $\theta_3 = 60^\circ$  and  $\mathbf{d}_4 = (4, 3)^T$ ,  $\theta_4 = 0^\circ$ . Poles comprising the opposite pole quadrilateral are calculated as  $\mathbf{P}_{12} = \mathbf{P}_1 = (-1.6360, 1.0000)^T$ ,  $\mathbf{P}_{23} = \mathbf{P}_3 = (1.7321, -0.4641)^T$ ,  $\mathbf{P}_{34} = \mathbf{P}_4 = (2.1340, 1.7679)^T$ , and  $\mathbf{P}_{14} = \mathbf{P}_2 = (-0.2586, 4.0173)^T$ . The first two coefficients of the center-point curve, calculated from Eqs. A-3 and A-4, are  $C_1 = -0.7852$  and  $C_2 = 0.9755$ . Moving

$\mathbf{P}_{1A}$  to infinity, Eq. A-20 is used to determine the corresponding  $\mathbf{P}_{4A} = (8.0768, 1.5319)^T$ . The two remaining vertices can be held as is, and the line of slide for  $\mathbf{P}_3$  will be perpendicular to the asymptote, having a slope  $n = C_2/C_1 = -1.2422$ . The resulting compatibility linkage has  $r_1 = 1.2595$ ,  $r_2 = 8.6981$ , and  $r_3 = 6.6513$  and is shown in Fig. A-9a. With these values, Eq. A-31 is satisfied, indicating that a link in the generating slider-crank is able to fully rotate and resulting in a bicursal center-point curve

Selecting  $\mathbf{P}_{2A} = (-0.3166, 2.5566)^T$ , Eqs. A-21 and A-22 can be used to determine the corresponding  $\mathbf{P}_{3A} = (1.2984, 0.6009)^T$ . With these vertices, an in-line slider-crank generating linkage is created as shown in Fig. A-9b. This is the most basic type of generating linkage. Note that the in-line slider-crank is not possible for unicursal center-point curve forms as  $r_1 = 0$  in Eq. A-31 will always have a rotating link.

### A-7.3 Example A-3: Double-point, Center-point Curve

Design positions are given as  $\mathbf{d}_1 = (2, -1)^T$ ,  $\theta_1 = 120^\circ$ ,  $\mathbf{d}_2 = (-1, -0.8406)^T$ ,  $\theta_2 = -75^\circ$ ,  $\mathbf{d}_3 = (0, 0)^T$ ,  $\theta_3 = -45^\circ$  and  $\mathbf{d}_4 = (1, 1)^T$ ,  $\theta_4 = 45^\circ$ . Poles comprising the opposite pole quadrilateral are calculated as  $\mathbf{P}_{12} = \mathbf{P}_1 = (0.4895, -1.1178)^T$ ,  $\mathbf{P}_{23} = \mathbf{P}_3 = (-2.0686, 1.4457)^T$ ,  $\mathbf{P}_{34} = \mathbf{P}_4 = (0.0000, 1.0000)^T$ , and  $\mathbf{P}_{14} = \mathbf{P}_2 = (2.8032, 0.6516)^T$ . The first two coefficients of the center-point curve, calculated from Eqs. A-3 and A-4, are  $C_1 = -2.2151$  and  $C_2 = 0.2451$ . Moving  $\mathbf{P}_{1A}$  to infinity, Eq. A-20 is used to determine the corresponding  $\mathbf{P}_{4A} = (2.0685, 1.1399)^T$ . The two remaining vertices can be held as is, and the line of slide for  $\mathbf{P}_3$  will be perpendicular to the asymptote, having a slope  $n = C_2/C_1 = -0.1107$ . The resulting compatibility linkage has  $r_1 = 0.2534$ ,  $r_2 = 3.6919$ , and  $r_3 = 3.4386$  and is shown in Fig. A-10. With these

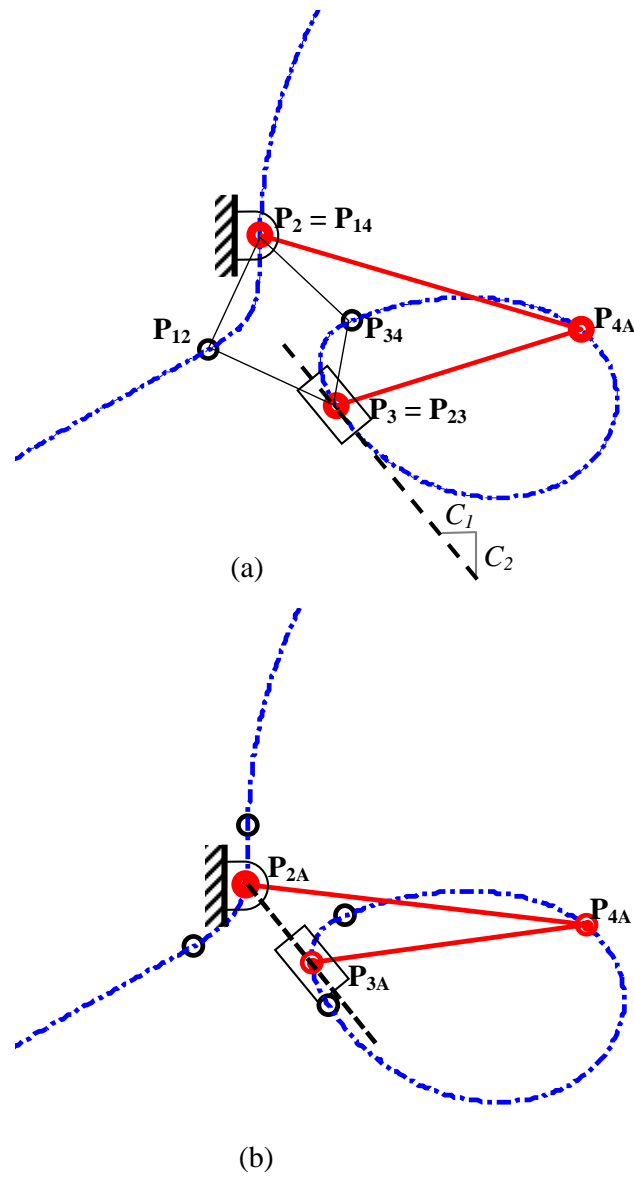


Figure A-9: Slider-crank compatibility linkage from example A-2.



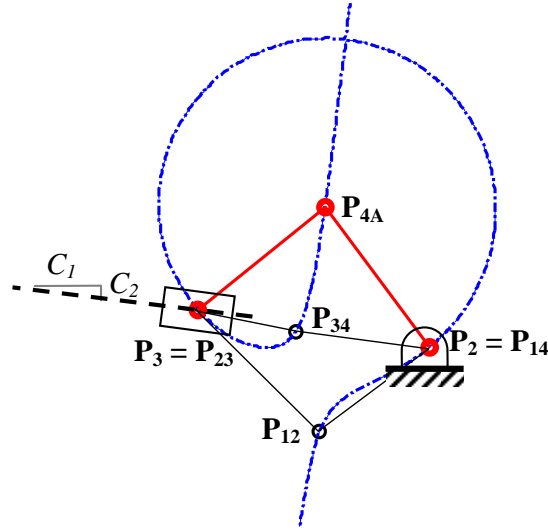


Figure A-10: Slider-crank compatibility linkage from example A-3.

values, Eq. A-31 becomes an equality producing a transition compatibility slider-crank in which the links are not aligned and which generates a double-point, center-point curve.

#### A-7.4 Example A-4: Circle-degenerate, Center-point Curve

Design positions are given as  $\mathbf{d}_1 = (0, 0)^T$ ,  $\theta_1 = -45^\circ$ ,  $\mathbf{d}_2 = (1, 1)^T$ ,  $\theta_2 = 45^\circ$ ,  $\mathbf{d}_3 = (2, -1)^T$ ,  $\theta_3 = 120^\circ$  and  $\mathbf{d}_4 = (1.2412, -2.8320)^T$ ,  $\theta_4 = -75^\circ$ . Poles comprising the opposite pole quadrilateral are calculated as  $\mathbf{P}_{12} = \mathbf{P}_1 = (0.0000, 1.0000)^T$ ,  $\mathbf{P}_{23} = \mathbf{P}_3 = (2.8032, 0.6516)^T$ ,  $\mathbf{P}_{34} = \mathbf{P}_4 = (1.7412, -1.9659)^T$ , and  $\mathbf{P}_{14} = \mathbf{P}_2 = (-4.6640, -3.7321)^T$ . The first two coefficients of the center-point curve, calculated from Eqs. A-3 and A-4, are  $C_1 = 2.1145$  and  $C_2 = -3.6020$ . Moving  $\mathbf{P}_{1A}$  to infinity, Eq. A-20 is used to determine the corresponding  $\mathbf{P}_{4A} = (4.4507, 1.6188)^T$ . The two remaining vertices can be held as is, and the line of slide for  $\mathbf{P}_3$  will be perpendicular to the asymptote, having a slope  $n = C_2/C_1 = -1.7034$ . The resulting compatibility linkage has  $r_1 = 8.6589$ ,  $r_2 = 10.5693$ , and  $r_3 = 1.9104$  and is shown in Fig. A-11.

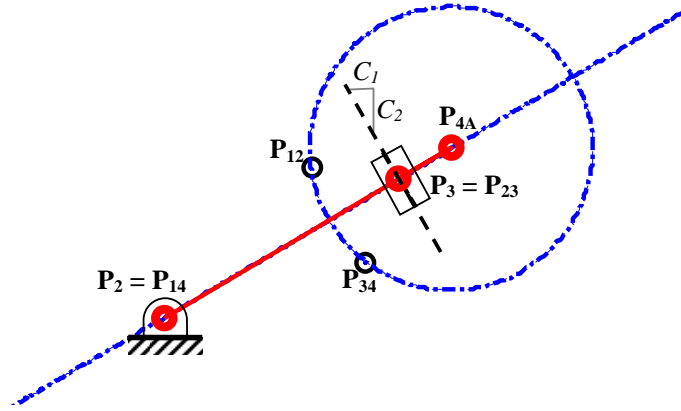


Figure A-11: Slider-crank compatibility linkage from example A-4.

With these values, Eq. A-31 becomes an equality producing a transition compatibility slider-crank in which the links are collinear and which generates a circle-degenerate, center-point curve. Notice in Fig. A-11 that  $P_{4A}$  is located at the center of the circle. Beyer [18] identifies that the focus of a circle-degenerate center-point curve is at the center of the circle.

#### A-7.5 Example A-5: Hyperbola-degenerate, Center-point Curve

Design positions are given as  $\mathbf{d}_1 = (0, 0)^T$ ,  $\theta_1 = -100^\circ$ ,  $\mathbf{d}_2 = (5, 0)^T$ ,  $\theta_2 = 50^\circ$ ,  $\mathbf{d}_3 = (10, -5)^T$ ,  $\theta_3 = 100^\circ$  and  $\mathbf{d}_4 = (10.7077, -6.0186)^T$ ,  $\theta_4 = 113^\circ$ . Poles comprising the opposite pole quadrilateral are calculated as  $\mathbf{P}_{12} = \mathbf{P}_1 = (2.5000, 0.6699)^T$ ,  $\mathbf{P}_{23} = \mathbf{P}_3 = (12.8613, 2.8613)^T$ ,  $\mathbf{P}_{34} = \mathbf{P}_4 = (14.8237, -2.4038)$ , and  $\mathbf{P}_{14} = \mathbf{P}_2 = (4.4624, -4.5952)^T$ . These poles form a parallelogram, and the first two coefficients of the center-point curve, calculated from Eqs. A-3 and A-4, are  $C_1 = C_2 = 0$ . Therefore, the procedure using Eq. A-20 is not applicable. Burmester [27] originally recognized that as the opposite pole quadrilateral is arranged as a parallelogram, the

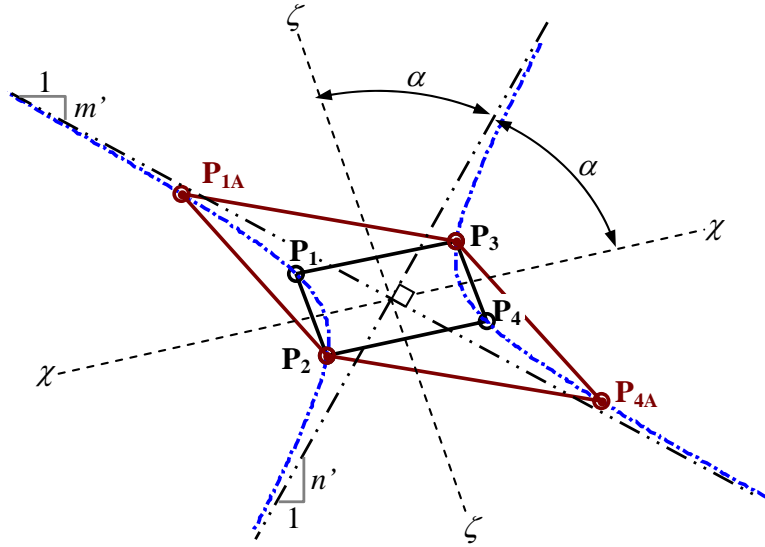


Figure A-12: Alternate compatibility linkage from example A-5.

center-point curve will degenerate into an equilateral hyperbola, as shown in Fig. A-12, and a circle at infinity.

With  $C_1 = C_2 = 0$ , Eqs. A-3 and A-4 dictate that as  $\mathbf{P}_1$  is moved to an alternate point  $\mathbf{P}_{1A}$ ,

$$q_{4A} = q_2 + q_3 - q_{1A}, \quad (\text{A-32})$$

$$p_{4A} = p_2 + p_3 - p_{1A}. \quad (\text{A-33})$$

Therefore, moving  $\mathbf{P}_{1A}$  to infinity,  $\mathbf{P}_{4A}$  will also move to negative infinity. With two vertices at infinity, and the resulting compatibility linkage is an RPRP, shown as bold red in Fig. A-13. The two remaining vertices are unaffected.

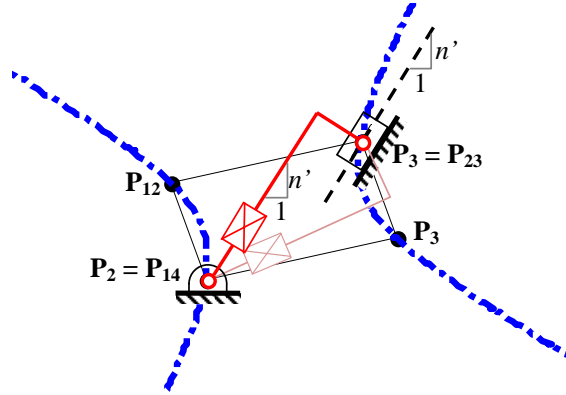


Figure A-13: RPRP compatibility linkage from example 5.

For an equilateral hyperbola,  $C_4 = -C_3$ , and the slopes of the two asymptotes (Salmon [71]) are

$$n', m' = \frac{C_5 \pm \sqrt{C_5^2 + 4C_3^2}}{2C_3}. \quad (\text{A-34})$$

The asymptote slope  $n'$  in Eq. A-34 also represents the line of slide for the prismatic joints of the compatibility linkage of Fig. A-13. For this hyperbola example,  $n' = 1.8184$ . The center-point curve is generated by tracking the coupler displacement pole as either prismatic joint is actuated. The assembly circuit shown bold red in Fig. A-13 will generate the circle at infinity. The hyperbola is generated by the alternate assembly circuit, shown in a muted red in Fig. A-13.

## A-8 Summary

This appendix explores the implications as a vertex of the compatibility linkage is selected at infinity. The resulting linkage is a slider-crank. A procedure is outlined to generate slider-cranks that serve as compatibility linkages. Further, a parameterization of the center-point curve by the crank angle of the slider-crank is given.

## BIBLIOGRAPHY

- [1] B. Hong and A. G. Erdman, "A method for adjustable planar and spherical four-bar linkage synthesis," *ASME J. of Mechanical Design*, vol. 127, no. 3, pp. 456–464, 2005.
- [2] A. G. Erdman, G. N. Sandor, and S. Kota, *Mechanism Design: Analysis and Synthesis*, 3rd ed. Englewood Cliffs, New Jersey: Prentice Hall, 2001, vol. 1.
- [3] S. Nesbit and M. Elzinga, "The application of path generation linkage synthesis to cyclic sports motions," *Sports Engineering*, vol. 10, no. 3, pp. 173–184, 2007.
- [4] J. T. Warner, A. E. Sherman, B. J. Fisher, and T. R. Chase, "Moving pivot specification for three precision position planar linkage synthesis," in *Proc. ASME International Design Engineering Technical Conference*, Brooklyn, NY, Aug. 3–6 2008, pp. DETC2008–49 040.
- [5] A. K. Mallik, A. Ghosh, and G. Ditttrich, *Kinematics Analysis and Synthesis of Mechanisms*. CRC Press, 1994.
- [6] P. L. Tso and K. C. Liang, "A nine-bar linkage for mechanical forming presses," *International Journal of Machine Tools and Manufacture*, vol. 42, no. 1, pp. 139–145, 2002.
- [7] G. N. Sandor and A. G. Erdman, *Advanced Mechanism Design: Analysis and Synthesis*. Englewood Cliffs, New Jersey: Prentice Hall, 1984, vol. 2.
- [8] S. Pramanik, "Kinematic synthesis of a six-member mechanism for automotive steering," *ASME J. of Mechanical Design*, vol. 124, no. 4, pp. 642–645, 2002.
- [9] J. A. Mirth, "Two precision positions of planar linkages with positional rectification," in *Proc. ASME International Design Engineering Technical Conference*, Irvine, CA, Sept. 24–28 1996, pp. MECH–1185.
- [10] A. Murray, J. Schmiedeler, and B. Korte, "Synthesis of planar, shape-changing rigid body mechanisms," *ASME J. of Mechanical Design*, vol. 130, no. 3, p. 032302, 2008.
- [11] J. Persinger, J. Schmiedeler, and A. Murray, "Synthesis of planar rigid-body mechanisms approximating shape changes defined by closed curves," *ASME J. of Mechanical Design*, vol. 131, no. 7, p. 071006, 2009.

- [12] F. Austin and W. V. Nostrand, "Shape control of an adaptive wing for transonic drag reduction," *SPIE Proceedings*, vol. 2447, pp. 45–55, 1995.
- [13] G. N. Washington, "Smart aperture antennas," *Journal of Smart Materials and Structures*, vol. 5, no. 6, pp. 801–805, 1996.
- [14] J. W. Martin, J. A. Main, and G. C. Nelson, "Shape control of deployable membrane mirrors," in *ASME Adaptive Structures and Materials Systems Conference*, Anaheim, CA, Nov. 15–20 1998, pp. 217–223.
- [15] P. Jardine, J. Flanagan, C. Martin, and B. Carpenter, "Smart wing shape memory alloy actuator design and performance," *SPIE Proceedings*, vol. 3044, pp. 48–55, 1997.
- [16] S. Ameduri, C. Espisito, and A. Concilio, "Active shape airfoil control through composite piezoceramic actuators," *SPIE Proceedings*, vol. 4327, pp. 641–650, 2001.
- [17] A. S. Hall, *Kinematics and Linkage Design*. Englewood Cliffs, New Jersey: Prentice Hall, 1961.
- [18] R. Beyer, *Kinematic Synthesis of Mechanisms*. New York: McGraw-Hill, 1963, translated by H. Kuenzel.
- [19] R. S. Hartenberg and J. Denavit, *Kinematic Synthesis of Linkages*. New York: McGraw-Hill, 1964.
- [20] O. Bottema and B. Roth, *Theoretical Kinematics*. New York: North-Holland Publishing Company, 1979.
- [21] R. Norton, *Kinematics and Dynamics of Machinery*, 4th ed. New York: McGraw-Hill, 2008.
- [22] K. J. Waldron and G. L. Kinzel, *Kinematics, Dynamics and Design of Machinery*, 2nd ed. New York, NY: John Wiley and Sons, 2004.
- [23] J. M. McCarthy, *Geometric Design of Linkages*. New York: Springer-Verlag, 2000.
- [24] H. Davis, T. Chase, and J. Mirth, "Circuit analysis of Stephenson chain six-bar mechanisms, mechanism synthesis and analysis," in *Proc. ASME International Design Engineering Technical Conference*, 1994, pp. 349–358.
- [25] J. Angeles and S. Bia, "Some special cases of the Burmester problem for four and five poses," in *Proc. ASME International Design Engineering Technical Conference*, Long Beach, CA, Sept. 24–28 2005, pp. DETC2005–84 871.
- [26] K. Brunthaler, M. Pfurner, and M. Husty, "Synthesis of planar four-bar mechanisms," *Trans. CSME*, vol. 30, no. 2, pp. 297–313, 2006.

- [27] L. Burmester, *Lehrbuch der Kinematic*. Leipzig, Germany: Verlag Von Arthur Felix, 1886.
- [28] C. H. Suh and C. W. Radcliffe, *Kinematics and Mechanism Design*. New York, NY: John Wiley and Sons, 1978.
- [29] Y. L. Sarkisyan, K. C. Gupta, and B. Roth, "Kinematic geometry associated with the least-square approximation of a given motion," *ASME J. of Engineering for Industry*, vol. 95, no. 2, pp. 503–510, 1973.
- [30] B. Ravani and B. Roth, "Motion synthesis using kinematic mappings," *ASME J. of Mechanisms, Transmissions and Automation in Design*, vol. 105, no. 2, pp. 460–467, 1983.
- [31] M. Hayes and P. Zsomer-Murray, "Solving the Burmester problem using kinematic mapping," in *Proc. ASME International Design Engineering Technical Conference*, Montreal, Canada, Sept. 29-Oct. 2 2002, pp. DETC2002–34 378.
- [32] H. P. Schrocker, M. Husty, and J. M. McCarthy, "Kinematic mapping based evaluation of assembly modes for planar four-bar synthesis," *ASME J. of Mechanical Design*, vol. 129, no. 9, pp. 924–929, 2007.
- [33] T. R. Chase and J. A. Mirth, "Circuits and branches of single-degree-of-freedom planar linkages," *ASME J. of Mechanical Design*, vol. 115, no. 2, pp. 223–230, 1993.
- [34] J. A. Mirth and T. R. Chase, "Circuit rectification for four precision position synthesis of four-bar and Watt six-bar linkages," *ASME J. of Mechanical Design*, vol. 117, no. 4, pp. 612–619, 1995.
- [35] S. S. Balli and S. Chand, "Defects in link mechanisms and solution rectification," *Mechanism and Machine Theory*, vol. 37, no. 9, pp. 851–876, 2002.
- [36] E. Filemon, "Useful ranges of centerpoint curves for design of crank and rocker linkages," *Mechanism and Machine Theory*, vol. 7, no. 1, pp. 47–53, 1972.
- [37] D. Foster and R. Cipra, "Assembly configurations and branches of planar single-input dyadic mechanisms," *ASME J. of Mechanical Design*, vol. 120, no. 3, pp. 381–386, 1998.
- [38] —, "An automatic method for finding the assembly configurations of planar non-single-input dyadic mechanisms," *ASME J. of Mechanical Design*, vol. 124, no. 1, pp. 58–67, 2002.
- [39] K. Wantanabe and H. Katoh, "Identification of motion domains of planar six-link mechanisms of the Stephenson-type," *Mechanism and Machine Theory*, vol. 39, no. 7, pp. 1081–1099, 2004.
- [40] F. Litvin and J. Tan, "Singularities in motion and displacement functions of constrained mechanical systems," *The International Journal of Robotics Research*, vol. 8, no. 2, pp. 30–43, 1989.

- [41] C. Gosselin and J. Angeles, "Singularity analysis of closed-loop kinematic chains," *IEEE Transactions on Robotics and Automation*, vol. 6, no. 3, pp. 281–290, 1990.
- [42] H. S. Yan and L. I. Wu, "The stationary configurations of planar six-bar kinematic chains," *Mechanism and Machine Theory*, vol. 23, no. 4, pp. 287–293, 1988.
- [43] K. J. Waldron, "The order problem of Burmester linkage synthesis," *ASME J. of Engineering for Industry*, vol. 97, no. 4, pp. 1405–1406, 1975.
- [44] —, "Graphical solution of the branch and order problems of linkage synthesis for multiply separated positions," *ASME J. of Engineering for Industry*, vol. 99, no. 3, pp. 591–597, 1977.
- [45] K. J. Waldron and R. T. Strong, "Improved solutions of the branch and order problems of Burmester linkage synthesis," *Mechanism and Machine Theory*, vol. 13, no. 2, pp. 199–207, 1978.
- [46] J. M. Prentis, "The pole triangle, Burmester theory and order and branching problems - I," *Mechanism and Machine Theory*, vol. 26, no. 1, pp. 19–30, 1991.
- [47] R. E. Keller, "Sketching rules for the curves of Burmester mechanism synthesis," *ASME J. of Engineering for Industry*, vol. 87, no. 5, pp. 155–160, 1965.
- [48] J. M. McCarthy, "The opposite pole quadrilateral as a compatibility linkage for parameterizing the center-point curve," *ASME J. of Mechanical Design*, vol. 115, no. 2, pp. 332–336, 1993.
- [49] A. P. Murray and J. M. McCarthy, "Center-point curves through six arbitrary points," *ASME J. of Mechanical Design*, vol. 119, no. 1, pp. 33–39, 1997.
- [50] C. Barker, "A complete classification of planar four-bar linkages," *Mechanism and Machine Theory*, vol. 130, no. 6, pp. 535–554, 1985.
- [51] J. Schaaf and J. Lammers, "Geometric characteristics of the center-point curve based on the kinematics of the compatibility linkage," in *Proc. of the ASME Design Engineering Technical Conference*, St. Louis, MO, Sept. 29–Oct. 21 1992.
- [52] T. R. Chase, A. G. Erdman, and D. R. Riley, "Improved center-point curve generation techniques for four-precision position synthesis using the complex number approach," *ASME J. of Mechanical Design*, vol. 107, no. 3, pp. 370–376, 1985.
- [53] A. Murray, M. Turner, and D. Martin, "Synthesizing single dof linkages via transition linkage identification," *ASME J. of Mechanical Design*, vol. 130, no. 2, p. 022301, 2008.
- [54] A. P. Murray and J. M. McCarthy, "Determining Burmester points from the analysis of a planar platform," *ASME J. of Mechanical Design*, vol. 117, no. 2, pp. 303–307, 1995.



- [55] J. A. Mirth and T. R. Chase, "Circuit analysis of Watt chain six-bar mechanisms," *ASME J. of Mechanical Design*, vol. 115, no. 2, pp. 214–222, 1993.
- [56] K. L. Ting and X. Dou, "Classification and branch identification of Stephenson six-bar chains," *Mechanism and Machine Theory*, vol. 31, no. 3, pp. 283–295, 1996.
- [57] C. Innocenti and V. Parenti-Castelli, "Singularity-free evolution from one configuration to another in serial and fully parallel manipulators," *ASME J. of Mechanical Design*, vol. 120, no. 1, pp. 73–99, 1998.
- [58] P. R. McAree and R. W. Daniel, "An explanation of never-special assembly changing motions for 3-3 parallel manipulators," *The International Journal of Robotics Research*, vol. 18, no. 6, pp. 556–574, 1999.
- [59] P. Wenger and D. Chablat, "Workspace and assembly-modes in fully parallel manipulators: A descriptive study," in *Advances in Robot Kinematics*. Kluwer Academic Publishers, 1998, pp. 117–126.
- [60] P. Wenger, D. Chablat, and M. Zein, "Degeneracy study of the forward kinematics of planar 3-RPR parallel manipulators," *ASME J. of Mechanical Design*, vol. 129, no. 12, pp. 1265–1268, 2007.
- [61] M. Zein, P. Wenger, and D. Chablat, "Singular curves and cusp points in the joint space of 3-RPR parallel manipulators," in *The International Journal of Robotics Research*, 2006.
- [62] —, "Non-singular assembly mode changing motions for 3-RPR parallel manipulators," *Mechanism and Machine Theory*, vol. 43, no. 4, pp. 480–490, 2008.
- [63] E. Macho, O. Altuzarra, C. Pinto, and A. Hernandez, "Transitions between multiple solutions of the direct kinematic problem," in *Advances in Robot Kinematics: Analysis and Design*. Springer Netherlands, 2008, vol. 5, pp. 301–310.
- [64] P. Kovacs and G. Mommel, "On the tangent-half-angle substitution," in *Computational Kinematics*, J. Angeles, Ed. Kluwer Academic Series, 1993, pp. 27–40.
- [65] C. W. Wampler, "Solving the kinematics of planar mechanisms," *ASME J. of Mechanical Design*, vol. 121, no. 3, pp. 387–391, 1999.
- [66] C. U. Galletti, "A note on modular approaches to planar linkage kinematic analysis," *Mechanism and Machine Theory*, vol. 21, no. 5, pp. 385–391, 1983.
- [67] T. S. Mruthunjaya, "Kinematic structure of mechanisms revisited," *Mechanism and Machine Theory*, vol. 38, no. 4, pp. 279–320, 2003.

- [68] E. Peisach, “Displacement analysis of linkages: Evolution of investigations in a historical aspect,” in *Proc. of the 3rd International Workshop on History of Machines and Mechanisms*, Shanghai, China, Mar. 15-16 2005, pp. 132–141.
- [69] N. I. Manolescu, “For a united point of view in the study of structural analysis of kinematic chains and mechanisms,” *J. of Mechanisms*, vol. 3, pp. 149–169, 1968.
- [70] E. Romaniak, “Methodology of the Assur group creation,” in *Proc. of the 12th IFToMM World Congress*, Besancon, France, June 17-21 2007, p. A898.
- [71] G. Salmon, *A Treatise on Conic Sections*, 6th ed. New York: Chelsea Publishing Co., 1954.